

12-5-2013 12:00 AM

## On Sensorless Collision Detection and Measurement of External Forces in Presence of Modeling Inaccuracies

Vahid Sotoudehnejad, *The University of Western Ontario*

Supervisor: Dr. Mehrdad R. Kermani, *The University of Western Ontario*

A thesis submitted in partial fulfillment of the requirements for the Doctor of Philosophy degree  
in Electrical and Computer Engineering

© Vahid Sotoudehnejad 2013

Follow this and additional works at: <https://ir.lib.uwo.ca/etd>



Part of the [Controls and Control Theory Commons](#), and the [Robotics Commons](#)

---

### Recommended Citation

Sotoudehnejad, Vahid, "On Sensorless Collision Detection and Measurement of External Forces in Presence of Modeling Inaccuracies" (2013). *Electronic Thesis and Dissertation Repository*. 1829.  
<https://ir.lib.uwo.ca/etd/1829>

This Dissertation/Thesis is brought to you for free and open access by Scholarship@Western. It has been accepted for inclusion in Electronic Thesis and Dissertation Repository by an authorized administrator of Scholarship@Western. For more information, please contact [wlsadmin@uwo.ca](mailto:wlsadmin@uwo.ca).

ON SENSORLESS COLLISION DETECTION AND MEASUREMENT  
OF EXTERNAL FORCES IN PRESENCE OF MODELING  
INACCURACIES

(Thesis format: Integrated-Article)

by

Vahid Sotoudehnejad

Graduate Program in Electrical and Computer Engineering

A thesis submitted in partial fulfillment  
of the requirements for the degree of  
Doctor of Philosophy

The School of Graduate and Postdoctoral Studies  
The University of Western Ontario  
London, Ontario, Canada

© Vahid Sotoudehnejad 2013

# Abstract

The field of human-robot interaction has garnered significant interest in the last decade. Every form of human-robot coexistence must guarantee the safety of the user. Safety in human-robot interaction is being vigorously studied, in areas such as collision avoidance, soft actuators, light-weight robots, computer vision techniques, soft tissue modeling, collision detection, etc. Despite the safety provisions, unwanted collisions can occur in case of system faults. In such cases, before post-collision strategies are triggered, it is imperative to effectively detect the collisions. Implementation of tactile sensors, vision systems, sonar and Lidar sensors, etc., allows for detection of collisions. However, due to the cost of such methods, more practical approaches are being investigated. A general goal remains to develop methods for fast detection of external contacts using minimal sensory information. Availability of position data and command torques in manipulators permits development of observer-based techniques to measure external forces/torques. The presence of disturbances and inaccuracies in the model of the robot presents challenges in the efficacy of observers in the context of collision detection. The purpose of this thesis is to develop methods that reduce the effects of modeling inaccuracies in external force/torque estimation and increase the efficacy of collision detection. It is comprised of the following four parts:

- The KUKA Light-Weight Robot IV+ is commonly employed for research purposes. The regressor matrix, minimal inertial parameters and the friction model of this robot are identified and presented in detail. To develop the model, relative weight analysis is employed for identification.
- Modeling inaccuracies and robot state approximation errors are considered simultaneously to develop model-based time-varying thresholds for collision detection. A metric is formulated to compare trajectories realizing the same task in terms of their collision detection and external force/torque estimation capabilities. A method for determining optimal trajectories with regards to accurate external force/torque estimation is also developed.
- The effects of velocity on external force/torque estimation errors are studied with and without the use of joint force/torque sensors. Velocity-based thresholds are developed and implemented to improve collision detection. The results are compared

with the collision detection module integrated in the KUKA Light-Weight Robot IV+.

- An alternative joint-by-joint heuristic method is proposed to identify the effects of modeling inaccuracies on external force/torque estimation. Time-varying collision detection thresholds associated with the heuristic method are developed and compared with constant thresholds.

In this work, the KUKA Light-Weight Robot IV+ is used for obtaining the experimental results. This robot is controlled via the Fast Research Interface and Visual C++ 2008. The experimental results confirm the efficacy of the proposed methodologies.

**Keywords:** Safety in Human-Robot Interaction, Robot Modeling, Relative Weight Analysis, External Force/Torque Observers, Collision Detection, Trajectory Planning



## Co-Authorship Statement

This thesis is written by Vahid Sotoudehnejad under supervision of Dr. Mehrdad R. Kermani. Parts of this material are published in peer-reviewed conference proceedings, or are under review in peer-reviewed journals and conferences.

- Chapter 1: V. Sotoudehnejad - Sole author
- Chapter 2:
  - V. Sotoudehnejad - Developed the methodology and experiment designs, programmed and modeled KUKA Light-Weight Robot IV+
  - M. R. Kermani - Proposed the problem and discussed the results
- Chapter 3:
  - V. Sotoudehnejad - Proposed model-based collision detection thresholds and studied effects of trajectories in external force/torque estimation, designed the experiments
  - M. R. Kermani - Introduced the underlying human-safety problems and discussed the design and results
- Chapter 4:
  - V. Sotoudehnejad - Developed the velocity-based thresholds and designed the experiments
  - M. R. Kermani - Discussed the results and reviewed the manuscript.
- Chapter 5:
  - V. Sotoudehnejad - Developed the time-varying thresholds, designed the experiments and conducted the simulations
  - M. R. Kermani - Discussed the design and results, proposed the simulations and reviewed the manuscript

## **Dedication**

To my family, and specially my mother for all she did.

## Acknowledgments

First and foremost, I'd like to express my sincere gratitude and appreciation to Dr. Mehrdad Kermani for giving me the opportunity to conduct this research at the Physical Human-Robot Interaction laboratory. His patience and understanding throughout the last four years gave me tremendous motivation. I'd also like to thank Dr. Roy Eagleson, Dr. Ana Luisa Trejos, Dr. O. Remus Tutunea-Fatan, and Dr. Mojtaba Ahmadi for serving as my committee members.

Special appreciation goes to Alex Shafer and Peyman Yadmellat for providing me with their invaluable experience. There is no doubt that this thesis would have been impossible without them. In addition I'd like to acknowledge my fellow colleagues Wenjun Li and Farzad Anooshahpour who have inspired me over the past few years.

I want to take this opportunity to give my heartfelt thanks to Vivian Wang, Zachary Lindop, Ron Brown, Chelsea Kirk, Mark Billing, Michelle Ponert, Jeff Rotman, Ali Fathi, Farshad Anooshahpour, and Shannon Quinn for many reasons.

I'd also like to thank Hayden Woodley for helpful discussions on statistical methods.

# Contents

<b>Abstract</b>	<b>ii</b>
<b>Co-Authorship Statement</b>	<b>iv</b>
<b>Dedication</b>	<b>v</b>
<b>Acknowledgments</b>	<b>vi</b>
<b>List of Figures</b>	<b>xi</b>
<b>List of Tables</b>	<b>xiii</b>
<b>List of Appendices</b>	<b>xv</b>
<b>1 Introduction</b>	<b>1</b>
1.1 Related Work . . . . .	1
1.1.1 Safe Actuation Mechanisms . . . . .	2
1.1.2 Collision Detection . . . . .	4
1.2 Accurate External Force/Torque Estimation . . . . .	5
1.2.1 Modeling Inaccuracies . . . . .	6
1.2.2 Time-Varying Collision Detection Thresholds . . . . .	7
1.2.3 Precision of External Torque Estimation with Regards to the Trajectory . . . . .	7
1.3 Thesis Outline and Organization . . . . .	7
1.4 Contributions and Publications . . . . .	9
<b>Bibliography</b>	<b>11</b>
<b>2 On Dynamic Model Identification of KUKA Light-Weight Robot IV+</b>	<b>16</b>

2.1	Introduction . . . . .	16
2.2	Preliminaries . . . . .	18
2.3	KUKA-LWR Controller Considerations . . . . .	18
2.4	Model Identification . . . . .	20
2.4.1	Motor-Side Friction Identification . . . . .	20
2.4.2	Link-Side Friction Identification . . . . .	23
2.4.3	Determining Minimal Inertial Parameters and Dynamic Model . . .	24
	Using Optimal Trajectories . . . . .	27
	Using the Inertia Matrix and the Gravity Vector . . . . .	28
	Using Relative Weight Analysis . . . . .	29
2.5	CONCLUSION . . . . .	31
<b>Bibliography</b>		<b>32</b>
<b>3</b>	<b>On Determining Collision Detection Thresholds and Trajectory Planning for Manipulators with Regards to External Torque Estimation Precision</b>	<b>34</b>
3.1	Introduction . . . . .	34
3.2	Manipulator Model and Collision Detection Residual . . . . .	36
3.3	Effects of Imprecise Modeling and Measurement on Estimating External Torques . . . . .	38
3.3.1	Dynamic Model Using Minimal inertial Parameters . . . . .	38
3.3.2	External Torque Estimation Errors . . . . .	39
3.4	Optimal Trajectories with Regards to Estimating External Torques . . . . .	41
3.4.1	Effects of Controller Design and Trajectory Planning on Accuracy of External Torque Measurement . . . . .	42
	Filter Design for Velocity and Acceleration Estimation - Objective A	42
	Controller Design - Objective A . . . . .	43
	Tachometer and Accelerometer Precision - Objective A . . . . .	43
	Optimal Trajectory Planning - Objective B . . . . .	43
3.4.2	Formulation of the Optimal Trajectories for External Torque Measurement . . . . .	44
3.4.3	Metric for External Torque Estimation Precision of Trajectories . .	47
3.5	Model-Based Collision Detection Thresholds . . . . .	47
3.6	Case Study . . . . .	49

3.6.1	Trajectories and the External Torque Estimation Precision Metric . .	50
3.6.2	Model-Based Thresholds and Collision Detection Results . . . . .	50
3.7	Discussions . . . . .	56
3.8	CONCLUSION . . . . .	57
<b>Bibliography</b>		<b>58</b>
<b>4</b>	<b>Velocity-Based Variable Thresholds for Improving Collision Detection in Manipulators</b>	<b>60</b>
4.1	Introduction . . . . .	60
4.2	Manipulator Modeling and Calculation of External Torques . . . . .	62
4.2.1	External Torque Observer Using Motor Torques . . . . .	62
4.2.2	Measuring External Torques Using Joint Torque Sensors . . . . .	63
4.3	Effects of Unmodeled Dynamics on Measuring External Torques . . . . .	64
4.3.1	Motor Torque Observer . . . . .	65
4.3.2	Joint Torque Sensor Observer . . . . .	66
4.3.3	Concurrent Use of Motor Torque Observer and Joint Torque Sensor Observer . . . . .	66
4.4	Velocity-Based Variable Thresholds for Collision Detection . . . . .	67
4.5	Case Study . . . . .	71
4.5.1	KUKA-LWR Considerations . . . . .	72
4.5.2	Parameter Adjustment of the Velocity-Based Variable Thresholds .	73
4.5.3	Comparison of Velocity-Based variable Thresholds with Constant Thresholds . . . . .	76
4.5.4	Comparison with the Collision Detection Module . . . . .	80
4.6	CONCLUSION . . . . .	80
<b>Bibliography</b>		<b>83</b>
<b>5</b>	<b>Improved Observer-Based Collision Detection Using Time-Variant Thresholds</b>	<b>85</b>
5.1	Introduction . . . . .	85
5.2	Manipulator Modeling, Friction Modeling and Collision Torque Observer .	87
5.3	Residue Error Bounds . . . . .	90
5.3.1	Constant Bounds . . . . .	90
5.3.2	Proposed Time-variant Bounds . . . . .	91

5.3.3	Implementation Notes . . . . .	94
5.4	Simulations . . . . .	96
5.4.1	Collision Detection . . . . .	97
5.4.2	Collision with Human Arm . . . . .	101
5.5	Experimental Results . . . . .	104
5.6	CONCLUSION . . . . .	107
<b>Bibliography</b>		<b>112</b>
<b>6</b>	<b>Concluding Remarks and Future Work</b>	<b>116</b>
6.1	Conclusions . . . . .	116
6.2	Suggestions for Future Work . . . . .	118
<b>Bibliography</b>		<b>121</b>
<b>A</b>	<b>Downloadable Files</b>	<b>123</b>
<b>B</b>	<b>Time-Domain Solution to the External Force/Torque Observer</b>	<b>124</b>
<b>Curriculum Vitae</b>		<b>125</b>

# List of Figures

1.1	Schematics of human-robot interaction . . . . .	2
1.2	Actuators with mechanical compliance . . . . .	3
1.3	KUKA Light-Weight Robot IV+ . . . . .	10
2.1	KUKA Light-Weight Robot IV+ . . . . .	17
2.2	Measurement results of the effective motor-side friction $BB_{\theta}^{-1}\tau_{fr}$ . . . . .	22
3.1	KUKA Light-Weight Robot IV+ . . . . .	51
3.2	Trajectories tracked by KUKA-LWR . . . . .	52
3.3	External torque residuals and their corresponding model-based collision detection thresholds for trajectory 1 in absence of collisions . . . . .	52
3.4	External torque residuals and their corresponding model-based collision detection thresholds in presence of collisions . . . . .	54
4.1	Schematic diagram of a single robot joint . . . . .	64
4.2	Simulated values of friction estimation error for a LuGre model with 15% parameter uncertainty . . . . .	68
4.3	Collision detection using a Hybrid III 50th male dummy . . . . .	71
4.4	Estimated values of $\hat{\tau}_{sfe}(\dot{q})$ and $\hat{\tau}_{fme}(\dot{q})$ for all joints of KUKA-LWR . . . . .	75
4.5	Torque sensor-based residuals $\hat{r}_s(t)$ and their respective upper and lower thresholds for joints 1-3 of KUKA-LWR in the absence of collision forces . . . . .	77
4.6	Torque sensor-based residuals $\hat{r}_s(t)$ , velocity-based variable thresholds, and constant thresholds for joints 1-3 of KUKA-LWR in the presence of collision forces . . . . .	77
4.7	Motor torque-based residuals $\hat{r}(t)$ , velocity-based variable thresholds, and constant thresholds for joints 1-3 of KUKA-LWR in the presence of collision forces . . . . .	78



4.8	Torque sensor-based residuals $\hat{r}_s(t)$ and their respective upper and lower thresholds for joints 1 and 4 of KUKA-LWR and the scaled acceleration signal from the Hybrid III 50th male dummy for a single collision . . . . .	81
5.1	Time-variant threshold concept . . . . .	87
5.2	Collision with KUKA Light-Weight Robot IV+ . . . . .	88
5.3	PUMA 560 . . . . .	97
5.4	Collision residue $\hat{r}(t)$ and thresholds $b_{2H}(t)$ and $b_{2L}(t)$ for a simulated PUMA 560. . . . .	99
5.5	Collision forces/torques applied to the last joint of PUMA 560 . . . . .	99
5.6	Collision residue $\hat{r}(t)$ compared to the collision torques $\tau_c$ for PUMA 560. .	100
5.7	Snapshots of a modeled human in LifeModeler software during two collisions with a robot (PUMA 560). . . . .	102
5.8	Collision forces between the human arm and an aluminum shaft held by PUMA 560. . . . .	102
5.9	Collision residue $\hat{r}(t)$ and upper and lower collision detection bounds for PUMA 560. . . . .	103
5.10	KUKA Light-Weight Robot IV+ . . . . .	105
5.11	Hysteretic nature of $\tau_{fre}$ in joint 1 of KUKA-LWR . . . . .	106
5.12	Collision residues $\hat{r}(t)$ and bounds $b_{2H}(t)$ and $b_{2L}(t)$ for KUKA-LWR in the absence of collision forces . . . . .	109
5.13	Collision residues $\hat{r}(t)$ , time-variant thresholds, and constant thresholds for KUKA-LWR in the presence of collision forces . . . . .	110

# List of Tables

2.1	PID gains for position control of KUKA-LWR via the FRI module . . . . .	20
2.2	Coulomb friction constants for effective motor-side friction $BB_{\theta}^{-1}\tau_{fr}$ in KUKA-LWR . . . . .	23
2.3	Coulomb friction constants of the link-side friction $\tau_{frL}$ in KUKA-LWR . . . . .	24
2.4	Modified Denavit-Hartenberg parameters of KUKA-LWR . . . . .	24
2.5	Classical inertial parameters of KUKA-LWR . . . . .	25
2.6	Formulation of minimal inertial parameters of KUKA-LWR using its classical inertial parameters . . . . .	26
2.7	Minimal Inertial Parameters of KUKA-LWR and the Regression Analysis Data . . . . .	30
3.1	Calculated $B_{\tilde{Q}}$ for different trajectories . . . . .	51
3.2	External torque estimation metric for different trajectories . . . . .	51
3.3	Comparison between different trajectories with regards to collision detection delays using model-based thresholds . . . . .	55
4.1	PID gains used via KUKA-LWR FRI module . . . . .	73
4.2	Estimated $\gamma \approx \gamma_s$ for all joints of KUKA-LWR . . . . .	76
4.3	Collision detection times with and without velocity-based thresholds in KUKA-LWR . . . . .	79
4.4	Collision detection delays of velocity-based and constant thresholds using torque sensor residuals and KUKA-LWR integrated collision detection module . . . . .	81
5.1	Simulated Trajectory Points . . . . .	97
5.2	PID Controller Gains for a Simulated PUMA 560. . . . .	98
5.3	Values of $\alpha$ , $\gamma$ and $\epsilon_{fr}$ for a Simulated PUMA 560. . . . .	98
5.4	Collision detection times in the first three joints of PUMA 560 . . . . .	101

5.5	Collision detection with the human arm using time-variant thresholds in the first three joints of PUMA 560. . . . .	104
5.6	PD controller values for KUKA-LWR . . . . .	106
5.7	Experimental values of $\alpha_H$ , $\alpha_L$ , $\gamma$ for KUKA-LWR . . . . .	107
5.8	Trajectory Points of KUKA-LWR . . . . .	108
5.9	Collision detection times in the first three joints of KUKA-LWR . . . . .	108

# List of Appendices

Appendix A Downloadable Files . . . . . 123

Appendix B Time-Domain Solution to the External Force/Torque Observer . . . . . 124

# Chapter 1

## Introduction

Physical human-robot interaction has become a major research area in the field of robotics, with the main objective of building robots that can coexist with humans in unstructured environments [1], [2], [3]. One of many challenges concerning human-robot interaction is to ensure safety of the user while physically interacting with the robot [4]. Accurate detection of human-robot collisions, as well as accurate estimation of external forces acting on the robot help to ensure the safety of the user [5]. For this reason, measurement of interaction forces and rapid detection of collisions with the robot is imperative.

Robots can sense their environment using vision, tactile, sonar, voice-based, and other such sensors. The cost of these sensors and their inherent complications may not be ideal. This research develops methodologies for collision detection and accurate force/torque estimation using minimal sensory information. To this end, this work presents methodologies to improve estimation of external forces/torques and collision detection in presence of modeling inaccuracies.

### 1.1 Related Work

A simple physical human-robot interaction diagram is shown in Fig. 1.1. The robot controller is responsible for taking into consideration the sensory information from the interaction to ensure the safety of the user. The amount of information available from the interaction determines if the robot is able to behave safely. The safety includes the controller design, post-collision strategies and the actuation mechanism. A lot of research is

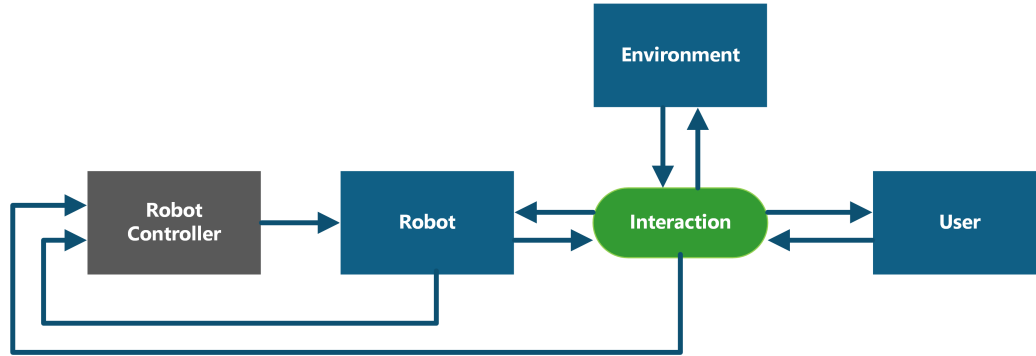


Figure 1.1: Schematics of human-robot interaction

done on safe robotic actuators. Fast and reliable collision detection is critical in order to activate post-collision strategies. We first review the actuation mechanisms that are related to the development of safe robots, with collision detection literature discussed after.

### 1.1.1 Safe Actuation Mechanisms

Unwanted collisions might occur in robots in case of faults, failure of collision avoidance systems, or any other unplanned changes in the environment. One way to achieve safety requirements is by adding proximity sensors to the robot [6], [7] or by adding extra paddings to the robot's surface [8]. Another method, proven to have intrinsic limitations, is active force control [9]. Safety issues have brought about technological innovations, most notably several generations of DLR's Zentrum für Luft- und Raumfahrt (DLR) robots [10]. Using joint torque sensors and accurate modeling, these robots are able to incorporate proper force control methods to assure safety of their users [11], [5].

Another method to realize a safe and interactive environment is creating intrinsically safe robots. Motor inertia is the main contributor to safety concerns [2]. Manipulators with mechanical compliance within the joints reduce total link inertia, where the total link inertia includes the motor inertia projected to the link side. One technique is distributed macro-mini actuation [12] that divides torque generation into high and low frequency components [13] (Figure 1.2a), where low frequency high power actuation occurs at the base of the robot while high frequency low power actuators are placed at the joints. Another way of adding mechanical compliance is Variable-Impedance Actuation (VIA) [14], [15]. VIA exploits the idea that slow motions are able to keep high impedance while fast motions need to have less impedance. VIA provides an overall smaller impedance than a regular

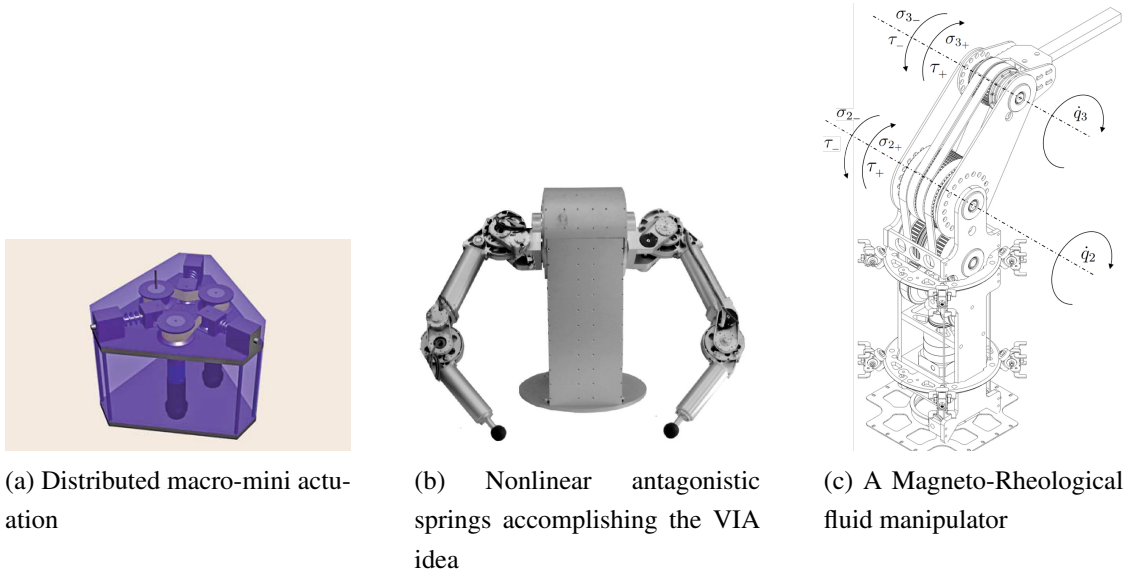


Figure 1.2: Actuators with mechanical compliance

actuation mechanism. A desired impedance can be achieved by varying the joint stiffness, damping and gear ratio. An actuator accomplishing this task by using antagonistic nonlinear springs is shown in Figure 1.2b. Its impedance is a function of time and depends on the state/motion of the actuator. One intriguing aspect of the VIA concept is that it can be implemented using various methods, such as arranging actuators at robot base, macro-mini actuation, and antagonistic arrangements. These manipulators, dubbed soft manipulators, require complex controllers which is an open area of research [16].

Magnetorheological-fluid (MR fluid) robots developed in our research group are another example of inherently safe robots (Figure 1.2c), where MR fluid was implemented in robot joints to realize safe mechanical compliance [17], [18], [19], [20], [21]. MR fluids were originally discovered in 1948 [22], but only recent advances in technology has made them a reliable engineering product [23], [24]. They have been used in various applications such as throttle valves [25], vehicle vibration dampers [26] and haptic actuation to improve stability and performance [27]. They have the ability to change their viscosity depending on the magnetic field that the fluid is exposed to. Research in Magnetorheological fluids has shown that their ability to change their viscosity can be used in manipulator joints to provide the ability to dynamically alter the joint compliance [18]. The physical properties of MR-fluids are used to decouple the motor inertia from the joint, allowing to have various degrees of compliancy while having high level of safety in the joint actuation.

The ability of the controller to cope with compliance and post-collision control laws is also an open research subject. However, no matter the actuation mechanism, compliance methods, or post-collision control laws, unexpected conditions may result in unwanted collisions that can be potentially dangerous to the user. The efficacy of post-collision strategies in ensuring the safety of the user, whether in compliant or not-compliant robots, is contingent on accurate and fast collision detection.

### 1.1.2 Collision Detection

Control laws for every manipulator to handle collisions are necessary. These laws become effective based on the sensory information available to the controller [8], [28]. This becomes more important given that there are robots being developed that employ Programming by Demonstration (PbD) [29]. PbD is the technique of mapping examples and their policies to actions. Such examples can be gathered from demonstrations performed by the user on the robot. PbD, in its modern form, attempts to replace rigid interfaces with more human-friendly interfaces. Human safety must be ensured before implementation of human-friendly interfaces.

In order to have safe physical human-robot interaction, rapid collision detection methods must be developed. Detection of collisions allows the trigger of post-collision strategies. It is shown that fast detection and appropriate implementation of post-collision strategies reduces the collision forces and consequently improves the safety of the physical human-robot interaction [5]. Detection of external forces using the robot model and position sensors was studied in [8] and [30]. The approach of using generalized momentum of the robot for collision detection was developed in [31]. Its application in post-collision reaction strategies was discussed in [5] and [32]. Adaptive control laws implemented in [33] and [34] were used to lower the constant thresholds. Constant thresholds are often used for the purpose of collision detection [5], [33] and are determined based on each robotic application. In case of safety in human-robot interaction, human pain tolerance levels can be used to determine the thresholds [28]. The studies mentioned above have employed constant thresholds for collision detection. Constant thresholds have the drawback that setting a low threshold might result in false-positive collision detection outcomes, and setting a high threshold might leave some collisions undetected. This drawback can be alleviated by using time-varying thresholds. Adaptive time-varying thresholds based on a fuzzy-logic



method were reported in [35]. Effects of physical modeling errors on the thresholds was also studied in [36]. However, a deterministic approach to time-varying thresholds that would consider all modeling inaccuracies along with the robot state approximations and trajectory planning was not investigated.

Chapter 3 of this work studies the complete model of a robot while considering all sources of modeling inaccuracies, i.e. uncertainties in minimal inertial parameters [37], sensor reading errors, as well as errors inherent in passband filters commonly used for obtaining velocity and acceleration approximations. All the mentioned inaccuracies are used simultaneously to develop the deterministic time-varying thresholds. To this end, estimation of external forces/torques is essential. As discussed before, the focus of this research is development of safe collision detection algorithms and accurate external force/torque measurement for robots, while avoiding costly and complex sensory information, such as tactile, visual or force sensors. Therefore only position sensors information, which are available in every manipulator, are considered. To this end, a study of external force/torque estimation methods using observers is required. Issues regarding modeling inaccuracies, time-varying collision detection thresholds, and impacts of trajectory on the estimations must be examined.

## 1.2 Accurate External Force/Torque Estimation

Safe robots should be aware of their surroundings and be capable of limiting the damage they might bring about to an acceptable minimum level. Two areas of robotics dealing with these issues are collision avoidance and collision detection. As this research thrives to develop safe HRI without adding additional sensors to what already exists in robot manipulators, collision avoidance would be out of the scope of this research as it requires workspace monitoring sensors.

A collision detection scheme based on the robot state, i.e. position and velocity data of the robot, is considered in our study. The accuracy of such a scheme depends on the accuracy of the robot model, which includes friction forces, link-specific information, motor parameters, joint elasticity, etc. Consequently, a dependable collision detection scheme relies heavily on the adopted modeling scheme. One thing that is common among industrial manipulators is the lack of accurate link and joint parameters. Hence a methodology that can deal with inaccuracies in the collision detection algorithm is of paramount importance. The manipulator dynamic equations allow implementation of observers for determining

externally applied forces and torques. Several observer-based methods have been proposed in the literature for obtaining the external forces/torques [38], [35], [39], [40], [5]. A nonlinear torque observer based on velocity residual was formulated in [35]. This approach did not use the complete robot dynamics for the development of a more accurate adaptive threshold. Another nonlinear torque observer was formulated in [39] for estimating friction torques in two link manipulators. This method however, could not be easily extended to robots with more than two joints. The implementation of high gain observers [40], for estimating external torques in robot manipulators, was proposed and discussed in detail in [5]. The observer in [5] is used in this work for estimation of external torques.

Investigating the modeling inaccuracies of a robot within the structure of torque observers such as [5] will lead to an effective method for detecting collisions based on the state of the robot at the time of collision. Modeling inaccuracies further motivate the need for time-varying thresholds to determine collisions.

### 1.2.1 Modeling Inaccuracies

External force/torque observers estimate external torques, or detect collisions, using the model and the state of the robot [30]. However, inaccuracy of the robot model and the presence of errors in velocity and acceleration estimations reduces the efficacy of the external force/torque observers.

The model of a manipulator consists of the actuator model, friction model, joint elasticity, and the minimal inertial parameters. Inaccuracy of the velocity and acceleration approximations must be considered alongside the imprecisions in parameter estimations of the model of the robot. Velocity and acceleration can be estimated by applying derivative filters to the position signal. Therefore the filter type along with potential robot trajectories help determine how accurate the velocity and acceleration estimations are. In case tachometers or accelerometers are available, the precision of these sensors must be taken into account. Also, controller design affects the external torque estimation as well. These concepts must also be considered in the general scheme of accurate external torque estimation.

Accuracy of external torque estimation also impacts the precision of collision detection. We propose time-varying thresholds based on the inaccuracies in modeling and sensor readings. Furthermore, precision of the collision detection method, based on the manipulator structure and the trajectory, can be determined by the proposed thresholds. Therefore a metric will be defined to address comparison between collision detection accuracy of dif-

ferent tasks or trajectories.

### 1.2.2 Time-Varying Collision Detection Thresholds

A particular formulation of serial link manipulators is given in this work which can be directly applied to determine the precision of external torque estimations. Upon investigating this modeling formulation, time-varying thresholds are developed for collision detection. In particular, effects of joint velocity on the collision detection thresholds are considered. Different scenarios of collision detection are experimented with different types of proposed thresholds using KUKA Light-Weight Robot IV+ (see Fig. 1.3). A heuristic procedure for improving time-varying collision detection thresholds on a joint-by-joint basis with inaccurate minimal inertial parameters is also proposed.

### 1.2.3 Precision of External Torque Estimation with Regards to the Trajectory

The robot dynamics, its model parameters, and the given task all affect the efficacy of external torque estimation methods. In particular, the trajectory that the robot takes to complete a given task might improve or deteriorate the collision detection capability of the external torque observers. By studying the effects of different trajectories simultaneously with modeling inaccuracies and robot state approximation errors, a metric is defined to compare trajectories with regards to external torque estimation and collision detection. By pairing this metric with its corresponding model-based time-varying threshold, collision detection capability of different trajectories and different robots can be compared.

## 1.3 Thesis Outline and Organization

In this thesis we study collision detection and measurement of external forces using external force/torque observers when modeling inaccuracies are present. The robot used for this research is KUKA Light-Weight Robot IV+ (KUKA-LWR) which has seven degrees of freedom. Considering that this work studies modeling inaccuracies in collision detection, modeling of KUKA-LWR was essential and is reported. An outline of the work in each chapter is as follows,

- In Chapter 2, modeling of KUKA-LWR is explored. This chapter starts with an introduction to serial link manipulators modeling techniques. An examination of the controller of KUKA-LWR is provided which helps in identifying its model. The experiments with regards to friction modeling are discussed and the regressor matrix and minimal inertial parameters of KUKA-LWR are obtained. To identify the minimal inertial parameters, a novel statistics-based method using relative weight analysis, see [41], is introduced. The modeling results of this section form the basis for the experiments in this thesis. The accuracy of the obtained model is verified by experiments.
- In Chapter 3, model-based collision detection thresholds are determined based on the modeling inaccuracies, trajectories and robot state estimations. First a particular formulation of manipulator dynamics based on minimal inertial parameters is provided. Based on this formulation, external force/torque estimation errors in presence of modeling uncertainty, sensor reading errors, and velocity and acceleration approximation errors are investigated. This formulation of force/torque estimation errors allows for definition of an optimization problem for determining the optimal trajectories with regards to external force/torque estimation precision. Metrics for comparing different trajectories in terms of external force/torque estimation are also proposed, along with controller design considerations related to external force/torque estimation errors. Based on the analysis of errors present in external force/torque estimations, model-based collision detection thresholds are proposed. Experiments are conducted on KUKA-LWR to compare different trajectories with regards to external torque estimation precision. Also, collision detection outcomes of the proposed model-based thresholds for different trajectories are compared.
- Chapter 4 proposes deterministic velocity-based collision detection thresholds using the high gain observer in [5]. Details of the external torque observers with and without joint torque sensors are described. The effects of inaccurate modeling and torque sensor reading errors on the solution of the external torque observers is studied. For this purpose, LuGre friction model is examined [42]. Strategies for minimizing the effects of such errors on torque observers are also discussed. Upon attempting to mitigate effects of modeling errors, velocity-based time-varying thresholds for collision detection are proposed. The proposed velocity-based thresholds are implemented on KUKA-LWR, which is equipped with joint torque sensors. Collision detection

capability of the proposed thresholds is compared to those obtained from uncompensated thresholds on KUKA-LWR. For this purpose, Endevco® Piezoresistive 2000 g accelerometers were installed in a Humanetics® Hybrid III 50th Male Dummy and were used to measure the detection delay between different collision detection methods. This comparison also includes the collision detection results of the COLLDETECTION module included by the manufacturer in the KUKA-LWR software.

- In Chapter 5, intuitive methods that can help in determining time-varying thresholds on a joint-by-joint basis are given. The mathematics behind the proposed intuitive methods for adjusting time-varying collision detection thresholds are provided. Of particular interest is the joint-by-joint study of the uncertainties in the physical parameters of the manipulators such as mass, inertia, center of gravity, etc. Simulation results of applying the proposed thresholds to PUMA 560 are given. This includes a model of a human developed using the LifeModeler® software, an MD ADAMS® software package. To evaluate a human-robot interaction algorithm, the amount of force exerted on a human should be analyzed. This could be achieved either using anthropomorphic dummies or software simulations. LifeModeler® is used as a simulation platform regarding human-robot collisions. The proposed scheme is then applied to KUKA-LWR robot. The results show that by using the proposed method, the effect of modeling inaccuracies in KUKA-LWR on external force/torque estimations can be partially mitigated which in turn improves collision detection results.
- Chapter 6 summarizes and concludes the work described in this thesis. It discusses future research directions and suggestions.

## 1.4 Contributions and Publications

This thesis is divided into four main chapters. The contributions of each chapter are as follows,

- Chapter 2 provides an original comprehensive systematic modeling of KUKA Light-Weight Robot IV+. The work is also novel in terms of implementing relative weight analysis for obtaining minimal inertial parameters in presence of noise. The results and the codes are available online for the robotic community use. This work is under review in a peer-reviewed journal.

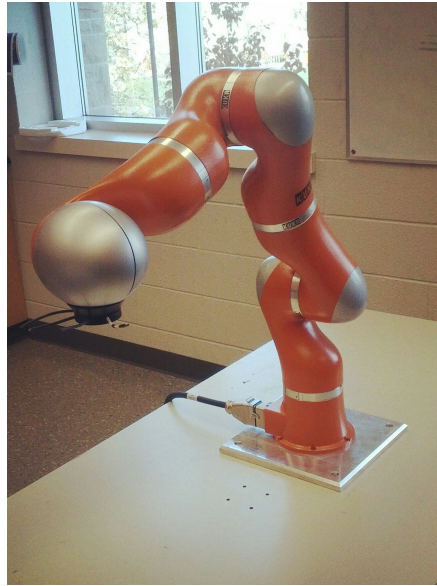


Figure 1.3: KUKA Light-Weight Robot IV+

- Chapter 3 is novel in terms of providing an original in-depth modeling error analysis of external force/torque observers. Optimal trajectories are formulated with regards to external force/torque estimation precision. Also, a new metric is defined to compare different trajectories with regards to external torque estimation precision. Novel model-based time-varying thresholds are proposed for the purpose of collision detection. The proposed methodologies are developed such that they can be applied to any serial link manipulator. However, in case of availability of more sensory information or the actuator mechanism model, the methodology can be easily expanded upon. This work is under review in a peer-reviewed journal.
- Chapter 4 investigates external force/torque observers to develop a new deterministic velocity-based time-varying threshold for collision detection. This work is under review in a peer-reviewed journal and conference proceedings.
- Chapter 5 proposed new heuristic methods to improve external force/torque estimation and collision detection without resorting to re-modeling of the robot. Parts of this work is published at conference proceedings [43], and is under review in a peer-reviewed journal.

## Bibliography

- [1] K. Ikuta, H. Ishii, and M. Nokata, "Safety evaluation method of design and control for human-care robots," *Int. J. of Robotics Research*, vol. 22, no. 5, pp. 281–297, 2003.
- [2] A. D. Santis, B. Siciliano, A. D. Luca, and A. Bicchi, "An atlas of physical human-robot interaction," *Mechanism and Machine Theory*, vol. 43, no. 3, pp. 253 – 270, 2008.
- [3] A. De Luca, F. Flacco, A. Bicchi, and R. Schiavi, "Nonlinear decoupled motion-stiffness control and collision detection/reaction for the vsa-ii variable stiffness device," in *Intelligent Robots and Systems (IROS), IEEE/RSJ International Conference on*, pp. 5487 –5494, 2009.
- [4] A. Pervez and J. Ryu, "Safe physical human robot interaction-past, present and future," *Journal of Mechanical Science and Technology*, vol. 22, pp. 469–483, 2008.
- [5] A. D. Luca, A. Albu-Schaffer, S. Haddadin, and G. Hirzinger, "Collision detection and safe reaction with the dlr-iii lightweight manipulator arm," in *Intelligent Robots and Systems, 2006 IEEE/RSJ International Conference on*, pp. 1623 –1630, oct. 2006.
- [6] E. Cheung and V. Lumelsky, "Proximity sensing in robot manipulator motion planning: system and implementation issues," *Robotics and Automation, IEEE Trans. on*, vol. 5, pp. 740 –751, dec 1989.
- [7] H. Iwata, H. Hoshino, T. Morita, and S. Sugano, "Force detectable surface covers for humanoid robots," in *Advanced Intelligent Mechatronics, Proceedings. 2001 IEEE/ASME International Conference on*, vol. 2, pp. 1205 –1210 vol.2, 2001.
- [8] K. Suita, Y. Yamada, N. Tsuchida, K. Imai, H. Ikeda, and N. Sugimoto, "A failure-to-safety "kyozon" system with simple contact detection and stop capabilities for safe human-autonomous robot coexistence," in *Robotics and Automation, Proceedings., 1995 IEEE International Conference on*, vol. 3, pp. 3089 –3096 vol.3, may 1995.
- [9] W. T. Townsend, "The effect of transmission design on force-controlled manipulator performance," tech. rep., Cambridge, MA, USA, 1988.
- [10] G. Hirzinger, A. Albu-Schaffer, M. Hahnle, I. Schaefer, and N. Sporer, "On a new generation of torque controlled light-weight robots," in *Robotics and Automation*,

- Proceedings 2001 ICRA. IEEE International Conference on*, vol. 4, pp. 3356 – 3363 vol.4, 2001.
- [11] A. Albu-Schffer and G. Hirzinger, “Cartesian compliant control strategies for light-weight, flexible joint robots,” *Control Problems in Robotics*, vol. 4, no. 1, pp. 135–152, 2002.
- [12] M. Zinn, O. Khatib, B. Roth, and J. K. Salisbury, “A new actuation approach for human friendly robot design,” in *International Symposium on Experimental Robotics, S. Angelo d’Ischia, I*, pp. 379–398, 2002.
- [13] A. Sharon, N. Hogan, and D. Hardt, “High bandwidth force regulation and inertia reduction using a macro/micro manipulator system,” in *Robotics and Automation, Proceedings., 1988 IEEE International Conference on*, pp. 126 –132 vol.1, apr 1988.
- [14] A. Bicchi and G. Tonietti, “Fast and ”soft-arm” tactics [robot arm design],” *Robotics Automation Magazine, IEEE*, vol. 11, pp. 22 – 33, june 2004.
- [15] A. Bicchi, S. Rizzini, and G. Tonietti, “Compliant design for intrinsic safety: general issues and preliminary design,” in *Intelligent Robots and Systems, Proceedings. 2001 IEEE/RSJ International Conference on*, vol. 4, pp. 1864 –1869 vol.4, 2001.
- [16] A. Bicchi, M. A. Peshkin, and J. E. Colgate, “Safety for physical human-robot interaction,” in *Springer Handbook of Robotics* (B. Siciliano and O. Khatib, eds.), pp. 1335–1348, Springer Berlin Heidelberg, 2008.
- [17] A. Shafer and M. Kermani, “Design and validation of a magneto-rheological clutch for practical control applications in human-friendly manipulation,” in *Robotics and Automation (ICRA), 2011 IEEE International Conference on*, pp. 4266–4271, 2011.
- [18] A. Shafer and M. Kermani, “On the feasibility and suitability of mr and er based actuators in human friendly manipulators,” in *Intelligent Robots and Systems (IROS), IEEE/RSJ International Conference on*, pp. 2904 –2909, 2009.
- [19] P. Yadmellat and M. Kermani, “Output torque modeling of a magneto-rheological based actuator,” in *IFAC World Congress*, vol. 18, pp. 1052–1057, 2011.



- [20] P. Yadmellat, A. Shafer, and M. Kermani, "Design and development of a single-motor, two-dof, safe manipulator," *Mechatronics, IEEE/ASME Transactions on*, vol. PP, no. 99, pp. 1–8, 2013.
- [21] P. Yadmellat, A. S. Shafer, and M. R. Kermani, "Design and development of a safe robot manipulator using a new actuation concept," in *Robotics and Automation (ICRA), 2013 IEEE International Conference on*, pp. 337–342, 2013.
- [22] J. Rabinow, "The magnetic fluid clutch," *American Institute of Electrical Engineers, Transactions of the*, vol. 67, pp. 1308 –1315, jan. 1948.
- [23] J. Carlson, "What makes a good MR fluid?," *Journal of intelligent material systems and structures*, vol. 13, no. 7-8, p. 431, 2002.
- [24] J. Huang, J. Zhang, Y. Yang, and Y. Wei, "Analysis and design of a cylindrical magneto-rheological fluid brake," *Journal of Materials Processing Technology*, vol. 129, no. 1-3, pp. 559–562, 2002.
- [25] O. Ashour, C. A. Rogers, and W. Kordonsky, "Magnetorheological fluids: Materials, characterization, and devices," *Journal of Intelligent Material Systems and Structures*, vol. 7, pp. 123–130, March 1996.
- [26] D. J. Peel, R. Stanway, and W. A. Bullough, "Experimental study of an er long-stroke vibration damper," in *Smart Structures and Materials 1997: Passive Damping and Isolation* (L. P. Davis, ed.), vol. 3045, pp. 96–107, SPIE, 1997.
- [27] J. An and D. soo Kwon, "Haptic experimentation on a hybrid active/passive force feedback device," in *Robotics and Automation, Proceedings. ICRA '02. IEEE International Conference on*, vol. 4, pp. 4217 – 4222 vol.4, 2002.
- [28] Y. Yamada, Y. Hirasawa, S. Huang, Y. Umetani, and K. Suita, "Human-robot contact in the safeguarding space," *Mechatronics, IEEE/ASME Trans. on*, vol. 2, pp. 230 –236, dec 1997.
- [29] A. Billard, S. Calinon, R. Dillmann, and S. Schaal, "Robot programming by demonstration," in *Springer Handbook of Robotics* (B. Siciliano and O. Khatib, eds.), pp. 1371–1394, Springer Berlin Heidelberg, 2008.

- [30] S. Takakura, T. Murakami, and K. Ohnishi, “An approach to collision detection and recovery motion in industrial robot,” in *Industrial Electronics Society, 1989. IECON '89., 15th Annual Conference of IEEE*, pp. 421–426 vol.2, nov 1989.
- [31] A. De Luca and R. Mattone, “Sensorless robot collision detection and hybrid force/motion control,” in *Robotics and Automation, 2005. ICRA 2005. Proceedings of the 2005 IEEE International Conference on*, pp. 999–1004, 2005.
- [32] S. Haddadin, A. Albu-Schaffer, A. De Luca, and G. Hirzinger, “Collision detection and reaction: A contribution to safe physical human-robot interaction,” in *Intelligent Robots and Systems, 2008. IROS 2008. IEEE/RSJ International Conference on*, pp. 3356–3363, 2008.
- [33] S. Morinaga and K. Kosuge, “Collision detection system for manipulator based on adaptive impedance control law,” in *Robotics and Automation, 2003. Proceedings. ICRA '03. IEEE International Conference on*, vol. 1, pp. 1080 – 1085 vol.1, sept. 2003.
- [34] T. Matsumoto and K. Kosuge, “Collision detection of manipulator based on adaptive control law,” in *Advanced Intelligent Mechatronics, 2001. Proceedings. 2001 IEEE/ASME International Conference on*, vol. 1, pp. 177–182 vol.1, 2001.
- [35] H. Sneider and P. Frank, “Observer-based supervision and fault detection in robots using nonlinear and fuzzy logic residual evaluation,” *Control Systems Technology, IEEE Trans. on*, vol. 4, pp. 274–282, May 1996.
- [36] W. Dixon, I. Walker, D. Dawson, and J. Hartranft, “Fault detection for robot manipulators with parametric uncertainty: a prediction error based approach,” in *Robotics and Automation, 2000. Proceedings. ICRA '00. IEEE International Conference on*, vol. 4, pp. 3628–3634 vol.4, 2000.
- [37] M. Gautier and W. Khalil, “A direct determination of minimum inertial parameters of robots,” in *Robotics and Automation, 1988. Proceedings., 1988 IEEE International Conference on*, pp. 1682–1687 vol.3, apr 1988.
- [38] S. Katsura, Y. Matsumoto, and K. Ohnishi, “Analysis and experimental validation of force bandwidth for force control,” *Industrial Electronics, IEEE Trans. on*, vol. 53, pp. 922 – 928, june 2006.

- [39] W.-H. Chen, D. Ballance, P. Gawthrop, and J. O'Reilly, "A nonlinear disturbance observer for robotic manipulators," *Industrial Electronics, IEEE Trans. on*, vol. 47, pp. 932–938, Aug. 2000.
- [40] A. Stotsky and I. Kolmanovsky, "Application of input estimation techniques to charge estimation and control in automotive engines," *Control Engineering Practice*, vol. 10, no. 12, pp. 1371–1383, 2002.
- [41] S. Tonidandel and J. LeBreton, "Relative importance analysis: A useful supplement to regression analysis," *Journal of Business and Psychology*, vol. 26, no. 1, pp. 1–9, 2011.
- [42] H. Olsson, K. Astrom, C. C. de Wit, M. Gafvert, and P. Lischinsky, "Friction models and friction compensation," *European Journal of Control*, vol. 4, no. 3, pp. 176–195, 1998.
- [43] V. Sotoudehnejad, A. Takhmar, M. Kermani, and I. Polushin, "Counteracting modeling errors for sensitive observer-based manipulator collision detection," in *Intelligent Robots and Systems (IROS), 2012 IEEE/RSJ International Conference on*, pp. 4315–4320, 2012.

## Chapter 2

# On Dynamic Model Identification of KUKA Light-Weight Robot IV+

### 2.1 Introduction

Serial link manipulators are commonly used in robotics research. Precise control of manipulators is a well-studied subject. In this respect, designing reliable controllers is made possible by obtaining the accurate model of the manipulator. Previous studies have attained the model of commonly used manipulators, such as PUMA 560 [1], [2], and Mitsubishi PA-10 [3], [4]. KUKA Light-Weight robot IV+ (KUKA-LWR), see Fig. 2.1, is a state-of-the-art manipulator that is put to use frequently in the robotics research community. Availability of an explicit model of KUKA-LWR would be beneficial in applications that involve position or force control, collision detection or human-robot interaction.

With recent advances in processing power, calculation of the formidable size of the explicit models of manipulators with several joints is not a major concern. The work in this thesis includes obtaining the KUKA-LWR dynamics without any simplifications in order to present a complete explicit model. The minimal inertial parameters, introduced in [5] and [6], are presented for KUKA-LWR along with the associated regressor matrix [5]. Experiments are designed for identification of parameters of the model of KUKA-LWR based on the methodology developed in [7] and [8] and the results are discussed. However, in order to achieve a more accurate model of KUKA-LWR, a larger data set than what is required by [7] is used to identify the minimal inertial parameters of KUKA-LWR. Furthermore, KUKA-LWR provides the user with the inertia matrix and the gravity vector, which can



Figure 2.1: KUKA Light-Weight Robot IV+

be used to identify the components of the minimal inertial parameters that affect the inertia matrix and the gravity vector. To this extent, regressor matrices based on the inertia matrix and the gravity vector are defined and the methodology to identify the minimal inertial parameters using such regressor matrices are presented. The results of the different identification procedures are compared. Also, using standard regression analysis procedures, the statistically insignificant model parameters are determined and removed from the model. Moreover, we propose using relative weight analysis, see [9], to measure the effect of each minimal inertial parameter in the modeling. This in turn allows us to distinguish the parameters with very small effect on the entire model. Removal of such parameters aid the user to avoid unnecessary computational complexity and obtain accurate estimations of the remaining minimal inertial parameters.

This paper covers the considerations specific to the KUKA-LWR manipulator for control and modeling, the process for the calculation of the explicit model, along with the modeling results. Due to the closed architecture of KUKA-LWR, some physical data specifically motor currents and motor positions are not accessible. This is taken into account during the modeling procedure and is explained in detail. Also, KUKA-LWR has an internal controller loop that can not be turned off, which must be examined as well. The organization of this paper is as follows. Section 2.2 provides the preliminaries for the model of flexible joint manipulators. In section 2.3, an examination of the KUKA-LWR controller is provided. Section 2.4, presents the methodology for and the results of modeling the friction of KUKA-LWR. Also, in this section the formulations of the regressor matrix and the mini-

mal inertial parameters of KUKA-LWR are obtained. This is followed by the identification procedures and their results. The implementation of relative weight analysis is described and its results are also discussed. Section 2.5 concludes this paper.

## 2.2 Preliminaries

The dynamic equations of a flexible joint manipulator are,

$$M(q)\ddot{q} + C(q, \dot{q})\dot{q} + g(q) = \tau_L - \tau_{fr_L} \quad (2.1a)$$

$$B\ddot{\theta} + DK^{-1}\dot{\tau}_J + \tau_J = \tau_m - \tau_{fr} \quad (2.1b)$$

$$\tau_L = DK^{-1}\dot{\tau}_J + \tau_J \quad (2.1c)$$

where  $q$  denotes the joint space position of the manipulator,  $M(q)$  is the link inertia matrix,  $C(q, \dot{q})$  is the centrifugal and Coriolis matrix,  $g(q)$  is the gravitational vector,  $\tau_L$  is the torque transmitted to the robot links via flexible joints, and  $\tau_{fr_L}$  is the friction torque from the manipulator links. Also,  $B$  is the motor inertia matrix,  $\theta$  is the motor position,  $K > 0$  is the diagonal joint stiffness matrix,  $D > 0$  is the diagonal joint viscosity matrix,  $\tau_J = K(\theta - q)$  is the joint elastic torque,  $\tau_m$  is the motor input torque to the flexible joint, and  $\tau_{fr}$  is the motor-side friction torque of the manipulator.

Details of friction models for  $\tau_{fr}$  and  $\tau_{fr_L}$  will be given in Section 2.4. Next section uses the flexible model described in (2.1) to explain the effects of internal controller feedback loops of KUKA-LWR.

## 2.3 KUKA-LWR Controller Considerations

KUKA-LWR manipulator can be programmed using KUKA Robot Language (KRL). While this language is easy to use, it does not allow the user to control the input motor command torques. KUKA-LWR allows the user to control the robot and select command torques using its Fast Research Interface module (FRI). This module connects an external computer to KUKA-LWR using a C++ library provided by the manufacturer. This interface allows the user to switch between different operation modes, e.g. Position Control or Impedance Control Mode. In the Impedance Control Mode, the user is able to select damping and stiffness coefficients. For further information, readers are encouraged to refer to the KUKA-LWR manual.

Controlling the robot via Position Control Mode is straightforward. The FRI module is capable of commanding custom trajectories to the manipulator. In this mode, there is no information available on the controlled motor torque. But given that KUKA-LWR is equipped with torque sensors, the measurements from these sensors suffice to model the physical parameters of the robot links, such as mass, centre of gravity, and link inertia matrix. The effects of motor inertia and the model of motor-side friction can not be investigated using the Position Control Mode. To that extent, Impedance Control Mode must be employed. In Impedance Control Mode, the user is able to command the desired torques. However, it must be noted that KUKA-LWR utilizes a state-of-the-art internal feedback loop using its joint torque sensor measurements to lower the effective motor inertia and the motor-side friction  $\tau_{fr}$ . This internal feedback loop alters the command torque. The details of this feedback loop, proposed in [10], are repeated here,

$$\tau_m = BB_\theta^{-1}u + (I - BB_\theta^{-1})\tau_J + (D - BB_\theta^{-1}D_s)K^{-1}\dot{\tau}_J \quad (2.2)$$

$B_\theta$  and  $D_s$  are selected by the KUKA-LWR controller, and  $u$  is the command torque. Readers are encouraged to refer to [10] for further information.

Considering (2.2), the transferred torque to the links  $\tau_L$  is,

$$\tau_L = u - B_\theta\ddot{\theta} - B_\theta B^{-1}\tau_{fr} + (D - D_s)K^{-1}\dot{\tau}_J \quad (2.3)$$

Moreover, when torque sensors reading errors in the internal feedback loop (2.2) are considered, the transferred torque to the links  $\tau_L$  is represented by,

$$\begin{aligned} \tau_L = & u - B_\theta\ddot{\theta} - B_\theta B^{-1}\tau_{fr} + (D - D_s)K^{-1}\dot{\tau}_J \\ & + (BB_\theta^{-1} - I)(\tilde{\tau}_J + DK^{-1}\dot{\tilde{\tau}}_J) \end{aligned} \quad (2.4)$$

Torque sensors readings might have a constant bias error due to their physical properties, or inaccurate calibration. Therefore  $\tau_L$  is estimated by,

$$\begin{aligned} \tau_L \approx & u - B_\theta\ddot{\theta} - BB_\theta^{-1}\tau_{fr} + (D - D_s)K^{-1}\dot{\tau}_J \\ & + (BB_\theta^{-1} - I)\tilde{\tau}_J \end{aligned} \quad (2.5)$$

By selecting zero damping and zero stiffness in the Impedance Control Mode, FRI makes it possible to control the command torque  $u$ . In order to control the robot position in the Impedance Control Mode, a PID controller with the values given in TABLE 2.1 is used. Position control of this manipulator in Impedance Control Mode allows identification of the friction model of KUKA-LWR. Next section studies the identification of KUKA-LWR by employing the controller details presented in this section.

Table 2.1: PID gains for position control of KUKA-LWR via the FRI module

Joint	P	I	D
1	8.25	0.52	4.12
2	70	4.37	35
3	7.75	4.84	3.1
4	25	1.56	12.5
5	2.5	1.56	1.0
6	1.61	2.0	0.8
7	1.57	2.0	0.79

## 2.4 Model Identification

This section covers the modeling of KUKA-LWR. It includes the experiments related to the friction model and the robot dynamic model. Effective identification of the dynamic model of a manipulator requires access to its friction model. To this end, first the experiments regarding the friction model of KUKA-LWR are discussed.

Information about transmission and mechanical design of KUKA-LWR is given in [11]. KUKA-LWR uses lightweight harmonic drives that account for the friction terms discussed in the next section.

### 2.4.1 Motor-Side Friction Identification

To measure friction in KUKA-LWR, experiments were designed to estimate  $\tau_{fr}$  and  $\tau_{frL}$  in (2.1a) and (2.1b). First we use the torque sensors installed in KUKA-LWR to measure  $\tau_{fr}$  separately from  $\tau_{frL}$ . To this effect, using (2.1c) and (2.4), the following is obtained,

$$\begin{aligned}
B_\theta B^{-1} \tau_{fr} = & u - \hat{\tau}_J - B_\theta \ddot{\theta} - D_s K^{-1} \dot{\hat{\tau}}_J \\
& + B_\theta B^{-1} (\tilde{\tau}_J + DK^{-1} \dot{\tilde{\tau}}_J)
\end{aligned} \tag{2.6}$$

Due to the internal feedback loop (2.2), only  $BB_\theta^{-1} \tau_{fr}$  affects the robot dynamics. Hence, only the identification of  $BB_\theta^{-1} \tau_{fr}$  is necessary for motor-side friction modeling of KUKA-LWR.

Friction modeling is a very well-studied subject in engineering and robotics [12], [13], [14]. Our work in this paper employs the methods proposed in [13] and [15] to find the friction



model of  $BB_\theta^{-1}\tau_{fr}$ . The LuGre model identification procedure from [13] is used to determine the model of  $\tau_{fr}$ . However, the results from constant velocity and sinusoidal-velocity experiments will show that a Coulomb model is sufficient. The following describes these experiments in detail.

To obtain the friction model of  $BB_\theta^{-1}\tau_{fr}$ , experiments with constant velocities are conducted on KUKA-LWR. Each robot joint was moved separately at various constant velocities between  $-2\text{rad/sec}$  to  $+2\text{rad/sec}$  with the resolution of  $0.16\text{rad/sec}$ . Equation (2.6) was used to obtain the motor-side friction estimations. The graphs shown in Fig. 2.2 summarize the experimental measurements of  $BB_\theta^{-1}\tau_{fr}$  versus joint velocity for all joint of KUKA-LWR. Also TABLE 2.2 lists the values of  $BB_\theta^{-1}\tau_{fr}$  for positive and negative velocities for each joint, respectively. These values are obtained from Fig. 2.2. In order to further investigate the properties of friction and torque measurement errors and to verify the results of Fig. 2.2, each joint of the robot was commanded to move at very slow velocities ranging from  $-0.11\text{ rad/sec}$  to  $+0.11\text{ rad/sec}$  with a resolution of  $0.01\text{rad/sec}$ . Using this data, the values of  $BB_\theta^{-1}\tau_{fr}$  for small positive and negative velocities for each joint were obtained. These values were consistent with those given in TABLE 2.2.

Furthermore, the friction identification method developed in [13] was implemented on KUKA-LWR to measure  $BB_\theta^{-1}\tau_{fr}$ . Sinusoidal trajectories were applied to the robot to obtain the motor-side friction  $BB_\theta^{-1}\tau_{fr}$  using (2.6). The plot of the results of  $BB_\theta^{-1}\tau_{fr}$  versus the sinusoidal joint velocities were similar to Fig. 2.2. Considering the results of the constant velocity and sinusoidal trajectory experiments, it is evident that the motor side friction  $BB_\theta^{-1}\tau_{fr}$  can be modeled using a Coulomb friction model, i.e.,

$$\hat{\tau}_{fr} = \begin{cases} C_+ & \dot{q}_j > 0 \\ C_- & \dot{q}_j < 0 \end{cases} \quad (2.7)$$

where  $C_+$  and  $C_-$  are positive and negative velocity Coulomb friction constants from TABLE 2.2.

During constant velocity experiments, the effect of  $B_\theta\ddot{\theta} - D_sK^{-1}\dot{\hat{\tau}}_J + BB_\theta^{-1}DK^{-1}\dot{\hat{\tau}}_J$  in (2.6) is negligible due to zero joint accelerations. The constant torque measurement bias  $\tilde{\tau}_J$  has an effect on the friction estimations through  $BB_\theta^{-1}\tilde{\tau}_J$ . However, this effect is very small and is responsible for the minor differences between the absolute values of  $C_+$  and  $C_-$  given in TABLE 2.2.

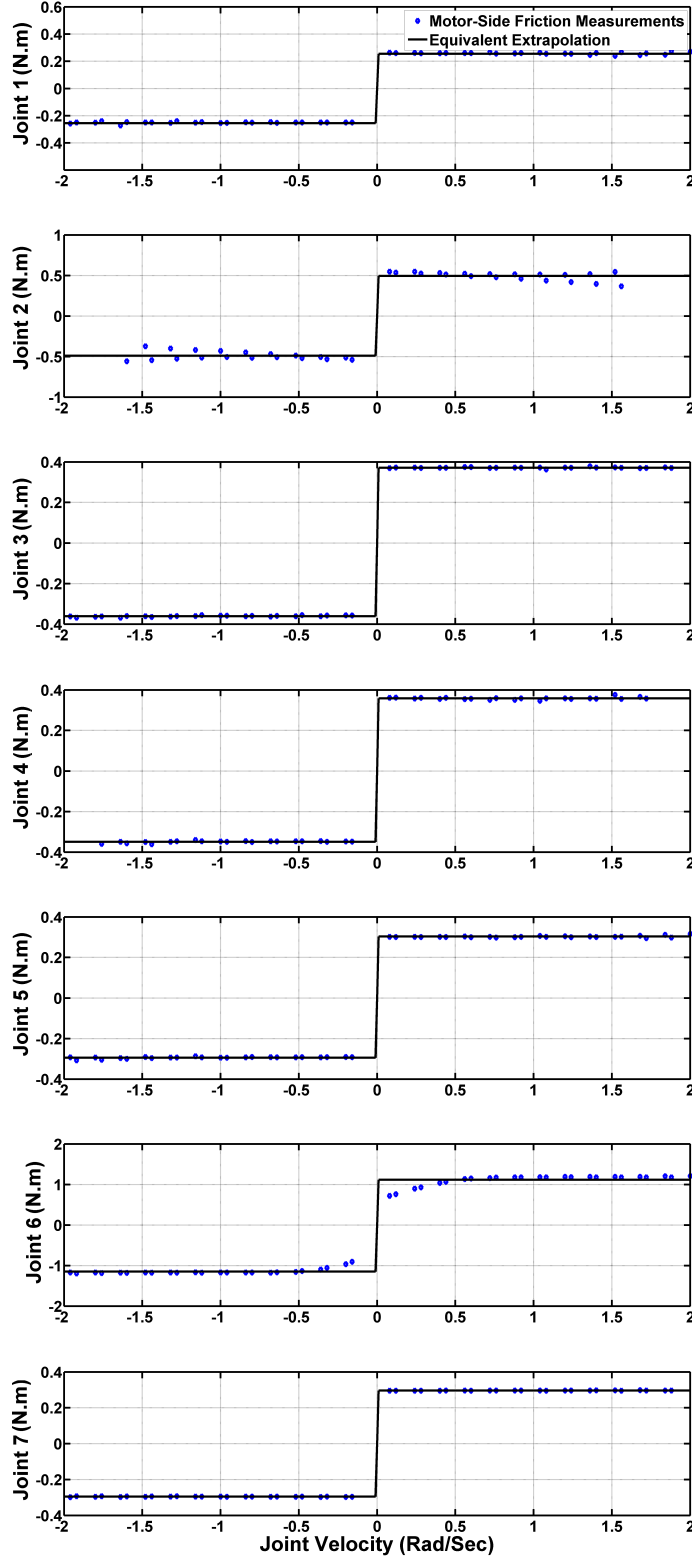
Figure 2.2: Measurement results of the effective motor-side friction  $BB_{\theta}^{-1}\tau_{fr}$

Table 2.2: Coulomb friction constants for effective motor-side friction  $BB_\theta^{-1}\tau_{fr}$  in KUKA-LWR

Joint	$BB_\theta^{-1}\tau_{fr}$ Negative Velocity (N.m) $C_-$	$BB_\theta^{-1}\tau_{fr}$ Positive Velocity (N.m) $C_+$
1	-0.2591	0.2508
2	-0.4939	0.4902
3	-0.3717	0.3609
4	-0.3581	0.3491
5	-0.3034	0.2945
6	-1.1174	1.1474
7	-0.2961	0.2954

### 2.4.2 Link-Side Friction Identification

This section covers the friction modeling of the link-side friction  $\tau_{frL}$  of KUKA-LWR as defined in (2.1a). Based on our experimental results, there's not a significant viscous component in the link-side friction of KUKA-LWR. Therefore, a Coulomb model is assumed for  $\tau_{frL}$ , i.e.,

$$\tau_{frL} = C_L \text{sgn}(\dot{q}) \quad (2.8)$$

where  $C_L$  is the Coulomb friction constant for  $\tau_{frL}$ , and  $\text{sgn}(\cdot)$  is the Signum function. Constant velocity experiments described in section 2.4.1 were used to measure  $C_L$  using (2.1a). Moving one joint at a constant velocity and keeping all the other joints at zero position leads to zero Coriolis and Centrifugal torques on the moving joint. Also, considering that during constant velocity experiments the acceleration is equal to zero,  $\tau_{frL}$  is obtained from (2.1a) by,

$$\tau_{frL} = DK^{-1}\ddot{\tau}_J + \tau_J - g(q) \quad (2.9)$$

The constant torque sensor bias must be considered in the link-side friction modeling. hence,

$$\tau_{frL} \approx DK^{-1}\dot{\hat{\tau}}_J + \hat{\tau}_J - \tilde{\tau}_J - g(q) \quad (2.10)$$

Table 2.3: Coulomb friction constants of the link-side friction  $\tau_{fr_L}$  in KUKA-LWR

Joint	$C_L$
1	0.9661
2	0.4561
3	0.9952
4	0.8136
5	0.2805
6	0.1313
7	0.1865

Table 2.4: Modified Denavit-Hartenberg parameters of KUKA-LWR

Link	$\alpha$ (Deg)	a	$\theta$	d (Meter)
1	0	0	$q_1$	0
2	90	0	$q_2$	0
3	-90	0	$q_3$	0.4
4	-90	0	$q_4$	0
5	90	0	$q_5$	0.39
6	90	0	$q_6$	0
7	-90	0	$q_7$	0

TABLE 2.3 shows the values of Coulomb friction for  $\tau_{fr_L}$  obtained using constant velocity experiments and by employing (2.10).

### 2.4.3 Determining Minimal Inertial Parameters and Dynamic Model

This section discusses the methodology we used for obtaining the minimal inertial parameters and dynamic model of KUKA-LWR.

The modified Denavit-Hartenberg (DH) parameters of KUKA-LWR as measured are given in TABLE 2.4. The DH parameters are necessary to obtain the regressor matrix and the minimal inertial parameters of a manipulator. Minimal inertial parameters were proposed in [5] as the minimal set of physical parameters that would determine the complete model

Table 2.5: Classical inertial parameters of KUKA-LWR

Link	XX	XY	XZ	YY	YZ	ZZ	mX	mY	mZ	m
1	0	0	0	0	0	ZZ <sub>1</sub>	0	0	0	0
2	XX <sub>2</sub>	0	0	YY <sub>2</sub>	YZ <sub>2</sub>	ZZ <sub>2</sub>	0	mY <sub>2</sub>	mZ <sub>2</sub>	m <sub>2</sub>
3	XX <sub>3</sub>	0	0	YY <sub>3</sub>	YZ <sub>3</sub>	ZZ <sub>3</sub>	0	mY <sub>3</sub>	mZ <sub>3</sub>	m <sub>3</sub>
4	XX <sub>4</sub>	0	0	YY <sub>4</sub>	YZ <sub>4</sub>	ZZ <sub>4</sub>	0	mY <sub>4</sub>	mZ <sub>4</sub>	m <sub>4</sub>
5	XX <sub>5</sub>	0	0	YY <sub>5</sub>	YZ <sub>5</sub>	ZZ <sub>5</sub>	0	mY <sub>5</sub>	mZ <sub>5</sub>	m <sub>5</sub>
6	XX <sub>6</sub>	0	0	YY <sub>6</sub>	YZ <sub>6</sub>	ZZ <sub>6</sub>	0	mY <sub>6</sub>	mZ <sub>6</sub>	m <sub>6</sub>
7	XX <sub>7</sub>	0	0	YY <sub>7</sub>	YZ <sub>7</sub>	ZZ <sub>7</sub>	0	mY <sub>7</sub>	mZ <sub>7</sub>	m <sub>7</sub>

of a manipulator, i.e.

$$M(q)\ddot{q} + C(q, \dot{q})\dot{q} + g(q) = Y(q, \dot{q}, \ddot{q})\Theta \quad (2.11)$$

where  $\Theta$  denotes the minimal inertial parameters vector, and  $Y$  denotes the regressor matrix. In order to find  $\Theta$ , the classical inertial parameters of KUKA-LWR must be determined [6]. Due to the symmetry of the robot, a few of the classic inertial parameters are equal to zero. These parameters, as defined in [5], are given in TABLE 2.5. The algorithm proposed in [6] was used to obtain the algebraic formulation of minimal inertial parameters  $\Theta$  from the classical inertial parameters. Based on this algorithm, 25 distinct minimal inertial parameters for KUKA-LWR were obtained. TABLE 2.6 provides the relationship between the minimal inertial parameters and the classical inertial parameters of KUKA-LWR. The regressor matrix  $Y$  of KUKA-LWR is also obtained. To find the regressor matrix  $Y$ , we rewrote the iterative Euler-Lagrange equations of manipulators in terms of the classical inertial parameters. This in turn led to an algorithm for finding the regressor matrix for serial link manipulators using MATLAB<sup>®</sup> Symbolic Toolbox. However, the KUKA-LWR regressor matrix  $Y$  is too large to be written down. The web link give in Appendix A contains a MATLAB<sup>®</sup> Symbolic Toolbox file that includes the  $Y(q, \dot{q}, \ddot{q})$  matrix.

We conduct identification experiments and employ equations (2.11) and (2.1) to identify the minimal inertial parameters of KUKA-LWR. In order to determine regression problem for identification of these parameters, (2.11) and (2.1c) are substituted in (2.1a), to obtain,

$$Y(q, \dot{q}, \ddot{q})\Theta - DK^{-1}\dot{\tau}_J = \tau_J - \tau_{frL} \quad (2.12)$$

A regression problem can be defined by substituting the measured data from the identifi-

Table 2.6: Formulation of minimal inertial parameters of KUKA-LWR using its classical inertial parameters

$\theta_1$ (kg.m)	$mY_2 + mZ_3 + l_3(m_3 + m_4 + m_5 + m_6 + m_7)$
$\theta_2$ (kg.m)	$mY_3 + mZ_4$
$\theta_3$ (kg.m)	$mY_4 - mZ_5 - l_5(m_5 + m_6 + m_7)$
$\theta_4$ (kg.m)	$mY_5 - mZ_6$
$\theta_5$ (kg.m)	$mY_6 + mZ_7$
$\theta_6$ (kg.m)	$mY_7$
$\theta_7$ (kg.m <sup>2</sup> )	$(m_3 + m_4 + m_5 + m_6 + m_7)l_3^2 + 2mZ_3l_3 + XX_2 - YY_2 + YY_3$
$\theta_8$ (kg.m <sup>2</sup> )	$XX_3 - YY_3 + YY_4$
$\theta_9$ (kg.m <sup>2</sup> )	$(m_5 + m_6 + m_7)l_5^2 + 2mZ_5l_5 + XX_4 - YY_4 + YY_5$
$\theta_{10}$ (kg.m <sup>2</sup> )	$XX_5 - YY_5 + YY_6$
$\theta_{11}$ (kg.m <sup>2</sup> )	$XX_6 - YY_6 + YY_7$
$\theta_{12}$ (kg.m <sup>2</sup> )	$XX_7 - YY_7$
$\theta_{13}$ (kg.m <sup>2</sup> )	$YZ_2$
$\theta_{14}$ (kg.m <sup>2</sup> )	$YZ_3$
$\theta_{15}$ (kg.m <sup>2</sup> )	$YZ_4$
$\theta_{16}$ (kg.m <sup>2</sup> )	$YZ_5$
$\theta_{17}$ (kg.m <sup>2</sup> )	$YZ_6$
$\theta_{18}$ (kg.m <sup>2</sup> )	$YZ_7$
$\theta_{19}$ (kg.m <sup>2</sup> )	$YY_2 + ZZ_1$
$\theta_{20}$ (kg.m <sup>2</sup> )	$(m_3 + m_4 + m_5 + m_6 + m_7)l_3^2 + 2mZ_3l_3 + YY_3 + ZZ_2$
$\theta_{21}$ (kg.m <sup>2</sup> )	$YY_4 + ZZ_3$
$\theta_{22}$ (kg.m <sup>2</sup> )	$(m_5 + m_6 + m_7)l_5^2 + 2mZ_5l_5 + YY_5 + ZZ_4$
$\theta_{23}$ (kg.m <sup>2</sup> )	$YY_6 + ZZ_5$
$\theta_{24}$ (kg.m <sup>2</sup> )	$YY_7 + ZZ_6$
$\theta_{25}$ (kg.m <sup>2</sup> )	$ZZ_7$

cation experiments into (2.12). This regression problem is given here,

$$\begin{bmatrix} Y(q_1, \dot{q}_1, \ddot{q}_1) \\ \vdots \\ Y(q_k, \dot{q}_k, \ddot{q}_k) \end{bmatrix} \Theta - \begin{bmatrix} \dot{\tau}_{J_1} \\ \vdots \\ \dot{\tau}_{J_k} \end{bmatrix} DK^{-1} = \begin{bmatrix} \tau_{J_1} - \tau_{fr_{Lk}} \\ \vdots \\ \tau_{J_k} - \tau_{fr_{Lk}} \end{bmatrix} \quad (2.13)$$

where the index  $k$  represents the number of data points. Based on this regression problem, the minimal inertial parameters of KUKA-LWR can be estimated. To this end, we use regression analysis to obtain and discuss the results of the following three methods; The optimal excitation trajectories [7], regression using the inertia matrix and gravity vector as measured by the FRI module, and random trajectories utilizing relative weight analysis [9].

### Using Optimal Trajectories

The accuracy of the identification process depends on the excitation trajectories. To model a serial link manipulator, suitable excitation trajectories must be determined. In this section the application of the optimal excitation trajectories method developed by Swevers et. al., [7] [8], is investigated to model KUKA-LWR. The optimal excitation trajectories in [7] are determined as sums of finite harmonic sine and cosine functions. By selecting such excitation trajectories, the noise in torque and position measurements can be reduced. Also their method significantly enhances approximation of velocity and acceleration based on band-pass filtering of position data. The excitation trajectory employed in our work is chosen to be a sum of twelve harmonic sine and cosine functions with the fundamental frequency of 0.009 Hertz. The optimization problem to find the optimal excitation trajectory from [7] is solved using the Optimization Toolbox in MATLAB®. The obtained optimal trajectories are not presented here for the sake of brevity.

The excitation trajectories are programmed in KUKA-LWR and tracked for 10 repetitions. Multiple repetitions allow averaging the data to minimize the effects of white noise on the identification results. The averaged data points, i.e. joint position measurements, velocity and acceleration approximations and joint torque sensor measurements, were substituted in the regression problem (2.13) to find the minimal inertial parameters of KUKA-LWR.

Our KUKA-LWR identification results obtained via the optimal trajectories method were far from the results obtained via the next two identification methods, i.e. using the mass matrix and the gravity vector, and using relative weight analysis. Also these results were not in accordance with the algebraic formulation of the minimal inertial parameters as given in TABLE 2.6.

Theoretically, the optimal excitation trajectories must obtain the best results for identification. However, in case of KUKA-LWR, the unmodeled dynamics outweighed the modeled dynamics. Given that unmodeled dynamics are not white noise, they can not be efficiently eliminated via the averaging process described in [7] and [8]. The sources of unmodeled dynamics in KUKA-LWR are the hysteresis in joint torque sensors and the friction. Also, the internal feedback loop for minimizing effective motor inertia, as described in (2.2), can possibly introduce additional unmodeled dynamics. Given these considerations, the identification results from the optimal excitation trajectories method are not provided here.

### Using the Inertia Matrix and the Gravity Vector

As we discussed before, the controller of KUKA-LWR computes and allows access to the mass matrix  $M(q)$  and the gravity vector  $g(q)$ . The minimal inertial parameters can be obtained from the mass matrix and the gravity vector. To this end, the relationship between the minimal inertial parameters and the mass matrix and the gravity vector are studied here. Minimal inertial parameters can be linearly separated for each component on the left-hand side of the dynamic model (2.11) by using,

$$g(q) = Y_g(q)\Theta \quad (2.14a)$$

$$M(q)\ddot{q} = Y_M(q, \ddot{q})\Theta \quad (2.14b)$$

Additionally,

$$M_i(q) = Y_{M_i}(q)\Theta \quad 1 \leq i \leq N \quad (2.15)$$

Where  $M_i(q)$  is the  $i$ th column of the inertia matrix  $M(q)$ . The web address given in Appendix A includes  $Y_g(q)$  and all  $Y_{M_i}(q)$  matrices.

Since the computed inertia matrix and the gravity vector do not contain any noise, it is not necessary to use optimal trajectories. Random fifth-order polynomial trajectories were followed by KUKA-LWR and the joint position measurements, velocity and acceleration estimations, along with joint torque sensor measurements were substituted in a regression problem that is derived from (2.14a) and (2.15). The obtained regression problem is solved and the results are given in TABLE 2.7. The t-statistic of the obtained values are also provided. Small t-statistic values indicate that the corresponding minimal inertial parameters were not considered, or equivalently set to be equal to zero, in the KUKA-LWR controller computation of the mass matrix and the gravity vector. The column "Final Estimation"



includes the resultant solution to the regression problem considering the t-statistics. The results of this column should be considered as the minimal inertial parameters that the KUKA-LWR controller uses to calculate the mass matrix and the gravity vector. The column "Contributing Terms" shows the components of the mass matrix or the gravity vector that were used in the regression analysis to identify the corresponding minimal inertial parameter.

The results of this section can be used to check the validity of the relative weight analysis method conducted in the next section. However, it should be noted that the actual values of the minimal inertial parameters of the KUKA-LWR robot modeled in this paper might be different than what is obtained in this section. This is in the light that FRI uses the minimal inertial parameters of a given prototype to compute the mass matrix and the gravity vector. Next section proposes implementing relative weight analysis to identify the minimal inertial parameters of KUKA-LWR.

### **Using Relative Weight Analysis**

This section uses relative weight analysis to augment regression results and obtain accurate minimal inertial parameters in presence of noise in the regression data. Relative weights are a method to determine the importance of each independent variable in multiple regression analysis [16]. Unlike standardized betas, relative weights partition the covariance of the predictors to obtain the importance of predictors in the regression analysis [9], [17]. Random fifth-order polynomial trajectories were tracked by KUKA-LWR to obtain the experimental data. To this end, 30 minutes of data was recorded. The long span the data was recorded in minimizes the effects of unmodeled dynamics in the regression results. The data was partitioned into smaller sections and the regression analysis was conducted on each segment. This was due to the memory limitations arising from the large size of the input data. The meta-analysis of the regression results of each minute of the experiment was conducted. As discussed in [18], by using the covariance matrices of individual regression results, meta-analysis provides the same results as if all the individual data were used in one regression analysis. An interesting aspect of relative weights is that they have this same property. Their meta-analysis results are equal to the outcomes of one relative weight analysis conducted on all the data.

Table 2.7: Minimal Inertial Parameters of KUKA-LWR and the Regression Analysis Data

Based on Regression Analysis Implementing Relative Weights										Based on the Inertia Matrix and the Gravity Vector from FRI				
Iteration 1					Iteration 2									
Regression Result	t-Statistic	Relative Weight	Contributing Joints	Significance	Regression Result	t-Statistic	Relative Weight	Contributing Joints	Final Estimation	Regression Result	t-Statistic	Contributing Terms	Final Estimation	
$\theta_1$	3.4577	47774	21.208 $J_2$	1	3.4623	41669	33.731 $J_2$	$J_2$	3.4623	3.4968	214600	$Y_g$	3.4968	
$\theta_2$	0.0098	239.79	0.1172 $J_{2,3}$	1	0.0078	269.98	0.142 $J_2$	$J_2$	0.0078	8.905E-5	10.12	$Y_g$	0	
$\theta_3$	-1.296	-26167	23.963 $J_{1,2,3,4}$	1	-1.3049	-25987	31.090 $J_{2,3,4}$	$J_{2,3,4}$	-1.304	-1.343	-46603	$Y_{M_{1,2,3,4}}, Y_g$	-1.343	
$\theta_4$	0.0469	1605.6	0.0186 $J_{1,2,3,4,5}$	1	0.0406	2321	41.3 $J_5$	$J_5$	0.0406	0.02398	84449	$Y_{M_5}$	0.02398	
$\theta_5$	0.0292	1099.2	1.4416 $J_{1,2,3,4,5,6}$	1	0.0308	1127	1.7964 $J_{2,3,4,5}$	$J_{2,3,4,5}$	0.0308	0.02628	4583.5	$Y_{M_{1,2,3,4,5,6}}, Y_g$	0.02628	
$\theta_6$	-0.0009	-36.646	0.1163 $J_{1,2,3,4,5,6,7}$	0	0	0	0	0	0	8.465E-5	19.996	$Y_{M_{1,2,3,4,5,6,7}}, Y_g$	$Y_g$	0
$\theta_7$	0.6465	92.644	2.9217 $J_{1,2}$	1	0.8633	199.45	1.7017 $J_{1,2}$	$J_{1,2}$	0.8633	1.2634	36448	$Y_{M_1}$	1.2634	
$\theta_8$	0.5357	77.246	1.6650 $J_{1,2,3}$	1	-0.6089	-139.22	0.2934 $J_{1,2,3}$	$J_{1,2,3}$	0	6.196E-3	200.01	$Y_{M_2}$	0	
$\theta_9$	0.9983	353.05	0.9901 $J_{1,2,3,4}$	1	0.43644	268.602	0.4554 $J_{1,2,3,4}$	$J_{1,2,3,4}$	0.43644	0.42847	19616	$Y_{M_{1,2,3}}$	0.42847	
$\theta_{10}$	0.0400	20.988	0.5136 $J_{1,2,3,4,5}$	0	0	0	0	0	0	3.991E-3	246.12	$Y_{M_{1,2,3,4}}$	0	
$\theta_{11}$	0.0938	116.94	1.0977 $J_6$	1	0.0517	68.518	1.511 $J_6$	$J_6$	0.0517	1.771E-3	145.27	$Y_{M_{2,4,5}}$	0	
$\theta_{12}$	-0.0283	-36.508	0.0101 $J_{1,2,3,4,5,6,7}$	0	0	0	0	0	0	3.9037E-6	42.671	$Y_{M_6}$	0	
$\theta_{13}$	-0.3549	-152.29	0.1614 $J_2$	1	-0.0806	-64.889	0.0195 $J_{1,2}$	$J_{1,2}$	0	-5.728E-4	-90.198	$Y_{M_{1,2}}$	0	
$\theta_{14}$	0.22157	120.72	0.0184 $J_{1,2,3}$	0	0	0	0	0	0	5.426E-4	74.199	$Y_{M_{1,2,3}}$	0	
$\theta_{15}$	0.01156	6.4731	0.0142 $J_{1,2,3,4}$	0	0	0	0	0	0	5.28E-4	118.95	$Y_{M_{1,3,4}}$	0	
$\theta_{16}$	-0.0272	-38.711	0.0138 $J_{1,2,3,4,5}$	0	0	0	0	0	0	4.241E-4	2477.6	$Y_{M_5}$	4.241E-4	
$\theta_{17}$	-0.0624	-115.79	0.0023 $J_{1,2,3,4,5,6}$	0	0	0	0	0	0	8.36E-6	104.15	$Y_{M_5}$	0	
$\theta_{18}$	-0.0079	-21.211	0.0015 $J_{1,2,3,4,5,6,7}$	0	0	0	0	0	0	-4.52E-6	-1.3651	$Y_{M_{2,4,5}}$	0	
$\theta_{19}$	-0.5739	-128.57	0.1588 $J_1$	0	0	0	0	0	0	0.0116	1258	$Y_{M_1}$	0.0116	
$\theta_{20}$	2.52087	235.99	5.8331 $J_2$	1	0.9200	391.63	0.2548 $J_2$	$J_2$	0.9200	1.2686	62400	$Y_{M_2}$	1.2686	
$\theta_{21}$	-0.1519	-127.53	0.0818 $J_3$	0	0	0	0	0	0	0.0108	1749.2	$Y_{M_{1,3}}$	0.0108	
$\theta_{22}$	1.01103	286.95	1.0283 $J_{1,2,3,4}$	1	0.2805	281.65	0.1245 $J_{1,2,3}$	$J_{1,2,3}$	0.2805	0.4328	22806	$Y_{M_{1,2,4}}$	0.4328	
$\theta_{23}$	0.6068	105.01	1.6295 $J_5$	1	-0.02852	-35.0780	0.2621 $J_{1,2,3,4}$	$J_{1,2,3,4}$	0	6.33E-3	51977	$Y_{M_5}$	6.33E-3	
$\theta_{24}$	0.0663	64.026	0.0750 $J_{1,2,3,4,5,6}$	0	0	0	0	0	0	4.421E-3	62476	$Y_{M_6}$	4.421E-3	
$\theta_{25}$	0.0789	121.418	0.4844 $J_6$	0	0	0	0	0	0	1.201E-4	419320	$Y_{M_7}$	1.201E-4	

The results of the regression meta-analysis are given in TABLE 2.7 in the column "Iteration 1". The "Regression Results" column shows the estimated minimal inertial parameters. The associated t-statistics and relative weights are also given. The "Contributing Joints" shows the joints that were involved in obtaining the regression data given in the table. Parameters with combined small t-statistics (less than 145) and relative weights (less than 0.5) are assumed to have a significance of zero and are marked out in the "Significance" column. The threshold for t-statistics depends on the amount of data available and must be determined on a case-by-case basis. The threshold for relative weights can be arbitrarily chosen to be small. However very small thresholds for relative weights tend to impair the efficacy of the relative weight-based method. A second regression analysis is conducted with only the remaining minimal inertial parameters. The results of this analysis is given in the column "Iteration 2". Once again, the minimal inertial parameters with combined small t-statistics and relative weights are marked out and shown with a "Final Estimation" of zero. The remaining parameters are calculated and given in the column "Final Estimation". This column shows the results of implementing relative weight analysis for obtaining minimal inertial parameters of KUKA-LWR. By comparing the Final estimation column of relative weight analysis with the results obtained from the mass matrix and gravity vector, the efficacy of the proposed methodology is verified.

## 2.5 CONCLUSION

This paper investigated the model of KUKA-Light Weight Robot IV+. The controller of KUKA-LWR is studied and its effect on the modeling procedure is discussed. Experiments and the results of friction modeling are presented in detail. The formulation of the regressor matrix and the minimal inertial parameters of KUKA-LWR are given. To identify the values of the minimal inertial parameters in presence of unmodeled dynamics, a novel regression-based method using relative weight analysis was developed. The relative weight analysis method allowed a systematic elimination of the parameters that do not have a significant effect on the dynamics of the robot. The values of the parameters identified using the proposed method are presented and verified.

## Bibliography

- [1] B. Armstrong, O. Khatib, and J. Burdick, “The explicit dynamic model and inertial parameters of the puma 560 arm,” in *Robotics and Automation. Proceedings. 1986 IEEE International Conference on*, vol. 3, 1986, pp. 510–518.
- [2] P. Corke and B. Armstrong-Helouvry, “A search for consensus among model parameters reported for the puma 560 robot,” in *Robotics and Automation, 1994. Proceedings., 1994 IEEE International Conference on*, 1994, pp. 1608–1613 vol.2.
- [3] C. Kennedy and J. Desai, “Modeling and control of the mitsubishi pa-10 robot arm harmonic drive system,” *Mechatronics, IEEE/ASME Transactions on*, vol. 10, no. 3, pp. 263–274, 2005.
- [4] N. Bompos, P. Artemiadis, A. Oikonomopoulos, and K. Kyriakopoulos, “Modeling, full identification and control of the mitsubishi pa-10 robot arm,” in *Advanced intelligent mechatronics, 2007 IEEE/ASME international conference on*, 2007, pp. 1–6.
- [5] M. Gautier and W. Khalil, “A direct determination of minimum inertial parameters of robots,” in *Robotics and Automation, 1988. Proceedings., 1988 IEEE International Conference on*, 1988, pp. 1682–1687 vol.3.
- [6] —, “Direct calculation of minimum set of inertial parameters of serial robots,” *Robotics and Automation, IEEE Transactions on*, vol. 6, no. 3, pp. 368–373, 1990.
- [7] J. Swevers, C. Ganseman, D. Tukel, J. De Schutter, and H. Van Brussel, “Optimal robot excitation and identification,” *Robotics and Automation, IEEE Transactions on*, vol. 13, no. 5, pp. 730–740, 1997.
- [8] J. Swevers, W. Verdonck, and J. De Schutter, “Dynamic model identification for industrial robots,” *Control Systems, IEEE*, vol. 27, no. 5, pp. 58–71, 2007.
- [9] S. Tonidandel and J. LeBreton, “Relative importance analysis: A useful supplement to regression analysis,” *Journal of Business and Psychology*, vol. 26, no. 1, pp. 1–9, 2011.
- [10] A. D. Luca, A. Albu-Schaffer, S. Haddadin, and G. Hirzinger, “Collision detection and safe reaction with the dlr-iii lightweight manipulator arm,” in *Intelligent Robots and Systems, 2006 IEEE/RSJ International Conference on*, oct. 2006, pp. 1623–1630.

- [11] A. Albu-Schaffer, S. Haddadin, C. Ott, A. Stemmer, T. Wimbock, and G. Hirzinger, "The dlr lightweight robot: design and control concepts for robots in human environments," *Industrial Robot: An International Journal*, vol. 34, no. 5, pp. 376–385, 2007.
- [12] C. Canudas de Wit, H. Olsson, K. Astrom, and P. Lischinsky, "A new model for control of systems with friction," *Automatic Control, IEEE Transactions on*, vol. 40, no. 3, pp. 419–425, mar 1995.
- [13] M. Kermani, R. Patel, and M. Moallem, "Friction identification and compensation in robotic manipulators," *Instrumentation and Measurement, IEEE Trans. on*, vol. 56, no. 6, pp. 2346–2353, dec. 2007.
- [14] J. Swevers, F. Al-Bender, C. Ganseman, and T. Projogo, "An integrated friction model structure with improved presliding behavior for accurate friction compensation," *Automatic Control, IEEE Transactions on*, vol. 45, no. 4, pp. 675–686, apr 2000.
- [15] H. Olsson, K. Astrom, C. C. de Wit, M. Gafvert, and P. Lischinsky, "Friction models and friction compensation," *European Journal of Control*, vol. 4, no. 3, pp. 176–195, 1998.
- [16] J. W. Johnson, "A heuristic method for estimating the relative weight of predictor variables in multiple regression," *Multivariate Behavioral Research*, vol. 35, no. 1, pp. 1–19, 2000.
- [17] J. M. J. W. Tonidandel, Scott; LeBreton, "Determining the statistical significance of relative weights," *Psychological Methods*, vol. 14, no. 4, pp. 387–399, 2009.
- [18] B. J. Becker and M.-J. Wu, "The synthesis of regression slopes in Meta-Analysis," *Statistical Science*, vol. 22, no. 3, pp. 414–429, 2007.

## **Chapter 3**

# **On Determining Collision Detection Thresholds and Trajectory Planning for Manipulators with Regards to External Torque Estimation Precision**

### **3.1 Introduction**

Robotic manipulators are increasingly employed in unstructured environments [1]. The quality of the physical interaction between a robot and its environment depends on how accurately the robot is able to estimate the interaction forces. In the area of human robot interaction, detection of contact forces between a human user and the manipulator is of particular importance with regards to the safety of the human user [2]. Successful integration of manipulators in unstructured environments relies on the precision the external forces are measured by the manipulator.

External forces can be obtained from tactile sensors and force/torque observers [3]. Tactile sensors are not commonly available in all manipulators and their cost and size is not always desirable. Force/torque observers only require the dynamic model of the robot. However, precise estimation of external forces using an observer requires precise modeling of the manipulator as well as accurate measurement of position, velocity and in some cases acceleration of manipulator joints. Predicated upon modeling-based external torque estimation using observers, this paper studies the effects of imprecise modeling of manipulators in

estimation of external torques.

Different external torque observers have been proposed for serial link manipulators [4], [5], [6]. The nonlinear fuzzy-based observer in [4] did not exploit the robot dynamics for the development of more precise residuals. In [5], the nonlinear torque observer was designed for two link manipulators. Their method can not be easily extended for manipulators with more joints. High gain observers [7] were used to define external torque observers for manipulators in [6]. We will use available estimations of joint accelerations and the manipulator model to estimate the external torques. It will be shown that the observer [6] can be described using the same format as the acceleration-based estimation method. This formulation has advantages in obtaining the optimal criteria for trajectory planning with regards to external torque estimations.

In this paper, optimal trajectories with regards to the precision of external torque estimations are determined. We will describe a particular formulation for serial link manipulator models using minimal inertial parameters [8]. This formulation separates the effects of position, velocity, acceleration and minimal inertial parameters in estimation of external torques. Using this separation technique, the external torque estimation errors are defined. We propose an optimization problem with regards to minimizing the external torque estimation errors. We express this optimization such that it can be solved using Euler-Lagrange equations. Furthermore, we propose a metric to compare trajectories in terms of their accuracy for external torque estimation. This metric is based on the objective function of the proposed optimization problem. Also, the problem of reliable collision detection is addressed by defining model-based thresholds. The novelty of the proposed thresholds is that all the imprecisions in the model of the manipulator and sensor measurements are considered. These imprecisions pertain to joint velocity and acceleration signals, and minimal inertial parameters. The effects of friction and controller on the proposed thresholds will also be discussed. Experiment are conducted to compare different trajectories with regards to the precision of the external torque estimations using the proposed metrics. The experimental results will further validate the proposed metrics and collision detection thresholds with regards to trajectory planning.

The structure of this paper is as follows. Section 3.2 describes manipulator modeling and external torque observers. In section 3.3, a particular formulation of manipulator modeling based on minimal inertial parameters is provided. External torque estimation errors based on this formulation are presented. In section 3.4, the optimization problem for determining the optimal trajectories with regards to external torque estimation precision is formulated.

Also, metrics for comparing different trajectories with regards to external torque estimation are presented. Section 3.5 presents model-based collision detection thresholds. Section 3.6 describes experiments comparing different trajectories with regards to external torque estimation. Also, collision detection outcomes of the proposed model-based thresholds for different trajectories are compared. Section 3.8 concludes the paper and discusses future work.

## 3.2 Manipulator Model and Collision Detection Residual

In this section, the modeling of serial link manipulators is covered. Also, an examination of external torque observers is provided.

Dynamic equation of a serial link manipulator is given by,

$$\mathbf{M}(q)\ddot{q} + \mathbf{B}(q)[\dot{q}\dot{q}] + \mathbf{C}(q)[\dot{q}]^2 + g(q) = \tau_L + \tau_d + \tau_c - \tau_{fr} \quad (3.1)$$

where  $q$  denotes the joint space position of the manipulator,  $\mathbf{M}(q)$  is the link inertia matrix,  $\mathbf{B}(q)$  is the matrix of Coriolis coefficients,  $\mathbf{C}(q)$  is the matrix of centrifugal coefficients, and  $g(q)$  is the gravitational vector. Also, in this equation  $[\dot{q}\dot{q}]$  is the Coriolis vector of joint velocity products defined as,

$$[\dot{q}\dot{q}] = [\dot{q}_1\dot{q}_2, \dot{q}_1\dot{q}_3, \dots, \dot{q}_{n-1}\dot{q}_n]^T \quad (3.2)$$

and  $[\dot{q}]^2$  is the vector of centrifugal squared velocity given by,

$$[\dot{q}]^2 = [\dot{q}_1^2, \dot{q}_2^2, \dots, \dot{q}_n^2]^T \quad (3.3)$$

Also, in equation (3.1),  $\tau_{fr}$  is the friction torque of the manipulator,  $\tau_d$  represents disturbance torque,  $\tau_c$  represents external torques acting on the manipulator, and  $\tau_L$  is the torque transferred to each link by the actuation mechanism.

Measurement of external torques  $\tau_c$  is made possible using external torque observers. Depending on the external torque observer definition, the observer results in different filtered forms of the external torque signal. In order to have a look at the filtered form, the observer discussed in [6] is examined here. This observer, commonly used for collision detection purposes, avoids obtaining joint accelerations by using the generalized momentum of the robot, i.e.,

$$p(t) = \mathbf{M}(q)\dot{q} \quad (3.4)$$



and is equal to the following residual for the external torques  $\tau_c$ ,

$$r(t) = K_I \left[ p(t) - \int_0^t (\tau_L + \mathbf{C}^T(q, \dot{q})\dot{q} - g(q) - \tau_{fr} + r) du - p(0) \right] \quad (3.5)$$

where  $K_I$  is the observer gain. In (3.5). The solution to  $r(t)$  represents the first-order filtered value of  $\tau_c$  [6], i.e.,

$$r(t) = \frac{K_I}{s + K_I} \tau_c \quad (3.6)$$

where  $s$  represents the Laplace transform. By Substituting  $\tau_c$  from (3.1) in (3.6),

$$r(t) = \frac{K_I}{s + K_I} \mathbf{M}(q)\ddot{q} + \frac{K_I}{s + K_I} \left[ \mathbf{B}(q)[\dot{q}\dot{q}] + \mathbf{C}(q)[\dot{q}]^2 + g(q) - \tau_L + \tau_{fr} \right] \quad (3.7)$$

The observer (3.5) assumes manipulator position and velocity are available. Therefore, an alternative to (3.7) is to use an observer that only filters the term that is acceleration dependent. Based on filtering the acceleration term, the following formulation of external torque residuals is given.

$$\hat{\tau}_c(t) = \mathbf{M}(q)\mathcal{F}(\ddot{q}) + \mathbf{B}(q)[\dot{q}\dot{q}] + \mathbf{C}(q)[\dot{q}]^2 + g(q) - \tau_L + \tau_{fr} \quad (3.8)$$

$\mathcal{F}(\ddot{q}) = \hat{\hat{q}}$  denotes the filter that estimates joint acceleration.  $\hat{\hat{q}}$  is the estimated joint acceleration.  $\mathcal{F}$  can be the first-order low pass filter defined in (3.6) or any other appropriate filter. The filter should be designed based on a case-by-case basis for each manipulator.  $\mathcal{F}$  would also depend on the availability of tachometers and accelerometers in each joint. Furthermore, the velocity might also need to be estimated using filters depending on the accuracy of the tachometers or estimation techniques.

The formulation (3.8) is pertinent to the analysis of external torque estimation precision provided in this paper. It is the simplest form of the external torque observers and can be directly obtained from (3.1). It will be used in the following sections for examining external torque measurements.

### 3.3 Effects of Imprecise Modeling and Measurement on Estimating External Torques

This section will first discuss the concept of minimal inertial parameters [8]. A particular formulation with regards to minimal inertial parameters will be introduced. This formulation will be used to investigate the effects of imprecise modeling and sensor measurements in external torque estimation. This investigation will form the basis for determining trajectories best suited for external torque estimation. It will also help determining collision detection thresholds that consider all modeling inaccuracies simultaneously.

#### 3.3.1 Dynamic Model Using Minimal inertial Parameters

Before studying the effects of imprecise modeling and measurement, it is necessary to write down manipulator dynamic equations using minimal inertial parameters.

Minimal inertial parameters of a manipulator were proposed in [8]. They are defined as the minimal set of physical parameters that would determine the model of a manipulator, i.e.

$$\mathbf{M}(q)\ddot{q} + \mathbf{B}(q)[\dot{q}\dot{q}] + \mathbf{C}(q)[\dot{q}]^2 + g(q) = \mathbf{Y}(q, \dot{q}, \ddot{q})\Theta \quad (3.9)$$

where  $\Theta$  is the Minimal inertial parameters, and  $\mathbf{Y}$  is the regressor matrix.

Furthermore, each term of (3.9) can be expressed in terms of minimal inertial parameters, i.e.,

$$M_i(q) = \mathbf{Y}_{M_i}^q(q)\Theta \quad 1 \leq i \leq n \quad (3.10a)$$

$$B_i(q) = \mathbf{Y}_{B_i}^q(q)\Theta \quad 1 \leq i \leq n(n-1)/2 \quad (3.10b)$$

$$C_i(q) = \mathbf{Y}_{C_i}^q(q)\Theta \quad 1 \leq i \leq n \quad (3.10c)$$

$$g(q) = \mathbf{Y}_g^q(q)\Theta \quad (3.10d)$$

Where the vectors  $M_i(q)$ ,  $B_i(q)$ , and  $C_i(q)$  are the  $i$ th column of the inertia matrix  $\mathbf{M}(q)$ , Coriolis matrix  $\mathbf{B}(q)$  and centrifugal matrix  $\mathbf{C}(q)$ , respectively. Also  $\mathbf{Y}^q$  denotes the dynamic matrix corresponding to each column of the inertia matrices  $\mathbf{M}(q)$ , Coriolis matrix  $\mathbf{B}(q)$ , centrifugal matrix  $\mathbf{C}(q)$ , and gravity vector  $g(q)$ .

In order to adopt a terminology that is simpler than (3.10), we define the following vector.

$$\mathbf{Q} = \begin{bmatrix} \ddot{q} \\ [\dot{q}\dot{q}] \\ [\dot{q}^2] \\ 1 \end{bmatrix} \quad (3.11)$$

where  $\mathbf{Q}$  is a  $l = \frac{n^2+3n+2}{2}$  dimensional vector. Using  $\mathbf{Q}$ , (3.9) can be written as,

$$\mathbf{Y}(q, \dot{q}, \ddot{q})\Theta = \sum_{k=1}^l \mathbf{Y}_k^q(q) \mathbf{Q}_k \Theta \quad (3.12)$$

where  $\mathbf{Y}_k^q(q)$  includes all  $\mathbf{Y}_{M_i}^q(q)$ ,  $\mathbf{Y}_{B_i}^q(q)$ ,  $\mathbf{Y}_{C_i}^q(q)$ ,  $\mathbf{Y}_g^q(q)$ . Also,  $\mathbf{Q}_k$  is the  $k$ th component of the vector  $\mathbf{Q}$ . In the next section, the formulation (3.12) will be applied for studying the effects of imprecise modeling in external torque estimation.

### 3.3.2 External Torque Estimation Errors

The external torque estimation error is defined as,

$$\tilde{\tau}_c(t) = \hat{\tau}_c(t) - \tau_c(t) \quad (3.13)$$

where  $\hat{\tau}_c$  is the estimated external torques and  $\tau_c$  is the actual external torques.

In order to obtain the external torque estimation errors, the ideal external torque residual must be considered. Based on (3.1), this ideal residual is equal to,

$$\begin{aligned} \tau_c(t) = & \mathbf{M}(q)\ddot{q} + \mathbf{B}(q)[\dot{q}\dot{q}] + \mathbf{C}(q)[\dot{q}]^2 \\ & + g(q) - \tau_L - \tau_d + \tau_{fr} \end{aligned} \quad (3.14)$$

By introducing (3.9) and (3.12) in the ideal residual (3.14), the following formulation of the ideal residual is obtained,

$$\tau_c(t) = \sum_{k=1}^l \mathbf{Y}_k^q(q) \mathbf{Q}_k \Theta - \tau_L - \tau_d + \tau_{fr} \quad (3.15)$$

Only an estimation of the parameters used in (3.15) are assumed to be available due to the disturbance torque  $\tau_d$ , and the errors in dynamic modeling, joint flexibility, friction modeling, and sensor measurements. Therefore, the external torque estimation corresponding to

the available parameters is written as,

$$\hat{\tau}_c(t) = \sum_{k=1}^l \mathbf{Y}_k^q(q) \hat{\mathbf{Q}}_k \hat{\Theta} - \hat{\tau}_L + \hat{\tau}_{fr} \quad (3.16)$$

where  $\hat{\mathbf{Q}}$ ,  $\hat{\Theta}$ ,  $\hat{\tau}_L$ ,  $\hat{\tau}_{fr}$  are the available estimations of  $\mathbf{Q}$ ,  $\Theta$ ,  $\tau_L$ ,  $\tau_{fr}$ . The joint position  $q$  can be measured with negligible measurement error. The value of  $Y(q)$  only depends on the Denavit-Hartenberg parameters of the manipulator which can always be measured very accurately. Therefore the benefit of using the particular formulation in (3.16) is the ability to linearly separate the effects of accurately measured joint position from estimated joint velocity, joint acceleration and minimal inertial parameters.

Next step for obtaining the external torque estimation error  $\tilde{\tau}_c$  is substituting (3.15) and (3.16) in (3.13), i.e.,

$$\begin{aligned} \tilde{\tau}_c(t) = & \sum_{k=1}^l \mathbf{Y}_k^q(q) [\hat{\mathbf{Q}}_k \hat{\Theta} - \mathbf{Q}_k \Theta] \\ & - \tilde{\tau}_L + \tau_d + \tilde{\tau}_{fr} \end{aligned} \quad (3.17)$$

The external torque estimation error  $\tilde{\tau}_c(t)$  can be described by using  $\tilde{\mathbf{Q}} = \hat{\mathbf{Q}} - \mathbf{Q}$  defined as,

$$\tilde{\mathbf{Q}} = \begin{bmatrix} \hat{\ddot{q}} - \ddot{q} \\ [\hat{\dot{q}}\hat{\dot{q}}] - [\dot{q}\dot{q}] \\ [\hat{q}^2] - [q^2] \\ 0 \end{bmatrix} \quad (3.18)$$

By substituting  $\tilde{\mathbf{Q}}$ , and  $\tilde{\Theta} = \hat{\Theta} - \Theta$  in (3.17), the external torque estimation error is written as,

$$\begin{aligned} \tilde{\tau}_c(t) = & \sum_{k=1}^l \mathbf{Y}_k^q(q) [\tilde{\mathbf{Q}}_k \hat{\Theta} + \mathbf{Q}_k \tilde{\Theta}] \\ & - \tilde{\tau}_L + \tau_d + \tilde{\tau}_{fr} \end{aligned} \quad (3.19)$$

The above formulation will be used for obtaining collision detection thresholds. Also, (3.19) will be used in the next section for determining the optimal trajectories with regards to external torque estimation precision.

### 3.4 Optimal Trajectories with Regards to Estimating External Torques

In this section we will introduce a novel optimal criteria with regards to trajectory planning for the purpose of accurate external torque estimation and collision detection. To the knowledge of the author, such criteria has not been defined previously in the literature. This criteria will be used as a metric for comparing trajectories with regards to external torque estimation. Also, the proposed criteria will be shown to help in finding collision detection thresholds in the next section.

The optimal trajectory problem formulation is as follows. In order to obtain the best estimation of external torques, the estimation error  $\tilde{\tau}_c(t)$  in (3.19) must be as small as possible. Minimization of the estimation error in (3.19) is feasible by minimizing an upper bound for absolute value of the torque estimation error at every joint. By introducing (3.12) in (3.19), an upper bound for the absolute value of  $\tilde{\tau}_{c_j}(t)$  is obtained as,

$$\begin{aligned} |\tilde{\tau}_{c_j}(t)| \leq & \left| \sum_{k=1}^l \mathbf{Y}_{k_j}^q(q) \tilde{Q}_k \hat{\Theta} + \mathbf{Y}_j(q, \dot{q}, \ddot{q}) \tilde{\Theta} \right. \\ & \left. - \tilde{\tau}_{L_j} + \tilde{\tau}_{fr_j} \right| + |\tau_{d_j}| \end{aligned} \quad (3.20)$$

where  $j$  denotes the  $j$ th row of the corresponding vector or matrix. Therefore, obtaining the most accurate external torque estimation is equivalent to solving the following multi-objective optimization problem,

$$\begin{aligned} \min_q |\tilde{\tau}_{c_j}(t)| \equiv \min_{q, \tilde{Q}} & \left\{ \left| \sum_{k=1}^l \mathbf{Y}_{k_j}^q(q) \tilde{Q}_k \hat{\Theta} + \mathbf{Y}_j(q, \dot{q}, \ddot{q}) \tilde{\Theta} \right. \right. \\ & \left. \left. - \tilde{\tau}_{L_j} + \tilde{\tau}_{fr_j} \right| \right\} \end{aligned} \quad (3.21)$$

Equation (3.21) is a functional optimization problem and its solution provides the trajectories that would result in the least external torque estimation error.

The optimization problem (3.21) is further studied by only using the first two terms of the objective function. If the model of the transmitted joint torque error  $\tilde{\tau}_L$  and friction modeling error  $\tilde{\tau}_{fr}$  are available, they should be considered in the optimization problem as well. When there's no information available on  $\tilde{\tau}_L$  and  $\tilde{\tau}_{fr}$ , the optimization problem (3.21) is simplified to the sum of two objectives:

- **Objective A:** Depends on the accuracy of velocity and acceleration estimations
- **Objective B:** Depends on the accuracy of minimal inertial parameter estimations and trajectory planning

$$\min_q |\tilde{\tau}_{c_j}(t)| \equiv \min_{q, \tilde{Q}} \left\{ \overbrace{\sum_{k=1}^l \mathbf{Y}_{k_j}^q(q) \tilde{Q}_k \hat{\Theta}}^{\text{Objective A}} + \underbrace{\mathbf{Y}_j(q, \dot{q}, \ddot{q}) \tilde{\Theta}}_{\text{Objective B}} \right\} \quad (3.22)$$

The two objective terms are separated as each has its own physical interpretation. Next, we will discuss each of these objective terms.

### 3.4.1 Effects of Controller Design and Trajectory Planning on Accuracy of External Torque Measurement

In the optimization problem (3.22), the objective A depends on the joint positions  $q$  and  $\tilde{Q}$  as defined in (3.18). The vector  $\tilde{Q}$  depends on the accuracy of velocity and acceleration estimations. Multiple factors contribute to the vector  $\tilde{Q}$  which are laid out below. The appropriate measures that must be taken to minimize the effect of each factor on  $\tilde{Q}$  are also discussed.

#### Filter Design for Velocity and Acceleration Estimation - Objective A

Filtering joint position data is a common practice for estimation of velocity and acceleration in robotic manipulators. Precision of velocity and acceleration estimation filters must be evaluated on a case-by-case basis for every manipulator.

Causal filters must be implemented for real-time estimation of external torques. Such filters are associated with a delay and are always a low-pass filter of the actual velocity or the acceleration signal. Therefore, a trajectory with high-frequency velocity or acceleration components impacts the effectiveness of such filters. To ensure accurate external torque measurements, trajectories with only low-frequency components must be planned. The cut-off frequency for these trajectories can be determined by the filters used for velocity and acceleration estimation. However, the actual trajectory that the manipulator follows

might include high-frequency components. These high-frequency components must be mitigated by designing a proper controller.

### **Controller Design - Objective A**

The next step after planning a low-frequency trajectory is ensuring that it is followed without high-frequency components.

High-frequency components in joint acceleration can occur for two reasons. First because of high-frequency components in the transmitted torque  $\tau_L$ . Such components can be avoided by implementing a controller that would only allow low-frequency controller outputs. Second, imperfect compensation of friction can lead up to high-frequency components in the trajectory. Accurate friction compensation is not usually possible for low velocities due to stiction and pre-sliding conditions [9]. Therefore, to ensure that the manipulator follows low-frequency trajectories, it is best to avoid low velocities when possible.

High-frequency components in joint velocity can occur as a result of high-frequency components in joint acceleration. Taking the measures discussed above to lower high-frequency components of joint acceleration will in turn ensure that joint velocity does not contain high-frequency components. However, high joint acceleration values can cause high-frequency components in the joint velocity. Therefore a cap must be set in the controller on transmitted torque  $\tau_L$  to make sure that joint velocity will not contain any high-frequency components.

### **Tachometer and Accelerometer Precision - Objective A**

In case tachometers and accelerometers are available in a manipulator,  $\tilde{Q}$  will depend on their precision. Their precision data can be used in the optimization problem (3.22). The precision of these sensors can significantly enhance the estimation of external torques. However, they are not commonly found in manipulators.

### **Optimal Trajectory Planning - Objective B**

In the optimization problem (3.22), the objective B depends on the robot trajectory and accuracy of the minimal inertial parameters  $\tilde{\Theta}$ . The value of  $\tilde{\Theta}$  depends on the modeling process. If the modeling is obtained using regression methods similar to [10],  $\tilde{\Theta}$  can be

estimated using the measured variances.

The effects of the robot trajectory on the objective B should be considered simultaneously with the objective A. To this purpose, the guidelines in section 3.4.1 must be followed. Next section introduces the formulation of the optimal trajectory planning problem with regards to the precision of external torque measurements.

### 3.4.2 Formulation of the Optimal Trajectories for External Torque Measurement

In this section, we will formulate the optimization problem for finding the best trajectories with regards to external torque measurement accuracy and collision detection. Such formulation will also determine a metric for assessing trajectories based on their suitability for external torque estimation.

To formulate the optimization problem, the multiple objective functions in (3.22) are considered. There are  $n$  objective functions in (3.22) where  $n$  is the number of the manipulator joints. We start with formulating the optimization problem for one joint and then we will expand the objective function to combine all joint objectives. For the joint  $j$  of the manipulator, the corresponding objective function from (3.22) at a given time  $t$  is equal to,

$$\begin{aligned} \text{OF}_j(t) = & \left| \sum_{k=1}^l \mathbf{Y}_{k_j}^q(q) \tilde{\mathbf{Q}}_k \hat{\Theta} \right. \\ & \left. + \mathbf{Y}_j(q, \dot{q}, \ddot{q}) \tilde{\Theta} \right| \quad \forall j : 1 \leq j \leq n \end{aligned} \quad (3.23)$$

Each joint might have different levels of importance with regards to accurate external torque estimations and collision detection. For example, with regards to safety, the end effector or joints with sharper exterior require better collision detection than other joints. Joints that their workspace might clamp the user require better collision detection as well. Therefore, weights must be assigned to each joint for the purpose of optimal trajectory planning with regards to external torque estimation. The weights are determined based on characteristics specific to each manipulator.

By denoting each joint-weight as  $w_j \geq 0$ , we define the following combined scalar objective



for trajectory optimization at any given time  $t$ ,

$$\begin{aligned} \text{OF}(t) &= \sum_{j=1}^n w_j \text{OF}_j(t) \\ &= \sum_{j=1}^n w_j \left| \sum_{k=1}^l \mathbf{Y}_{k_j}^q(q) \tilde{\mathbf{Q}}_k \hat{\Theta} + \mathbf{Y}_j(q, \dot{q}, \ddot{q}) \tilde{\Theta} \right| \end{aligned} \quad (3.24)$$

$\text{OF}(t)$  is a function of time. Depending on the manipulator's purpose, there are time periods when the external torque measurements must be as precise as possible. For example, when the manipulator is performing a collaborative task with a human, sensitive collision detection is very important. Therefore, the  $\text{OF}(t)$  must be time-weighted. Using the weighting function  $w_t(t)$ , we define the following definite integral as the objective function, i.e.,

$$\begin{aligned} \text{OBJ}[q] &= \int_{t_s}^{t_f} w_t(t) \sum_{j=1}^n w_j \left| \sum_{k=1}^l \mathbf{Y}_{k_j}^q(q) \tilde{\mathbf{Q}}_k \hat{\Theta} + \right. \\ &\quad \left. + \mathbf{Y}_j(q, \dot{q}, \ddot{q}) \tilde{\Theta} \right| dt \end{aligned} \quad (3.25)$$

where  $t_s$  and  $t_f$  denote the starting and finish times for the time span under consideration for trajectory planning.

The effect of  $\tilde{\mathbf{Q}}$  in  $\text{OBJ}[q]$  can be simplified by following the recommendations regarding controller design in section 3.4.1. These recommendations provide us with an upper bound on  $|\tilde{\mathbf{Q}}|$ , i.e.,

$$B_{\tilde{\mathbf{Q}}} : \quad |\tilde{\mathbf{Q}}_k| \leq B_{\tilde{\mathbf{Q}}_k}, \quad 1 \leq k \leq l \quad (3.26)$$

We discussed in section 3.4.1 that the minimal inertial parameters are determined with a confidence interval. The confidence interval of minimal inertial parameters is mathematically represented by an upper bound,

$$B_{\tilde{\Theta}} : \quad |\tilde{\Theta}_p| \leq B_{\tilde{\Theta}_p}, \quad 1 \leq p \leq n_p \quad (3.27)$$

where  $n_p$  is the number of minimal inertial parameters. By introducing (3.26) and (3.27) in (3.25), the objective function  $\text{OBJ}[q]$  is written as,

$$\begin{aligned} \text{OBJ}[q] &= \int_{t_s}^{t_f} w_t(t) \sum_{j=1}^n w_j \left( \sum_{k=1}^l |\mathbf{Y}_{k_j}^q(q) \hat{\Theta}| B_{\tilde{\mathbf{Q}}_k} \right. \\ &\quad \left. + \sum_{p=1}^{n_p} |\mathbf{Y}_{jp}(q, \dot{q}, \ddot{q})| B_{\tilde{\Theta}_p} \right) dt \end{aligned} \quad (3.28)$$

The objective function  $\text{OBJ}[q]$  must be minimized in terms of the trajectory  $q$  to obtain the optimal trajectories with regards to the precision of the external torque measurement. The minimization problem associated with the objective function  $\text{OBJ}[q]$  is,

$$\min_q \text{OBJ}[q] \quad (3.29)$$

The optimization problem (3.29) is a calculus of variation problem and its solution can be found by implementing the Euler-Lagrange equations. However, Euler-Lagrange equations require differentiability of the integrand of the optimization objective (3.28). The absolute value operator  $|\cdot|$  does not satisfy the differentiability requirement. By replacing  $|\cdot|$  with a differentiable substitute, i.e.  $f(x) = (\epsilon + x^2)^{\frac{1}{2}}$ , where  $\epsilon$  is a small regularization constant, the optimization objective (3.28) is written as,

$$\text{OBJ}[q] = \int_{t_s}^{t_f} L(t, q, \dot{q}, \ddot{q}) dt \quad (3.30a)$$

$$\begin{aligned} L(t, q, \dot{q}, \ddot{q}) = & w_t(t) \sum_{j=1}^n w_j \left( \sum_{k=1}^l f(\mathbf{Y}_{k_j}^q(q) \hat{\Theta}) B_{\tilde{Q}_k} \right. \\ & \left. + \sum_{p=1}^{n_p} f(\mathbf{Y}_{jp}(q, \dot{q}, \ddot{q}) B_{\tilde{\Theta}_p} \right) \end{aligned} \quad (3.30b)$$

The solution to the trajectory optimization problem (3.29) using (3.30) is equivalent to the solution to the following Euler-Lagrange equation,

$$\frac{\delta L}{\delta q} - \frac{d}{dt} \left( \frac{\delta L}{\delta \dot{q}} \right) + \frac{d^2}{dt^2} \left( \frac{\delta L}{\delta \ddot{q}} \right) = 0 \quad (3.31)$$

The objective  $\text{OBJ}[q]$  must be optimized on the trajectory  $q$ , subject to boundary conditions. The boundary conditions are determined as  $q(t_s) = q_s$ ,  $q(t_f) = q_f$ ,  $\dot{q}(t_s) = \dot{q}_s$ ,  $\dot{q}(t_f) = \dot{q}_f$  and the workspace boundaries. The trajectory determined from the Euler-Lagrange equation (3.31) will be the optimal trajectory between  $q_s$  and  $q_f$  with regards to the precision of external torque estimations. Further investigation of the solution (3.31) is out of the scope of this paper and will be subject of future work.

So far the formulation of the optimal trajectories with regards to the precision of the external torque estimation is determined. Moreover, the formulation (3.28) can be applied as a metric to compare different trajectories.

### 3.4.3 Metric for External Torque Estimation Precision of Trajectories

Programming a manipulator with the proposed optimal trajectory might not always be of interest. There are robotic application when the robot trajectory has to be determined by different trajectory planning procedures. In cases where solving the optimization problem is not of interest, the objective (3.28) can be used to compare different trajectories in terms of external torque estimation precision. The comparison capability of the objective (3.28) motivates the following external torque estimation metric,

$$EM[q] = OBJ[q] \quad (3.32)$$

where  $EM$  denotes estimation metric. This metric can be further expanded to include the effects of unmodeled friction dynamics and joint elasticity.

In the next section, the formulation of the upper bound for external torque estimation error in (3.20) will help to determine model-based collision detection thresholds. These thresholds can be used for any serial link manipulator and any trajectory. However, the proposed thresholds are minimized when the trajectory obtained from the optimization problem (3.29) is used.

## 3.5 Model-Based Collision Detection Thresholds

Constant thresholds are usually implemented for the purpose of collision detection [6], [11], [12]. In this section, novel varying thresholds for collision detection for robotic manipulators are proposed. We will investigate the combined effect of inaccurate modeling and imprecise sensor measurement to determine the proposed thresholds. For this purpose, we will use the particular formulation of external torque estimation error  $\tilde{\tau}_c(t)$  in (3.19).

By substituting  $Q = \hat{Q} - \tilde{Q}$  in (3.19),  $\tilde{\tau}_c(t)$  is written as,

$$\begin{aligned} \tilde{\tau}_c(t) = & \sum_{k=1}^l \mathbf{Y}_k^q(q) [\tilde{Q}_k \hat{\Theta} + \hat{Q}_k \tilde{\Theta} - \tilde{Q}_k \tilde{\Theta}] \\ & - \tilde{\tau}_L + \tau_d + \tilde{\tau}_{fr} \end{aligned} \quad (3.33)$$

We use the formulation (3.33) in determining an upper bound for the absolute value of  $\tilde{\tau}_c(t)$  by using only the measured signals and available minimal inertial parameter estimations.

By substituting (3.12) in (3.33) the upper bound for torque estimation error at joint  $j$  of the manipulator is obtained as,

$$\begin{aligned} |\tilde{\tau}_{c_j}(t)| \leq & \left| \sum_{k=1}^l \mathbf{Y}_{k_j}^q(q) [\tilde{\mathcal{Q}}_k \hat{\Theta} - \tilde{\mathcal{Q}}_k \tilde{\Theta}] + \mathbf{Y}_j(q, \hat{q}, \hat{\dot{q}}) \tilde{\Theta} \right| \\ & + |\tilde{\tau}_{L_j}| + |\tilde{\tau}_{fr_j}| + |\tau_{d_j}| \end{aligned} \quad (3.34)$$

The bounds  $B_{\tilde{\mathcal{Q}}}$  and  $B_{\tilde{\Theta}}$  for  $|\tilde{\mathcal{Q}}|$  and  $|\tilde{\Theta}|$ , defined in (3.26) and (3.27), hold true by following the recommendations in section 3.4.1. By introducing  $B_{\tilde{\mathcal{Q}}}$  and  $B_{\tilde{\Theta}}$  in (3.34), the upper bound is simplified as  $B_{c_j}(t)$ ,

$$|\tilde{\tau}_{c_j}(t)| \leq B_{c_j}(t) \quad (3.35)$$

where

$$\begin{aligned} B_{c_j}(t) = & \sum_{k=1}^l \left| \mathbf{Y}_{k_j}^q(q) \hat{\Theta} \right| B_{\tilde{\mathcal{Q}}_k} + \sum_{p=1}^{n_p} \sum_{k=1}^l \left| \mathbf{Y}_{k_{jp}}^q(q) \right| B_{\tilde{\mathcal{Q}}_k} B_{\tilde{\Theta}_p} \\ & + \sum_{p=1}^{n_p} \left| \mathbf{Y}_{jp}(q, \hat{q}, \hat{\dot{q}}) \right| B_{\tilde{\Theta}_p} + |\tilde{\tau}_{L_j}| + |\tilde{\tau}_{fr_j}| + B_{d_j} \end{aligned} \quad (3.36)$$

where  $B_d$  is the upper bound for the disturbance torque such that for every joint  $|\tau_{d_j}| < B_{d_j}$ . If there is information available related to the imprecise model of the actuators  $\tilde{\tau}_L$  and friction  $\tilde{\tau}_{fr}$ , it must be included in the bound (3.36). The proposed time-varying bound  $B_{c_j}(t)$  can be used as a collision detection threshold. If for any joint  $j$ ,  $|\tilde{\tau}_{c_j}(t)|$  crosses  $B_{c_j}(t)$  a collision is detected and post-collision strategies must be executed. The detection of collision at a given time  $t$  is formulated as,

$$\exists j : 1 \leq j \leq n \quad \text{s.t.} \quad |\tilde{\tau}_{c_j}(t)| > B_{c_j}(t) \Rightarrow \text{Collision} \quad (3.37)$$

The thresholds  $B_{c_j}(t)$  integrate the effects of trajectory planning, estimation error of minimal inertial parameters, velocity and acceleration filters, and actuator and friction modeling. As a result, these thresholds adjust to all modeling and measurement inaccuracies in a manipulator. Furthermore, implementing the optimization trajectory obtained from (3.29) minimizes the contribution of  $\sum_{k=1}^l \left| \mathbf{Y}_{k_j}^q(q) \hat{\Theta} \right| B_{\tilde{\mathcal{Q}}_k}$  and  $\mathbf{Y}(q, \hat{q}, \hat{\dot{q}})$  to the proposed threshold. This minimization lowers the collision detection thresholds and is desirable.

In a large number of applications, external torques are expected to be zero. This condition, considering (3.13), is equivalent to,

$$\tau_c(t) = 0 \quad \Rightarrow \quad \hat{\tau}_c(t) = \tilde{\tau}_c(t) \quad (3.38)$$

Therefore when expected external torques are zero, collision detection condition (3.37) is simplified as,

$$\exists j : 1 \leq j \leq n \quad \text{s.t.} \quad |\hat{\tau}_{c_j}(t)| > B_{c_j}(t) \Rightarrow \text{Collision} \quad (3.39)$$

The condition (3.39) shows the usage of the proposed thresholds for collision detection. The variable thresholds  $B_{c_j}(t)$  are a novel method to detect collisions in serial link manipulators. Furthermore, the current formulation allows comparison between different trajectories and different manipulators in terms of collision detection capability. This is highly valuable in cases when the manipulator is interacting with unstructured environments. Next section will present experimental results that use the proposed thresholds (3.36). The result will demonstrate the efficacy of the proposed metric for external torque estimation precision (3.32) by comparing collision detection between different trajectories.

## 3.6 Case Study

In this section, a KUKA Light-Weight Robot IV+ (KUKA-LWR), Fig. 3.1, is used to implement the proposed methods for comparing external torque measurement precision of different trajectories. Collision detection time-delays of the manipulator using the residual (3.16) are measured. The collision detection delays are shown to be consistent with the external torque estimation precision metric (3.32).

The setup of KUKA-LWR manipulator is as follows. The set of minimal inertial parameters and the regressor matrix (3.9) of KUKA-LWR are obtained using the algorithm in [8]. The values of the minimal inertial parameters of KUKA-LWR are identified by implementing regression modeling techniques. The modeling results are not provided here for the sake of brevity. Regression-based modeling of serial link manipulators is discussed in detail in [10]. Moreover, KUKA-LWR is controlled via the Fast Research Interface (FRI) which allows controlling the robot and access to the position and torque sensors measurements. Also, of the seven joints of KUKA-LWR, only joints 1, 2 and 4 are moved and joints 3, 5, 6 and 7 are kept at the zero position throughout the experiments of this section. The reason behind this choice is that joints 1, 2 and 4 are the first 3 joints that allow arbitrary positioning of the end-effector. The other joints are not moved for simplicity.

### 3.6.1 Trajectories and the External Torque Estimation Precision Metric

This section describes the desired trajectories used for validating the proposed model-based threshold and the external torque estimation metric. The external torque estimation precision metrics are calculated using (3.32) for all trajectories.

All three desired trajectories have the same starting and final position. The desired trajectories are specified for joints 1, 2 and 4, see Fig. 3.2, and are piece-wise fifth order polynomials. In order to calculate the corresponding external torque estimation precision metric for these trajectories the following assumptions pertaining to  $B_{\tilde{Q}}$  and  $B_{\tilde{\Theta}_p}$  are made.  $B_{\tilde{Q}}$  is calculated by adding a white noise to the trajectory signal. The resulting trajectory is filtered using the fifth-order Butterworth filter which was implemented for estimating velocity and acceleration. This filtered trajectory is substituted in (3.18) to calculate  $B_{\tilde{Q}}$  for the desired trajectories in Fig. 3.2. The calculated values of  $B_{\tilde{Q}}$  are given in TABLE 3.1. Since the frequency content of the trajectories are almost similar, the values of  $B_{\tilde{Q}}$  are almost equal for all the trajectories. Also, it is assumed that the minimal inertial parameters are determined with a certainty of two percent, i.e.,

$$B_{\tilde{\Theta}_p} = 0.02 |\tilde{\Theta}_p|, \quad 1 \leq p \leq n_p \quad (3.40)$$

Based on the above assumptions, the external torque estimation precision metrics for the trajectories in Fig. 3.2 are calculated and given in TABLE 3.2. Section 3.4.3 concluded that smaller precision metrics result in more accuracy in external torque estimation. Therefore, the results in TABLE 3.2 predict that trajectories 1 and 2 have better external torque estimation than trajectory 3.

Predictions of the external torque estimation precision metric can not be confirmed without access to the actual values of the interaction forces and torques. However, collision detection efficiency using the model-based thresholds (3.36) can be used to confirm the predictions of the proposed metrics in TABLE 3.2.

### 3.6.2 Model-Based Thresholds and Collision Detection Results

In this section, model-based thresholds (3.36) are calculated for the given desired trajectories in absence and with presence of collisions.

The manipulator is commanded to track the desired trajectories without any external collisions. The trajectories in Section 3.6.1 are chosen such that they would only have either

Table 3.1: Calculated  $B_{\bar{Q}}$  for different trajectories

Trajectory 1	Trajectory 2	Trajectory 3
0.37725	0.37694	0.37724
0.37717	0.37701	0.37715
0.37705	0.37717	0.37706
$4.7029e^{-5}$	$4.7452e^{-5}$	$4.818e^{-5}$
$4.6268e^{-5}$	$4.6215e^{-5}$	$4.7028e^{-5}$
$4.5749e^{-5}$	$4.568e^{-5}$	$4.5749e^{-5}$
$4.7562e^{-5}$	$4.8007e^{-5}$	$4.9527e^{-5}$
$4.6502e^{-5}$	$4.6902e^{-5}$	$4.687e^{-5}$
$4.5008e^{-5}$	$4.4684e^{-5}$	$4.4655e^{-5}$
0	0	0

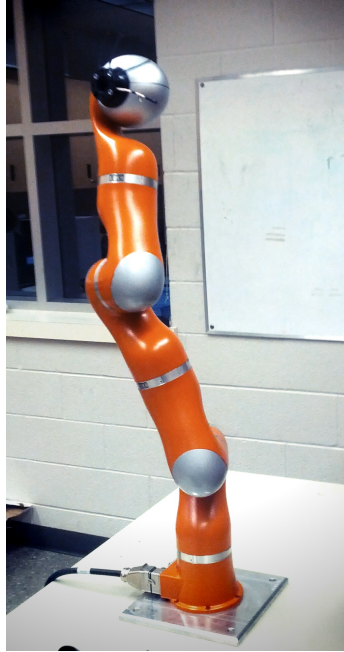


Figure 3.1: KUKA Light-Weight Robot IV+

Table 3.2: External torque estimation metric for different trajectories

	Trajectory 1	Trajectory 2	Trajectory 3
Metric	19.422	19.433	20.668

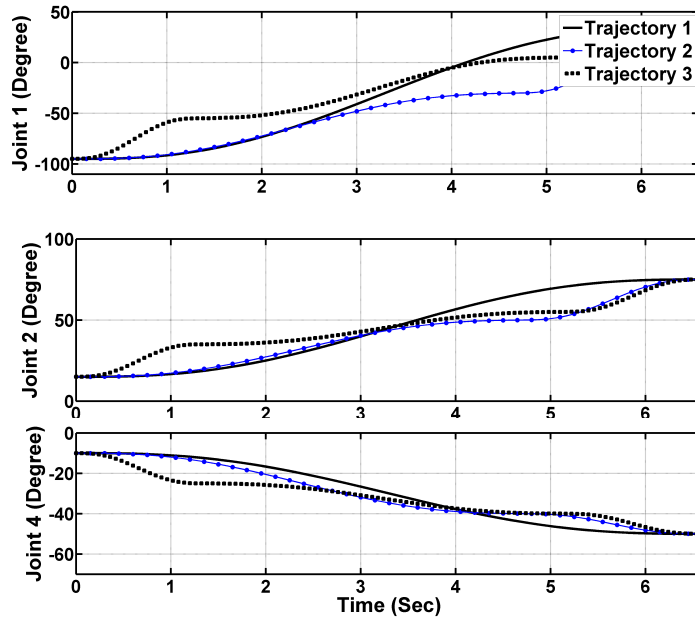


Figure 3.2: Trajectories tracked by KUKA-LWR

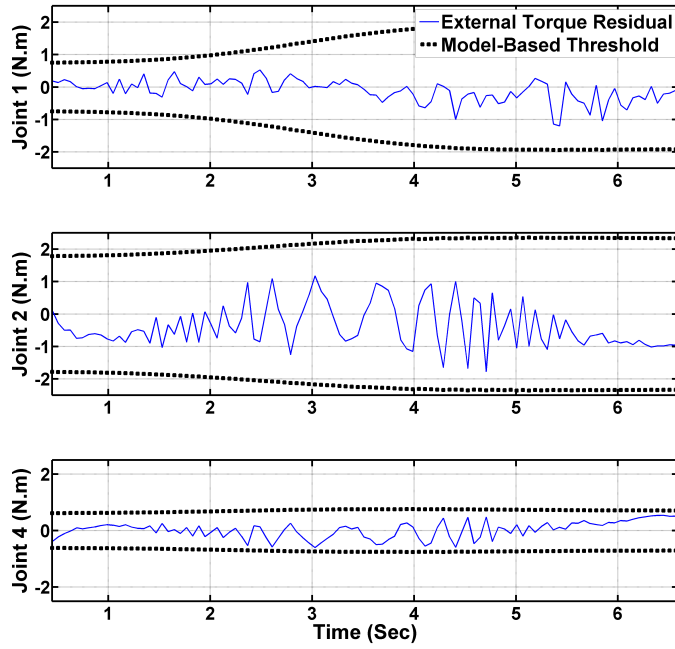


Figure 3.3: External torque residuals and their corresponding model-based collision detection thresholds for trajectory 1 in absence of collisions



positive or negative velocity at each joint. This reduces the non-linear effects of friction present at low velocities. Given that low-velocity friction non-linearities do not exist in this experiment, the friction torque term  $\hat{\tau}_{fr}$  in (3.16) can be estimated using Coulomb-viscous friction model. Through experiments not provided here for the sake of brevity, the value of coulomb friction is calculated for each joint. Also, viscous friction is measured and is found to be negligible for all joints.

KUKA-LWR is equipped with joint torque sensors. Joint torque sensor measurements are available via the FRI module used to control the manipulator. In our experiments joint torque sensors are used to measure the transferred torque to the links  $\hat{\tau}_L$  in the external torque estimation observer (3.16).

The external torque residuals are calculated using (3.16) and the corresponding model-based collision detection thresholds (3.36) are calculated for joints 1, 2 and 4 of KUKA-LWR. The results of this experiment for trajectory 1 are shown in Fig 3.3. The residuals of the trajectories 1 and 2 are not shown for the sake of brevity. Fig. 3.3 confirms that the residuals do not pass the model-based thresholds in absence of external torques.

Next, the KUKA-LWR manipulator is commanded to track the same trajectories but in presence of multiple collisions. The collisions are applied by colliding human arm with the manipulator. The resulting external torque residuals and model-based thresholds are given in Fig. 3.4 for all three trajectories. Collisions are detected using the criteria (3.39).

The actual collision times are given in TABLE 3.3 along with collision detection delays for all the three trajectories. Collision detection delays are the time elapsed between the moment of actual collision and the moment the model-based thresholds detect the collision using (3.39). The average collision detection delays are also calculated for the three trajectories. The results show that trajectory 3 has the slowest collision detection capability compared to trajectories 1 and 2. This result is in agreement with the high external torque precision metrics for trajectory 3 as given in TABLE 3.2. Trajectories 1 and 2 have similar collision detection capability which is predicted by their almost equal external torque precision metric in TABLE 3.2.

In this section we provided experimental results that show low external torque estimation metric (3.32) corresponds to better collision detection accuracy. Therefore, the proposed metric is a viable method for comparing different trajectories when the manipulator is expected to measure the external forces/torques. Also, the proposed model-based thresholds (3.36) were shown to be effective for collision detection purposes. In the next section, discussions pertaining to the effects of friction, environment dynamics and object manipu-

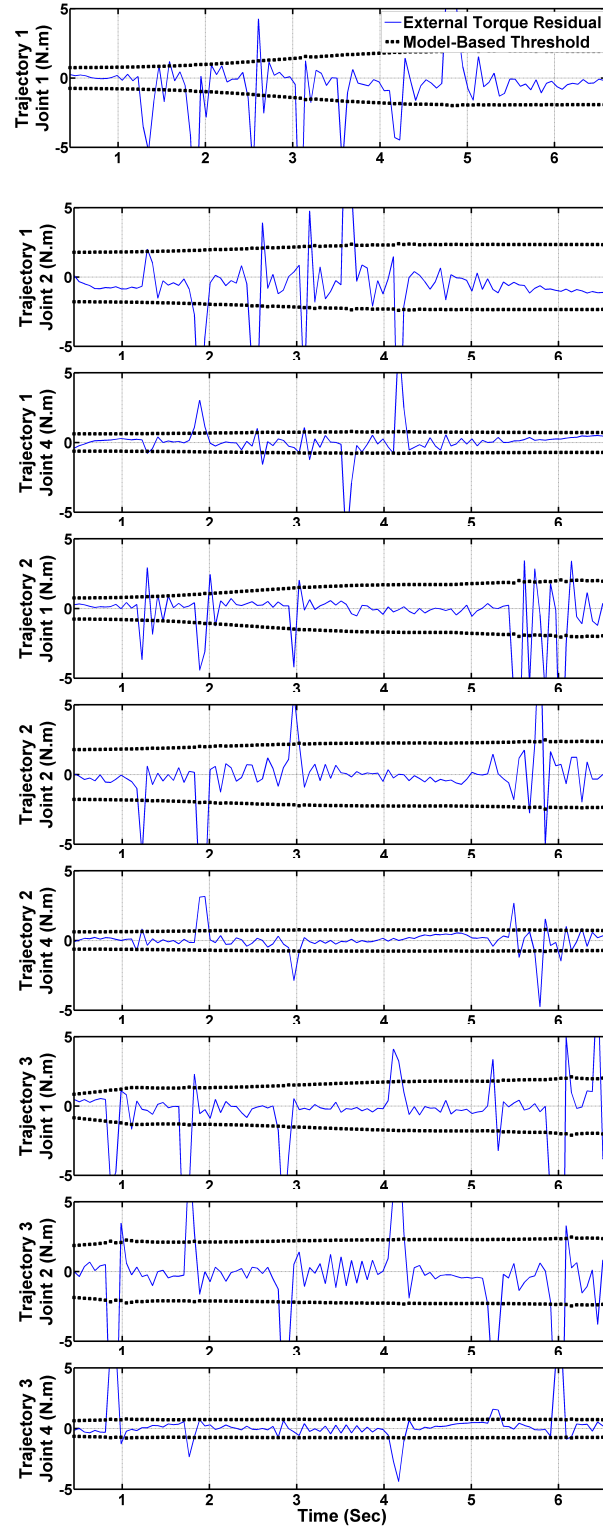


Figure 3.4: External torque residuals and their corresponding model-based collision detection thresholds in presence of collisions

Table 3.3: Comparison between different trajectories with regards to collision detection delays using model-based thresholds

Trajectory 1		Trajectory 2		Trajectory 3	
Collision Occurs (Sec)	Detection Delay (Sec)	Collision Occurs (Sec)	Detection Delay (Sec)	Collision Occurs (Sec)	Detection Delay (Sec)
1.250	0.018	1.148	0.022	0.825	0.018
1.791	0.018	1.852	0.017	1.656	0.021
2.465	0.007	2.910	0.021	2.770	0.023
3.020	0.017	5.470	0.011	4.030	0.029
3.520	0.012	5.751	0.001	5.175	0.018
4.127	0.007	5.996	0.007	5.876	0.022
4.740	0.021	—	—	6.387	0.012
Average Collision Detection Delay (Sec) 0.014		Average Collision Detection Delay (Sec) 0.013		Average Collision Detection Delay (Sec) 0.020	

lation are provided.

### 3.7 Discussions

As we have discussed earlier, external force/torque estimation without tactile sensors relies on the accuracy of the dynamic model of the manipulator along with the precision of available sensors. Therefore, the suitability of using external force/torque observers such as (3.16) depends on the particular application and available sensory information. However, the following general remarks can be made.

1. *Effects of Friction:* Depending on the manipulator, friction can form a major part of the dynamics. Accurate model of friction can enhance external torque estimation significantly. However, modeling friction at low-velocities is not always straightforward. If friction is not compensated properly by the controller, it can affect tracking the desired trajectory. Insufficient compensation of friction can be interpreted as noise by the controller, which in turn can result in fluctuation of the input torque and acceleration. The presence of acceleration fluctuation components increases the acceleration-dependent terms in external torque observer (3.16), external torque estimation precision metric (3.32), and model-based thresholds (3.36). Therefore, designing a manipulator with low friction components along with trajectory planning that avoids very low-velocities and velocity-direction changes is preferable.
2. *Unanticipated Dynamics:* Collisions were used in this paper as a form of external forces/torques. Collisions can be considered as the simplest form of an external environment interruption of the normal manipulator operation. It should be noted that the external environment can exhibit dynamics that can not originate from inaccuracies in dynamic modeling of the manipulator. Future work should review methods to identify the dynamics of the measured external torques. Comparing the identified external torque dynamics with the dynamics present in the manipulator has the potential become a technique to determine presence of external forces/torques.
3. *Object Manipulation:* The mass and inertia matrix of an object the robot performs manipulation tasks on may not be available. In such cases, the object can be modeled as part of the minimal inertial parameters of the manipulator. The uncertainty of the

mass and the inertia of the object can be included in the uncertainty of the minimal inertial parameters  $B_{\hat{\Theta}}$  in (3.27). This in turn means that the external torque estimation precision metric (3.32), model-based thresholds (3.36), and optimal trajectories with regards to external torque estimation (3.29), can be adjusted for manipulation of unknown objects via  $B_{\hat{\Theta}}$ . Therefore, this work has developed thresholds and metrics for estimation of external torques when the manipulation of an unknown object is performed.

## 3.8 CONCLUSION

In this paper we examined external torque estimation and collision detection in serial link manipulators by considering modeling inaccuracies and trajectories. We formulated optimal trajectories based on the precision of the external torque estimations. The optimal trajectories for a given manipulator with given modeling inaccuracies result in the most accurate external torque estimation and collision detection outcomes. Also, our method resulted in a metric for comparing different trajectories and manipulators with regards to external torque estimation. We proposed model-based thresholds that adapt based on the manipulator's position, velocity and acceleration. Collision detection experiments were conducted using different trajectories and the proposed thresholds. The experiments confirm that a trajectory with smaller collision detection metric results in more accurate collision detection outcomes. Future work will consider joint elasticity and friction in the proposed model-based thresholds. Moreover, a comprehensive study is needed that would simultaneously consider controller design, trajectory generation and the structure of the manipulator in term of precision of external torque estimation.

## Bibliography

- [1] A. D. Santis, B. Siciliano, A. D. Luca, and A. Bicchi, “An atlas of physical human-robot interaction,” *Mechanism and Machine Theory*, vol. 43, no. 3, pp. 253 – 270, 2008.
- [2] A. Pervez and J. Ryu, “Safe physical human robot interaction-past, present and future,” *Journal of Mechanical Science and Technology*, vol. 22, pp. 469–483, 2008.
- [3] V. Sotoudehnejad, A. Takhmar, M. Kermani, and I. Polushin, “Counteracting modeling errors for sensitive observer-based manipulator collision detection,” in *Intelligent Robots and Systems (IROS), 2012 IEEE/RSJ International Conference on*, oct. 2012, pp. 4315 –4320.
- [4] H. Sneider and P. Frank, “Observer-based supervision and fault detection in robots using nonlinear and fuzzy logic residual evaluation,” *Control Systems Technology, IEEE Transactions on*, vol. 4, no. 3, pp. 274 –282, May 1996.
- [5] W.-H. Chen, D. Ballance, P. Gawthrop, and J. O’Reilly, “A nonlinear disturbance observer for robotic manipulators,” *Industrial Electronics, IEEE Transactions on*, vol. 47, no. 4, pp. 932 –938, Aug. 2000.
- [6] A. D. Luca, A. Albu-Schaffer, S. Haddadin, and G. Hirzinger, “Collision detection and safe reaction with the dlr-iii lightweight manipulator arm,” in *Intelligent Robots and Systems, 2006 IEEE/RSJ International Conference on*, oct. 2006, pp. 1623 –1630.
- [7] A. Stotsky and I. Kolmanovsky, “Application of input estimation techniques to charge estimation and control in automotive engines,” *Control Engineering Practice*, vol. 10, no. 12, pp. 1371 – 1383, 2002.
- [8] M. Gautier and W. Khalil, “A direct determination of minimum inertial parameters of robots,” in *Robotics and Automation, 1988. Proceedings., 1988 IEEE International Conference on*, 1988, pp. 1682–1687 vol.3.
- [9] M. Kermani, R. Patel, and M. Moallem, “Friction identification and compensation in robotic manipulators,” *Instrumentation and Measurement, IEEE Transactions on*, vol. 56, no. 6, pp. 2346 –2353, dec. 2007.

- [10] J. Swevers, W. Verdonck, and J. De Schutter, “Dynamic model identification for industrial robots,” *Control Systems, IEEE*, vol. 27, no. 5, pp. 58–71, 2007.
- [11] S. Morinaga and K. Kosuge, “Collision detection system for manipulator based on adaptive impedance control law,” in *Robotics and Automation, 2003. Proceedings. ICRA '03. IEEE International Conference on*, vol. 1, sept. 2003, pp. 1080 – 1085 vol.1.
- [12] S. Takakura, T. Murakami, and K. Ohnishi, “An approach to collision detection and recovery motion in industrial robot,” in *Industrial Electronics Society, 1989. IECON '89., 15th Annual Conference of IEEE*, nov 1989, pp. 421 –426 vol.2.

## **Chapter 4**

# **Velocity-Based Variable Thresholds for Improving Collision Detection in Manipulators**

### **4.1 Introduction**

Safety in human-robot interaction has become an important research area in recent years. In order to allow robots to share their workspace with humans, it is important to build safety modules that ensure safe operation of the robot in unstructured environments [1], [2], [3], [4]. Safe human-robot interactions can be achieved using different technologies, e.g. safety paddings, compliant actuators, light-weight robots, collision avoidance systems, and collision detection.

When robots and humans share a common workspace, immediate removal of unwanted collisions is crucial to the human safety. Without a collision avoidance system, or in case of collision avoidance system failure, human safety will depend on post-collision safety strategies. Accurate collision detection ensures that active post-collision strategies, which are designed to prevent injuries to humans, are employed as soon as possible. Collisions can be detected either with or without tactile sensors. Considering the cost and the size of tactile sensors, it is more favourable if the robot is able to detect collisions without such sensors. The use of joint torque sensors in robot joints is an alternative solution. The most cost effective method is to use force/torque residual observers to estimate external torques exerted on the robot by the environment.



Several observer-based methods without using torque sensors have been proposed in the literature for obtaining the values of external torques [5], [6], [7], [8], [9]. A nonlinear torque observer based on velocity residual was formulated in [6]. This approach did not use the complete robot dynamics for the development of a more accurate adaptive threshold. Another nonlinear torque observer was formulated in [7] for estimating friction torques in two link manipulators. This method however, could not be easily extended to robots with more than two joints. The implementation of high gain observers [8], for estimating external torques in robot manipulators, was proposed and discussed in detail in [9] and is used in this paper for the calculation of external torque residuals.

To detect collisions in manipulators, accurate modeling of the robot dynamics and the friction is essential for external torque observers with or without joint torque sensors. This paper describes how collision detection in manipulators can be improved if the dynamic modeling errors, friction compensation errors and sensor errors are taken into consideration. We propose techniques for finding estimations of the modeling and sensor errors without resorting to complete remodeling of the robot. The proposed techniques are developed for robots with and without joint torque sensors and are used to introduce velocity-based variable thresholds. It is shown that by compensating the torque residual thresholds with the velocity-based variable thresholds, collisions can be detected more accurately compared to uncompensated thresholds. Experimental results on a robot equipped with joint torque sensors are used to show the efficacy of our method.

The organization of this paper is as follows. Section 4.2 covers manipulator modeling equations for rigid and flexible joint robots. Also, in this section, details of external torque observers with and without joint torque sensors are described. Section 4.3 analyzes the effects of inaccurate modeling and torque sensor reading errors on external torque observers. Strategies for minimizing the effects of such errors on torque observers are also discussed. In section 4.4, velocity-based variable thresholds for collision detection are proposed. In section 4.5, the proposed velocity-based thresholds are implemented on a KUKA-LWR robot that is equipped with joint torque sensors. Collision detection capability of the proposed thresholds is compared to those obtained from uncompensated thresholds on the KUKA-LWR. This comparison also includes the results of the COLLDTECTION module included by the manufacturer in the KUKA-LWR software. Section 4.6 concludes the paper and discusses future work.

## 4.2 Manipulator Modeling and Calculation of External Torques

A manipulator's dynamic equation is given by,

$$M(q)\ddot{q} + C(q, \dot{q})\dot{q} + g(q) = \tau_m + \tau_d + \tau_c - \tau_{fr} \quad (4.1)$$

where  $q$  denotes the joint space position of the manipulator,  $M(q)$  is the link inertia matrix,  $C(q, \dot{q})$  is the Centrifugal and Coriolis matrix, and  $g(q)$  is the gravitational vector. Also in this equation,  $\tau_m$  represents the motor torque,  $\tau_{fr}$  is the friction torque of the manipulator,  $\tau_d$  represents the disturbance torque, and  $\tau_c$  represents external torques acting on the manipulator.

In what follows, two methods for observing external torques with and without torque sensors are discussed.

### 4.2.1 External Torque Observer Using Motor Torques

Various external torque observers have been proposed in the literature, including high gain observers and sliding mode observers [8], observers based on adaptive control law [10], and nonlinear disturbance observers [7]. A common drawback among these observers is their complex dynamics, which in case of error analyses leads to further complications. In this paper, we use the observer discussed in [9] which can be applied to any manipulator without further modifications. This observer uses the generalized momentum of the robot i.e.,

$$p(t) = M(q)\dot{q} \quad (4.2)$$

and is defined as the following N-dimensional residual for the external torques  $\tau_c$ ,

$$r(t) = K_I \left[ p(t) - \int_0^t (\tau_m + \tau_d + C^T(q, \dot{q})\dot{q} - g(q) - \tau_{fr} + r) du - p(0) \right] \quad (4.3)$$

where  $N$  is the number of robot joints, and  $K_I$  is the observer gain. In (4.3),  $r(t)$  represents the first-order filtered value of  $\tau_c$  [9], i.e.  $r(t) = K_I \tau_c / (s + K_I)$ , where  $s$  represents the Laplace transform. Accurate calculation of  $r(t)$  is not possible due to the existence of errors in dynamic modeling, joint flexibility, friction modeling, sensor readings, and disturbance

torque  $\tau_d$ . Hence, one is limited to,

$$\hat{r}(t) = K_I \left[ \hat{p}(t) - \int_0^t (\hat{\tau}_m + \hat{C}^T(\hat{q}, \dot{\hat{q}}) \dot{\hat{q}} - \hat{g}(\hat{q}) - \hat{\tau}_{fr} + \hat{r}) du - \hat{p}(0) \right] \quad (4.4)$$

where the hatted values are the approximations obtained through either modeling, online calculations, or real-time sensor readings. The solution of the differential equation (4.4) with respect to  $\hat{r}(t)$  is given by,

$$\hat{r}(t) = K_I \left[ \hat{p}(t) - K_I \left( e^{-K_I t} * \hat{p}(t) \right) - K_I \left( e^{-K_I t} * (\hat{\tau}_m + \hat{C}^T(\hat{q}, \dot{\hat{q}}) \dot{\hat{q}} - \hat{g}(\hat{q}) - \hat{\tau}_{fr}) \right) \right] \quad (4.5)$$

where  $*$  denotes convolution (for more details see Appendix B). The initial value  $\hat{p}(0)$  has only a transient effect on  $\hat{r}(t)$  and is ignored in (4.5). The external torque residual in equation (4.4) is approximately zero as long as there is no collision [9], i.e.,

$$\tau_c(t) = 0 \implies \hat{r}(t) \approx 0 \quad (4.6)$$

In order to use  $\hat{r}(t)$  for detecting collisions, the simplest method is to choose a constant threshold  $b$  for  $\hat{r}(t)$  so that upon exceeding this threshold, i.e.,  $|\hat{r}(t)| > b$ , post-collision routines are triggered. It is a common practice to define such thresholds for collision detection [9], and determine the threshold values experimentally as the maximum value of  $|\hat{r}(t)|$  in the absence of external forces [10], [11].

### 4.2.2 Measuring External Torques Using Joint Torque Sensors

Availability of force/torque sensors in robot joints provides another method for measuring external torques. These sensors measure the sum of external forces/torques and manipulator dynamics, i.e.,

$$\tau_s = M_s(q) \ddot{q} + C_s(q, \dot{q}) \dot{q} + g_s(q) - \tau_{d_s} - \tau_c + \tau_{fr_L} \quad (4.7)$$

where the subscript  $s$  denotes the parameters measured at the location of the torque sensors.  $\tau_{d_s}$  is the disturbance at the torque sensors, and  $\tau_{fr_L}$  is the part of the friction that can be measured by the torque sensors. In Fig. 4.1, a general schematic of a robotic joint is

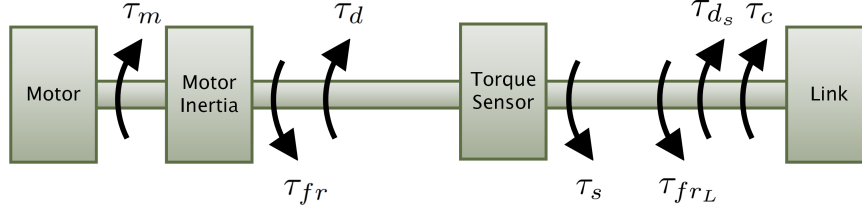


Figure 4.1: Schematic diagram of a single robot joint

depicted to show the relative locations of the torques acting on the joint.

In order to avoid using the estimated values of joint accelerations to calculate  $\tau_c$ , an observer similar to (4.3) can be used,

$$r_s(t) = K_I \left[ p_s(t) - \int_0^t (\tau_s + \tau_{ds} + C_s^T(q, \dot{q})\dot{q} - g_s(q) - \tau_{frL} + r_s) du - p_s(0) \right] \quad (4.8)$$

Similar to (4.4), using available estimations, the corresponding observer for  $\hat{\tau}_c$  is given by,

$$\hat{r}_s(t) = K_I \left[ \hat{p}_s(t) - \int_0^t (\hat{\tau}_s + \hat{C}_s^T(\hat{q}, \hat{\dot{q}})\hat{\dot{q}} - \hat{g}_s(\hat{q}) - \hat{\tau}_{frL} + \hat{r}_s) du - \hat{p}_s(0) \right] \quad (4.9)$$

In the same manner as in (4.5), the solution to (4.9) with respect to  $\hat{r}_s$  is given by,

$$\hat{r}_s(t) = K_I \left[ \hat{p}_s(t) - K_I (e^{-K_I t} * \hat{p}_s(t)) \right] - K_I (e^{-K_I t} * (\hat{\tau}_s + \hat{C}_s^T(\hat{q}, \hat{\dot{q}})\hat{\dot{q}} - \hat{g}_s - \hat{\tau}_{frL})) \quad (4.10)$$

The accuracy of the observers (4.4) and (4.9) is prone to modeling and measurement errors. In the next section, the effects of these errors are calculated and methods for overcoming these inaccuracies, with and without torque sensors, are discussed.

### 4.3 Effects of Unmodeled Dynamics on Measuring External Torques

Unmodeled dynamics appear in the calculation of external torques. In this section, the effects of such dynamics on the torque observers given in (4.4) and (4.9) are examined and

approaches for minimizing their impact on external torque measurements are presented. The formulation of unmodeled dynamics provided in this section will be used in Section 4.4 to define Velocity-Based Variable Thresholds.

### 4.3.1 Motor Torque Observer

The effect of inaccurate modeling on external torque observers is defined as the difference between the actual external torques and the observed external torques. For the observer (4.4), this effect is equal to the following residual,

$$\tilde{r}(t) = \hat{r}(t) - r(t) \quad (4.11)$$

where  $\tilde{r}(t)$  can be obtained in the same way described for  $\hat{r}(t)$  in Appendix B. Hence,

$$\begin{aligned} \tilde{r}(t) = & K_I \left[ \tilde{p}(t) - K_I \left( e^{-K_I t} * \tilde{p}(t) \right) \right] \\ & - K_I \left( e^{-K_I t} * (\tilde{\tau}_m - \tau_d + \tilde{v} - \tilde{g} - \tilde{\tau}_{fr}) \right) \end{aligned} \quad (4.12)$$

in that  $\tilde{\tau}_m = \hat{\tau}_m - \tau_m$ ,  $\tilde{p}(t) = \hat{M}(\hat{q})\hat{\dot{q}} - M(q)\dot{q}$ ,  $\tilde{v}(t) = \hat{C}^T(\hat{q}, \hat{\dot{q}})\hat{\dot{q}} - C^T(q, \dot{q})\dot{q}$ ,  $\tilde{g}(t) = \hat{g}(\hat{q}) - g(q)$ , and  $\tilde{\tau}_{fr} = \hat{\tau}_{fr} - \tau_{fr}$ . Here we define two terms that contribute to (4.12) and are caused by modeling inaccuracies. The first term is due to friction modeling errors and inaccuracies in estimating motor torques, i.e.,

$$\tau_{fm_e} = \tilde{\tau}_{fr} - \tilde{\tau}_m \quad (4.13)$$

The second term is the effect of dynamic modeling errors in (4.12),

$$\begin{aligned} \tilde{h}(t) \triangleq & K_I \left[ \tilde{p}(t) - K_I \left( e^{-K_I t} * \tilde{p}(t) \right) \right] \\ & - K_I \left( e^{-K_I t} * (\tilde{v} - \tilde{g}) \right) \end{aligned} \quad (4.14)$$

The problem of improving the external torque observers, is equivalent to the problem of estimating or minimizing  $\tau_{fm_e}(t)$  and  $\tilde{h}(t)$ . One method for keeping  $\tilde{h}(t)$  as small as possible, in the absence of external torques, is to use the adaptive controller proposed in [10], which minimizes the dependency of the residual to  $\tilde{p}(t)$ ,  $\tilde{v}(t)$ , and  $\tilde{g}(t)$ . This paper will propose the velocity-based variable thresholds to reduce the effects of  $\tau_{fm_e}(t)$  and  $\tilde{h}(t)$  on collision detection outcomes.

In the next section, the suitability of employing joint torque sensors in reducing the effects of inaccurate modeling is studied.

### 4.3.2 Joint Torque Sensor Observer

When torque sensors are employed for the calculation of external torques, the external torque residual (4.9) must be implemented. Similar to (4.11), the effect of measurement and modeling errors in the external torque residual (4.9) is equal to,

$$\tilde{r}_s(t) = \hat{r}_s(t) - r_s(t) \quad (4.15)$$

Consequently, in the same way as in (4.12),  $\tilde{r}_s(t)$  can be expressed as,

$$\begin{aligned} \tilde{r}_s(t) = & K_I \left[ \tilde{p}_s(t) - K_I (e^{-K_I t} * \tilde{p}_s(t)) \right] \\ & - K_I (e^{-K_I t} * (\tilde{\tau}_s - \tau_{d_s} + \tilde{v}_s - \tilde{g}_s - \tilde{\tau}_{frL})) \end{aligned} \quad (4.16)$$

where  $\tilde{\tau}_s = \hat{\tau}_s - \tau_s$ ,  $\tilde{p}_s = \hat{p}_s - p_s$ ,  $\tilde{v}_s = \hat{v}_s - v_s$ ,  $\tilde{g}_s = \hat{g}_s - g_s$ , and  $\tilde{\tau}_{frL} = \hat{\tau}_{frL} - \tau_{frL}$ . Using similar arguments as in (4.13) and (4.14), the following two term in (4.16) contribute to modeling inaccuracies,

$$\tau_{sfe} = \tilde{\tau}_s - \tilde{\tau}_{frL} \quad (4.17)$$

$$\begin{aligned} \tilde{h}_s(t) = & K_I \left[ \tilde{p}_s(t) - K_I (e^{-K_I t} * \tilde{p}_s(t)) \right] \\ & - K_I (e^{-K_I t} * (\tilde{v}_s - \tilde{g}_s)) \end{aligned} \quad (4.18)$$

In the absence of external torques,  $\tilde{h}_s(t)$ , similar to  $\tilde{h}(t)$ , can be kept as small as possible using the adaptive controller in [10].

### 4.3.3 Concurrent Use of Motor Torque Observer and Joint Torque Sensor Observer

In this section, the combined effect of unmodeled dynamics when both motor torque observer and joint torque observer are implemented is discussed. When joint torque sensors are installed, the sum of two of the unmodeled terms, namely  $\tau_{fme}$  defined in (4.13) and  $\tau_{sfe}$  defined in (4.17), can be obtained by subtracting (4.1) from (4.7),

$$\begin{aligned} & \left[ \hat{\tau}_s - \hat{\tau}_{frL} - \tau_{sfe} + \tau_{d_s} \right] - \left[ \hat{\tau}_m - \hat{\tau}_{fr} + \tau_{fme} + \tau_d \right] = \\ & \left[ M_s(q)\ddot{q} + C_s(q, \dot{q})\dot{q} + g_s(q) \right] - \left[ M(q)\ddot{q} + C(q, \dot{q})\dot{q} + g(q) \right] \end{aligned} \quad (4.19)$$

An estimation of  $\hat{\tau}_{f_{m_e}} + \hat{\tau}_{s_{f_e}}$  is then given by,

$$\begin{aligned} \hat{\tau}_{s_{f_e}} + \hat{\tau}_{f_{m_e}} &\approx [\hat{\tau}_s - \hat{\tau}_{f_{rL}}] - [\hat{\tau}_m - \hat{\tau}_{f_r}] - [\hat{M}_s(\hat{q})\hat{\dot{q}} \\ &+ \hat{C}_s(\hat{q}, \hat{\dot{q}})\hat{\dot{q}} + \hat{g}_s(\hat{q})] + [\hat{M}(\hat{q})\hat{\dot{q}} + \hat{C}(\hat{q}, \hat{\dot{q}})\hat{\dot{q}} + \hat{g}(\hat{q})] \end{aligned} \quad (4.20)$$

Furthermore, if the manipulator has only revolute joints, and if the torque sensors are installed on the same axis the motors are installed on, then using the Euler-Lagrange equations it can be shown that  $g_s(q) = g(q)$  and  $C_s(q, \dot{q})\dot{q} = C(q, \dot{q})\dot{q}$ . Consequently the estimation in (4.20) will simplify to,

$$\begin{aligned} \hat{\tau}_{s_{f_e}} + \hat{\tau}_{f_{m_e}} &\approx [\hat{\tau}_s - \hat{\tau}_{f_{rL}}] - [\hat{\tau}_m - \hat{\tau}_{f_r}] \\ &- \hat{M}_s(\hat{q})\hat{\dot{q}} + \hat{M}(\hat{q})\hat{\dot{q}} \end{aligned} \quad (4.21)$$

In (4.20) and (4.21),  $\hat{\tau}_m$  can be estimated using motor currents. The estimations  $\hat{\tau}_{f_r}$  and  $\hat{\tau}_{f_{rL}}$  are the friction models that were used in the observers (4.4) and (4.9).

The applicability of (4.20) and (4.21) to external torque measurement largely depends on the relative accuracy of  $\hat{\tau}_{f_{m_e}}$  and  $\hat{\tau}_{s_{f_e}}$ . The value of  $\hat{\tau}_{f_{m_e}} + \hat{\tau}_{s_{f_e}}$  by itself cannot be used to reduce the effects of modeling accuracies in the residuals (4.12) and (4.16). Hence, further examination of these residuals is required to estimate  $\hat{\tau}_{f_{m_e}}$  and  $\hat{\tau}_{s_{f_e}}$  using (4.21).

In the next section, we propose the velocity-based variable thresholds for collision detection by utilizing the available information on the inaccuracies of  $\hat{\tau}_{s_{f_e}}$  and  $\hat{\tau}_{f_{m_e}}$ , and by using approximations for  $\tilde{h}(t)$  and  $\tilde{h}_s(t)$ . To this effect, we employ the formulation of the unmodeled dynamics of serial link manipulators provided in this section.

## 4.4 Velocity-Based Variable Thresholds for Collision Detection

In this section we introduce velocity-based thresholds for the purpose of collision detection in industrial manipulators with modeling inaccuracies.

First, we analyze the effects of inaccurate friction modeling on collision detection thresholds. Given that most friction models, e.g. LuGre model, are velocity dependent, inaccurate modeling of friction results in velocity-dependent errors. To further elaborate on this matter, the effects of parameter uncertainty on the LuGre model are considered in the following

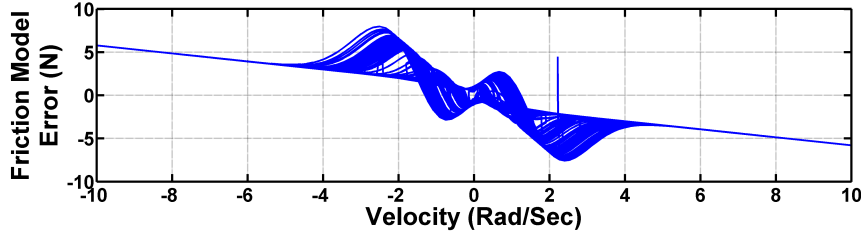


Figure 4.2: Simulated values of friction estimation error for a LuGre model with 15% parameter uncertainty

simulation results.

The LuGre friction model is defined as follows [12],

$$\dot{z} = \dot{q} - \frac{\sigma_0 |\dot{q}|}{s(\dot{q})} z; \quad (4.22a)$$

$$\tau_{fr} = \sigma_1 \dot{z} + \sigma_0 z + \sigma_2 \dot{q}; \quad (4.22b)$$

$$s(\dot{q}) = F_c + (F_s - F_c) e^{-\alpha |\dot{q}|} \quad (4.22c)$$

where  $z$  represents the deflection of bristle-like elements used for characterizing the friction force in the model,  $\tau_{fr}$  is the friction torque,  $\sigma_0$ ,  $\sigma_1$ , and  $\sigma_2$  are the stiffness, damping and viscous friction coefficients, respectively, and  $F_c$  and  $F_s$  are Coulomb and stiction friction torques, respectively. Also,  $\alpha$  represents the nature of the transitions between  $F_c$  and  $F_s$  in  $s(\dot{q})$ . A Monte Carlo simulation on a LuGre friction model with a maximum of 15% uncertainty in all the parameters is conducted. The inputs to the LuGre model are 500 fourth-order polynomial velocity trajectories of different lengths throughout a total time span of 1000 seconds. Fig. 4.2 shows the results of this simulation, i.e.  $\tilde{\tau}_{fr} = \hat{\tau}_{fr} - \tau_{fr}$ .

From Fig. 4.2, it is clear that the friction modeling error  $|\tilde{\tau}_{fr}| = |\hat{\tau}_{fr} - \tau_{fr}|$  is dependent on the velocity, i.e.

$$|\tilde{\tau}_{fr}(t)| \leq \beta(\dot{q}) \quad (4.23)$$

where,

$$\beta(\dot{q}_0) = \max_t |\tilde{\tau}_{fr}(t)|, \quad \forall \dot{q}(t) = \dot{q}_0 \quad (4.24)$$

Thus, for any mechanical system with friction including manipulators, it can be safely assumed that a function  $\beta(\dot{q})$  exists that determines the maximum friction modeling error for any given velocity. This concept will be later used to determine the velocity-based variable



thresholds.

The second step in determining the collision detection thresholds is considering the unmodeled dynamics. We use an approximation of  $\tilde{h}(t)$  and  $\tilde{h}_s(t)$ , introduced in [13], for the velocity-based variable thresholds. These approximations are

$$\tilde{h}(t) \approx \gamma \hat{h}(t) \quad (4.25)$$

where,

$$\begin{aligned} \hat{h}(t) \triangleq & K_I \left[ \hat{p}(t) - K_I \left( e^{-K_I t} * \hat{p}(t) \right) \right] \\ & - K_I \left( e^{-K_I t} * (\hat{v} - \hat{g}) \right) \end{aligned} \quad (4.26)$$

and similarly,

$$\tilde{h}_s(t) \approx \gamma_s \hat{h}_s(t) \quad (4.27)$$

where,

$$\begin{aligned} \hat{h}_s(t) \triangleq & K_I \left[ \hat{p}_s(t) - K_I \left( e^{-K_I t} * \hat{p}_s(t) \right) \right] \\ & - K_I \left( e^{-K_I t} * (\hat{v}_s - \hat{g}_s) \right) \end{aligned} \quad (4.28)$$

$\gamma$  and  $\gamma_s$  are constants that are adjusted for every joint individually.

In order to define the velocity-based variable thresholds for the residuals (4.4) and (4.9), the robot dynamics during collision-free periods are considered. Considering that the estimations of  $\tau_{fme}(t)$  and  $\tilde{h}(t)$  are available, (4.13) and (4.14) are introduced into (4.12) to obtain a residual signal without systematic modeling inaccuracies. This residual, in the absence of external forces, can be approximated to be zero and is equal to,

$$\hat{r}_c(t) = \hat{r}(t) - \tilde{h}(t) - K_I \left( e^{-K_I t} * \tau_{fme} \right) \approx 0 \quad (4.29)$$

Furthermore, by including the approximation of  $\tilde{h}(t)$  given in (4.25),

$$\hat{r}_c(t) \approx \hat{r}(t) - \gamma \hat{h}(t) - K_I \left( e^{-K_I t} * \hat{\tau}_{fme} \right) \approx 0 \quad (4.30)$$

In a similar manner, estimations of  $\tau_{sfe}(t)$  and  $\tilde{h}_s(t)$  allow introducing (4.17), (4.18) and (4.27) into (4.16) to obtain the following residual signal,

$$\hat{r}_{s,c}(t) \approx \hat{r}_s(t) - \gamma_s \hat{h}_s(t) + K_I \left( e^{-K_I t} * \hat{\tau}_{sfe} \right) \approx 0 \quad (4.31)$$

We will use the signals  $\hat{r}_c(t)$  and  $\hat{r}_{s,c}(t)$  to define the velocity-based variant thresholds for the standard residuals  $\hat{r}(t)$  and  $\hat{r}_s(t)$ . To this effect, we use the notion of velocity-dependent friction modeling described in (4.23) and apply it to (4.30) to arrive at,

$$L_{\hat{r}}(\dot{q}) < \hat{r}_c(t) < U_{\hat{r}}(\dot{q}) \quad (4.32)$$

where  $L_{\hat{r}}(\dot{q})$  and  $U_{\hat{r}}(\dot{q})$  are the lower and upper bounds of the residual  $\hat{r}_c(t)$ , respectively. These bounds should be determined experimentally. Substituting  $\hat{r}_c(t)$  from (4.30) into (4.32) yields,

$$\begin{aligned} L_{\hat{r}}(\dot{q}) &< \hat{r}(t) - \gamma \hat{h}(t) \\ &- K_I \left( e^{-K_I t} * \hat{\tau}_{f_{m_e}}(\dot{q}) \right) < U_{\hat{r}}(\dot{q}) \end{aligned} \quad (4.33)$$

consequently,

$$LT_{\hat{r}}(t) < \hat{r}(t) < UT_{\hat{r}}(t) \quad (4.34)$$

in that,

$$UT_{\hat{r}}(t) = U_{\hat{r}}(\dot{q}) + \gamma \hat{h}(t) + K_I \left( e^{-K_I t} * \hat{\tau}_{f_{m_e}}(\dot{q}) \right) \quad (4.35)$$

and,

$$LT_{\hat{r}}(t) = L_{\hat{r}}(\dot{q}) + \gamma \hat{h}(t) + K_I \left( e^{-K_I t} * \hat{\tau}_{f_{m_e}}(\dot{q}) \right) \quad (4.36)$$

$UT_{\hat{r}}$  and  $LT_{\hat{r}}$  respectively are the velocity-based upper and lower thresholds for the motor torque-based external torque observer  $\hat{r}(t)$  defined in (4.4).

For the external torque observer using joint torque sensors, i.e.  $\hat{r}_s(t)$  as defined in (4.9), one can similarly obtain,

$$LT_{\hat{r}_s}(t) < \hat{r}_s(t) < UT_{\hat{r}_s}(t) \quad (4.37)$$

where  $UT_{\hat{r}_s}$  and  $LT_{\hat{r}_s}$  respectively are the upper and lower velocity-based thresholds for  $\hat{r}_s(t)$ , and are equal to,

$$UT_{\hat{r}_s}(t) = U_{\hat{r}_s}(\dot{q}) + \gamma_s \hat{h}_s(t) - K_I \left( e^{-K_I t} * \hat{\tau}_{s_e}(\dot{q}) \right) \quad (4.38)$$

$$LT_{\hat{r}_s}(t) = L_{\hat{r}_s}(\dot{q}) + \gamma_s \hat{h}_s(t) - K_I \left( e^{-K_I t} * \hat{\tau}_{s_e}(\dot{q}) \right) \quad (4.39)$$

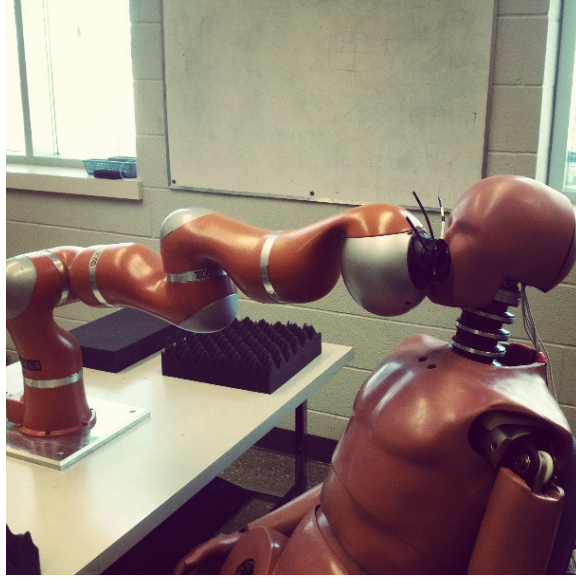


Figure 4.3: Collision detection using a Hybrid III 50th male dummy

Similar to (4.32),  $L_{\hat{r},s}(\dot{q})$  and  $U_{\hat{r},s}(\dot{q})$ , are determined experimentally as the lower and upper bounds of the residual  $\hat{r}_{s,c}(t)$  in (4.31).

Constant thresholds are often used for the purpose of collision detection [9], [10]. Our proposed thresholds (4.35), (4.36), (4.38), and (4.39) are velocity-dependent in terms of  $\hat{\tau}_{s_e}(\dot{q})$  and  $\hat{\tau}_{f_{me}}(\dot{q})$ , and time-variant in terms of  $\hat{h}(t)$  and  $\hat{h}_s(t)$ . These variable thresholds are more realistic and result in more true-positive outcomes in collision detection.

In what follows, we cover a case study on the application of the proposed velocity-based variable thresholds in a torque sensor equipped robot. Moreover, the performance of the factory-integrated collision detection module on this robot is compared to the performance of the proposed time-variant thresholds.

## 4.5 Case Study

In this section, our proposed methodology for improving collision detection using velocity-based thresholds for external torque observers described in section 4.4 is examined on a KUKA Light-Weight Robot IV+, hereafter KUKA-LWR, shown in Fig. 4.3.

### 4.5.1 KUKA-LWR Considerations

KUKA-LWR is a flexible joint robot, which is modeled as,

$$M_s(q)\ddot{q} + C_s(q, \dot{q})\dot{q} + g_s(q) = \tau_L + \tau_d + \tau_c - \tau_{frL} \quad (4.40a)$$

$$B\ddot{\theta} + DK^{-1}\dot{\tau}_s + \tau_s = \tau_m - \tau_{fr_m} \quad (4.40b)$$

$$\tau_L = DK^{-1}\dot{\tau}_s + \tau_s \quad (4.40c)$$

where  $\tau_m$  is the controlled motor torque,  $B$  is the motor inertia matrix,  $\theta$  is the motor position,  $K$  is the diagonal joint stiffness matrix,  $D$  is the diagonal joint viscosity matrix,  $\tau_s = K(\theta - q)$  is the elastic torque measured by the torque sensors,  $\tau_{fr_m}$  is the friction torque of the motors,  $\tau_{frL}$  is the friction torque of the links, and  $\tau_L$  is the torque transferred to the manipulator's links.

By replacing  $\tau_m$  and  $\tau_{fr}$  with  $\tau_L$  and  $\tau_{frL}$ , respectively, every equation derived in sections 4.2-4.4 holds true for the flexible joint model (4.40). Therefore, the velocity-based variable thresholds (4.34-4.39) are valid for flexible joint robots as well.

KUKA-LWR employs a state-of-the-art internal feedback loop from the torque sensors to the input motor torque which successfully reduces the effective motor friction  $\tau_{fr_m}$  and the effective motor inertia  $B\ddot{\theta}$ . We briefly review the details of this internal feedback loop originally proposed in [9] for the benefit of our discussion. In the proposed feedback loop in [9], the controlled motor torque is given by,

$$\tau_m = BB_\theta^{-1}u + (I - BB_\theta^{-1})\tau_s + (D - BB_\theta^{-1}D_s)K^{-1}\dot{\tau}_s \quad (4.41)$$

where  $u$  is the command torque and the values of  $B_\theta$  and  $D_s$  are determined by the KUKA-LWR controller. Readers are encouraged to refer to [9] for further information. This torque feedback loop is mentioned here since torque sensor reading errors affect the controlled motor torque  $\tau_m$  in (4.41) and thereby  $\tau_L$ , and the velocity-based thresholds.

Considering (4.40b), (4.40c), and (4.41), the transferred torque to the links is given by,

$$\tau_L = u - B_\theta\ddot{\theta} - BB_\theta^{-1}\tau_{fr_m} + (D - D_s)K^{-1}\dot{\tau}_s \quad (4.42)$$

Furthermore, considering the torque sensor errors  $\tilde{\tau}_s$ , (4.42) becomes,

$$\begin{aligned} \tau_L = & u - B_\theta\ddot{\theta} - B_\theta B^{-1}\tau_{fr_m} + (D - D_s)K^{-1}\dot{\tau}_s \\ & + (B_\theta B^{-1} - I)(\tilde{\tau}_s + DK^{-1}\dot{\tau}_s) \end{aligned} \quad (4.43)$$

Table 4.1: PID gains used via KUKA-LWR FRI module

Joint	P	I	D
1	8.25	0.52	4.12
2	70	4.37	35
3	7.75	4.84	3.1
4	25	1.56	12.5
5	2.5	1.56	1.0
6	1.61	2.0	0.8
7	1.57	2.0	0.79

The torque sensors in KUKA-LWR must be calibrated. An inaccurate calibration results in a constant bias. Considering such a constant bias in torque sensor readings and assuming a small  $B_\theta$ , one can conclude that

$$\tau_L \approx u + (B_\theta B^{-1} - I)\tilde{\tau}_s \quad (4.44)$$

These result are used in the next section to justify the biases in the velocity-dependent terms of the proposed thresholds.

In our experiments, the Fast Research Interface (FRI) module of KUKA-LWR was used to control the robot. In order to provide a motor command torque to KUKA-LWR, the FRI module needed to run in the Impedance Control mode. The Impedance Control mode includes automatic gravity compensation. We used a PID controller with the gains listed in TABLE 4.1 via the FRI module, together with the automatic gravity compensation, for the purpose of position control.

#### 4.5.2 Parameter Adjustment of the Velocity-Based Variable Thresholds

The values of  $\gamma$ ,  $L_{\hat{r}}(\dot{q})$  and  $U_{\hat{r}}(\dot{q})$ , and the measurements of  $\hat{\tau}_{fme}(\dot{q})$  in (4.35) and (4.36) can be adjusted simultaneously. Similarly, the values of  $\gamma_s$ ,  $L_{\hat{r}_s}(\dot{q})$  and  $U_{\hat{r}_s}(\dot{q})$ , and the measurements of  $\hat{\tau}_{sfe}(\dot{q})$  in (4.38) and (4.39) can be obtained simultaneously. To this effect, two least square problems based on (4.30) and (4.31) must be used to obtain the parameters

of the proposed velocity-based thresholds. These two least square problems are,

$$\min_{\gamma, \hat{\tau}_{fme}(\dot{q})} \left\{ \gamma \hat{h}(t) + K_I \left( e^{-K_I t} * \hat{\tau}_{fme}(\dot{q}) \right) - \hat{r}(t) \right\} \quad (4.45)$$

$$\min_{\gamma_s, \hat{\tau}_{sfe}(\dot{q})} \left\{ \gamma_s \hat{h}_s(t) + K_I \left( e^{-K_I t} * \hat{\tau}_{sfe}(\dot{q}) \right) - \hat{r}_s(t) \right\} \quad (4.46)$$

For the motor torque residual in (4.34), for every set of collision free data, the least square solution to (4.45) can be used to determine the values of  $\gamma$  and  $\hat{\tau}_{fme}(\dot{q})$ .  $L_{\hat{r}}(\dot{q})$  and  $U_{\hat{r}}(\dot{q})$  can be obtained by the maximum error for each velocity in the least square solution to (4.45). A similar method can be used to determine  $\gamma_s$ ,  $\hat{\tau}_{sfe}(\dot{q})$ ,  $L_{\hat{r}_s}(\dot{q})$ , and  $U_{\hat{r}_s}(\dot{q})$  in (4.37-4.39) by solving (4.46).

Also, the internal feedback loop (4.41) integrated in the KUKA-LWR controller selects the effective motor inertia  $B_\theta$  as a small value. A small value of  $B_\theta$  corresponds to the following,

$$M(q) \approx M_s(q) \implies \begin{cases} \gamma \approx \gamma_s \\ h(t) \approx h_s(t) \end{cases} \quad (4.47)$$

In order to obtain the data required for formulating the least-square problems of (4.45) and (4.46), fifth-order-polynomial trajectories between random set points were followed in the absence of any collisions and the values of  $\hat{h}(t)$ ,  $\hat{r}(t)$ ,  $\hat{h}_s(t)$ ,  $\hat{r}_s(t)$  were calculated. Moreover, the values of  $\dot{q}$  were quantized with the resolution of 0.06 Rad/Sec. Since KUKA-LWR is equipped with torque sensors, we used (4.21) to combine the two least square problems (4.45) and (4.46) into one single least square problem. As a result, the values of  $\gamma \approx \gamma_s$ ,  $\hat{\tau}_{fme}(\dot{q})$ , and  $\hat{\tau}_{sfe}(\dot{q})$  were found simultaneously.

Fig. 4.4 shows  $\hat{\tau}_{fme}(\dot{q})$ , and  $\hat{\tau}_{sfe}(\dot{q})$  obtained for all seven joints of KUKA-LWR. The graphs in Fig. 4.4 have a constant bias which is explained by (4.44). The values of  $\gamma \approx \gamma_s$  are given in TABLE 4.2.

Constant thresholds and velocity-based variable thresholds based on TABLE 4.2, Fig. 4.4, and (4.34-4.39) were calculated for a trajectory of fifth-order polynomial in the absence of external torques. Fig. 4.5 shows the torque sensor based residuals  $\hat{r}_s(t)$  for joints 1-3, and their respective velocity-based variable upper and lower thresholds,  $UT_{\hat{r}_s}(t)$  and  $LT_{\hat{r}_s}(t)$ . Similar results were obtained for joints 4-7, as well as for the motor torque based observer  $\hat{r}(t)$ , which are not presented here for the sake of brevity.

It should be noted that the data provided in this paper from KUKA-LWR depends on the

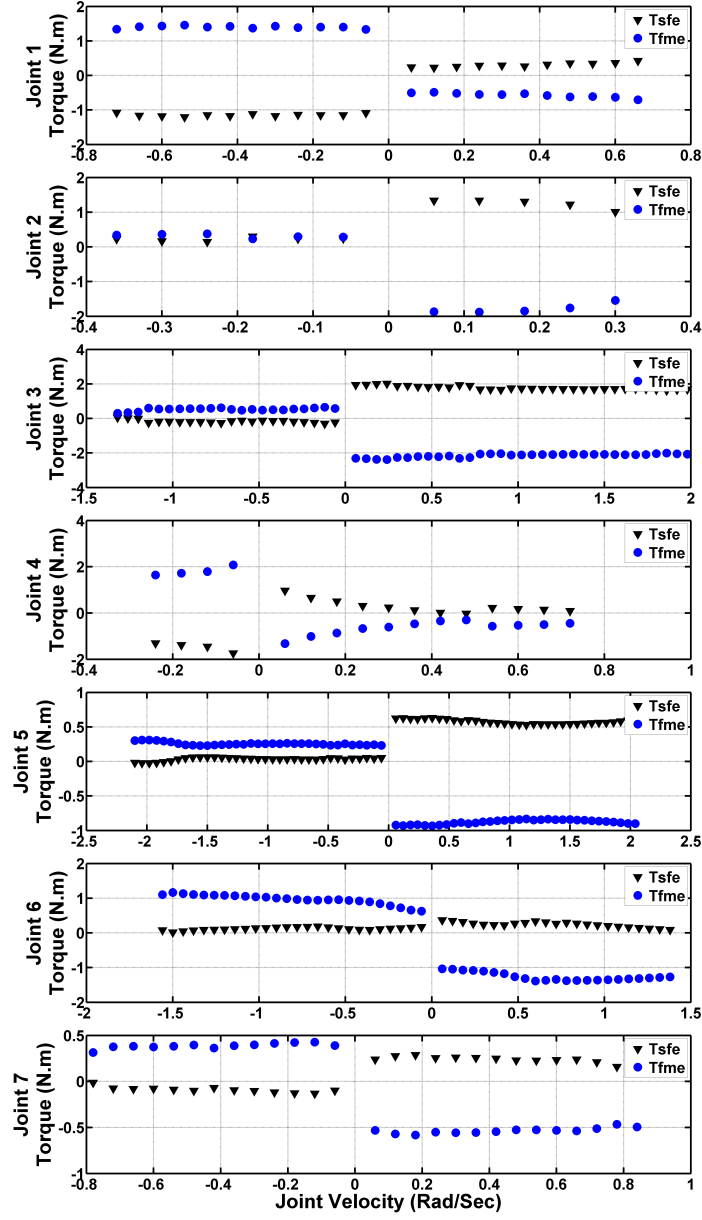


Figure 4.4: Estimated values of  $\hat{\tau}_{sfe}(\dot{q})$  and  $\hat{\tau}_{fme}(\dot{q})$  for all joints of KUKA-LWR

Table 4.2: Estimated  $\gamma \approx \gamma_s$  for all joints of KUKA-LWR

Joint	$\gamma$
1	0.002
2	$5.06 \times 10^{-4}$
3	0.005
4	0.001
5	-0.0054
6	0.0188
7	-0.0592

calibration of the robot and is subject to change if a different robot is used. However, the methodology to calculate the velocity-based thresholds remains unchanged for any manipulator with or without joint torque sensors. In the next two sections, we compare the efficacy of the proposed thresholds, constant thresholds, and the factory-integrated collision detection module of KUKA-LWR.

### 4.5.3 Comparison of Velocity-Based variable Thresholds with Constant Thresholds

In this section, collision detection of external torque observers, defined in (4.5) and (4.10), using proposed velocity-based variable thresholds is compared to collision detection using constant thresholds. In order to demonstrate the performance of the proposed thresholds, random external impact forces were applied by an individual's forearm colliding with the second joint of the robot while the robot was following an arbitrary fifth-order polynomial trajectory. The torque sensor-based residuals  $\hat{r}_s(t)$  and their respective velocity-based thresholds were calculated. The results for joints 1-3 are shown in Fig. 4.6. Motor torque-based residuals  $\hat{r}(t)$  and their velocity-based thresholds for joints 1-3 are also shown in Fig. 4.7. Similar results were obtained for joints 4-7 which are not included for the sake of brevity. TABLE 4.3 lists the times of detecting each collision using velocity-based thresholds and the relative delays that occur if constant thresholds are used instead. The results of TABLE 4.3 underscore the importance of the proposed velocity-based thresholds in collision detection.



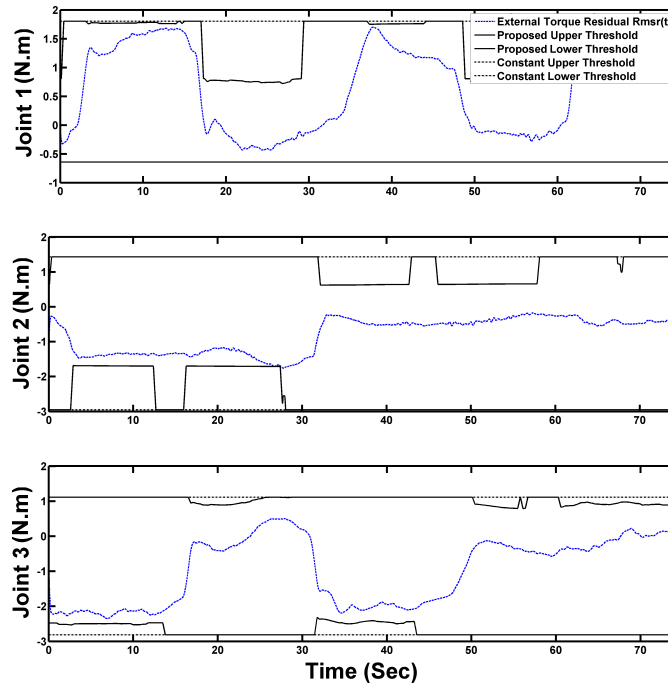


Figure 4.5: Torque sensor-based residuals  $\hat{r}_s(t)$  and their respective upper and lower thresholds for joints 1-3 of KUKA-LWR in the absence of collision forces

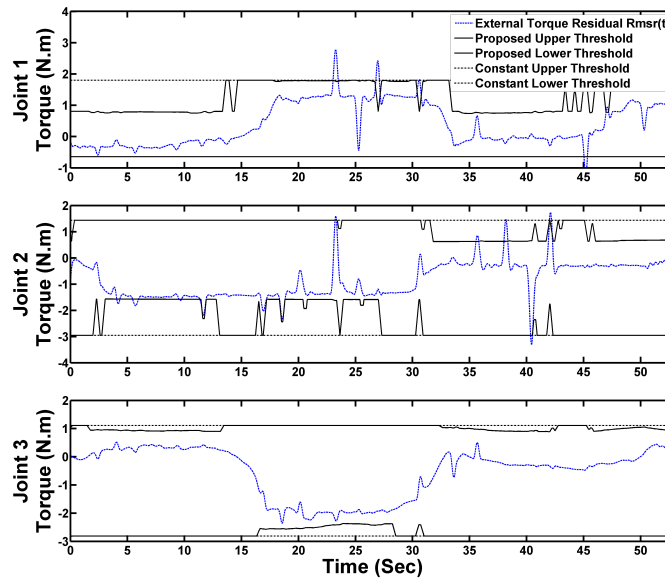


Figure 4.6: Torque sensor-based residuals  $\hat{r}_s(t)$ , velocity-based variable thresholds, and constant thresholds for joints 1-3 of KUKA-LWR in the presence of collision forces

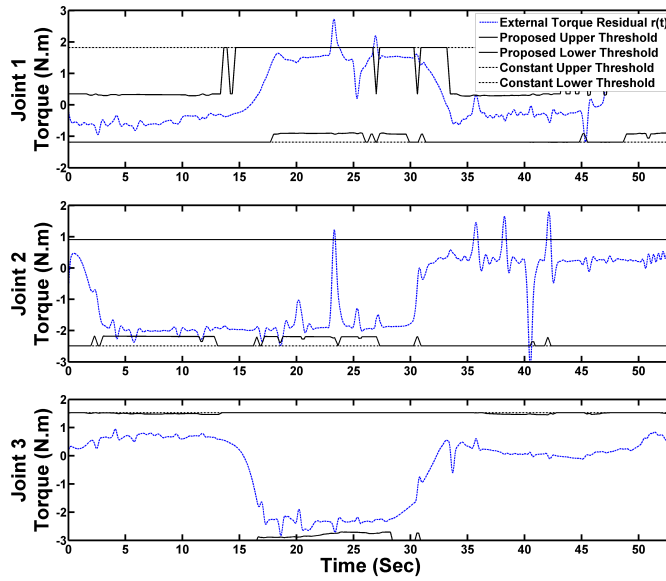


Figure 4.7: Motor torque-based residuals  $\hat{r}(t)$ , velocity-based variable thresholds, and constant thresholds for joints 1-3 of KUKA-LWR in the presence of collision forces

Table 4.3: Collision detection times with and without velocity-based thresholds in KUKA-LWR

Collision Count	Velocity-Based Threshold Detection time (Sec) Using $\hat{r}_s$	Constant Threshold Detection Delay (Sec) Using $\hat{r}_s$	Velocity-Based Threshold Detection time (Sec) Using $\hat{r}$	Constant Threshold Detection Delay (Sec) Using $\hat{r}$
1	2.18	0.02	2.17	0.04
2	4.06	Does Not Detect	4.18	Does Not Detect
3	5.45	0.07	5.54	0.06
4	9.31	0.0	9.63	Does Not Detect
5	11.35	Does Not Detect	11.42	Does Not Detect
6	13.67	0.0	13.73	Does Not Detect
7	16.74	0.0	17.05	Does Not Detect
8	18.70	Does Not Detect	18.46	Does Not Detect
9	20.02	0.0	20.18	0.0
10	23.04	0.0	23.01	0.0
11	26.75	0.04	26.72	0.03
12	30.40	0.16	30.36	Does Not Detect
13	35.57	Does Not Detect	35.53	0.0
14	38.02	0.14	38.05	0.0
15	40.35	0.0	40.39	0.0
16	42.01	0.0	41.94	0.0
17	45.04	0.0	45.22	Does Not Detect
18	46.98	Does Not Detect	47.00	Does Not Detect

#### 4.5.4 Comparison with the Collision Detection Module

This section compares the performance of constant and velocity-based variable thresholds with the KUKA-LWR factory-integrated collision detection module, i.e., COLLDTECTION. A Hybrid III 50th Male dummy as shown in Fig. 4.3 was used in these tests to measure the detection delays between the three methods. Endevco<sup>®</sup> Piezoresistive 2000 g accelerometers were installed in the dummy's head for collision detection, alongside KUKA-LWR integrated COLLDTECTION module. Both constant and velocity-based thresholds were used in these tests. The robot was repeatedly moved to collide with the dummy's head. Fig. 4.8 demonstrates the torque sensor-based residuals, constant and velocity-based variable thresholds for joints 1 and 4, as well as the accelerometer output obtained in one collision experiment with the dummy. Only the results for joints 1 and 4 are shown as these are the joints that can detect the collision. It is assumed that the accelerometer readings detect collisions instantly. TABLE 4.4 compares the delays in collision detection between the three methods, namely COLLDTECTION, constant thresholds, and velocity-based variable thresholds. The weaker performance of the COLLDTECTION module compared to the constant thresholds could be attributed to the calibration of the joint torque sensors, even though standard techniques provided by KUKA were employed to calibrate these sensors properly. As observed, the results clearly show that the proposed velocity-based variable thresholds are faster in detecting collisions in comparison to the other two methods.

## 4.6 CONCLUSION

In this paper we examined external torque residuals for serial link manipulators. The accuracy of these residuals for the purpose of collision detection was assessed and new velocity-based variable thresholds for detecting collisions using the residuals were proposed. It was shown that velocity-based variable thresholds, determined based on modeling errors and torque sensor inaccuracies, resulted in more accurate collision detection than constant thresholds. Experimental results validated that the proposed thresholds could improve the capability of the external torque observers for detecting collisions. The velocity-based methodology presented in this paper is a general technique that is applicable to any serial link manipulator.

Future works will combine the proposed thresholds with adaptive modeling techniques

Table 4.4: Collision detection delays of velocity-based and constant thresholds using torque sensor residuals and KUKA-LWR integrated collision detection module

Experiment Number	Velocity-Based Threshold Detection Delay (Sec) Using $\hat{r}_s$	Constant Threshold Detection Delay (Sec) Using $\hat{r}_s$	COLLDETECTION Module Detection Delay (Sec)
1	0.0964	0.1081	0.8132
2	0.1071	0.1218	0.8357
3	0.0784	0.0911	0.6038
4	0.1101	0.1756	0.7820
5	0.1478	0.2015	0.8226
6	0.0883	0.1430	0.7426
Average	0.1047	0.1402	0.7667

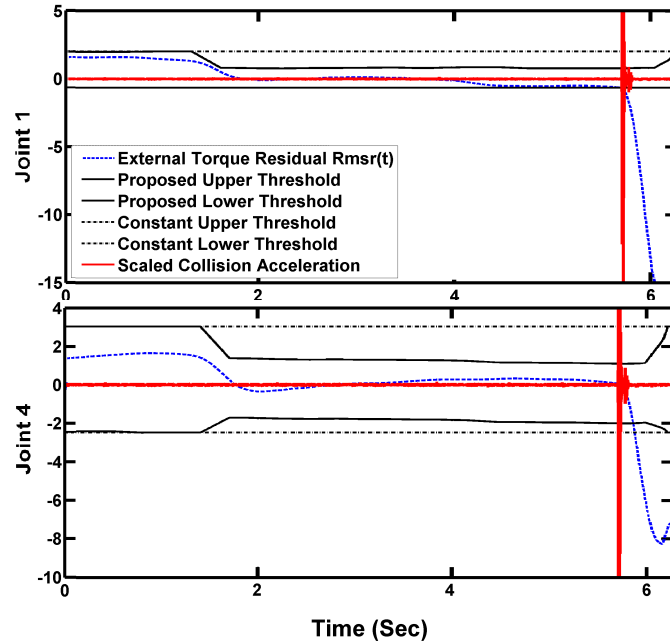


Figure 4.8: Torque sensor-based residuals  $\hat{r}_s(t)$  and their respective upper and lower thresholds for joints 1 and 4 of KUKA-LWR and the scaled acceleration signal from the Hybrid III 50th male dummy for a single collision

and acceleration based collision detection. Moreover, we will obtain the velocity-based variable thresholds for Magneto-Rheological fluid robots. Such robots have an inherently safe structure for the purpose of human-robot interaction. Comparing collision detection in Magneto-Rheological robots and KUKA-LWR using the proposed thresholds will help determine how different actuation mechanisms can assist in creating a safe environment for human-robot interaction.

## Bibliography

- [1] K. Ikuta, H. Ishii, and M. Nokata, "Safety evaluation method of design and control for human-care robots," *International Journal of Robotics Research*, vol. 22, pp. 281–297, May 2003.
- [2] A. D. Santis, B. Siciliano, A. D. Luca, and A. Bicchi, "An atlas of physical human-robot interaction," *Mechanism and Machine Theory*, vol. 43, no. 3, pp. 253 – 270, 2008.
- [3] A. De Luca, F. Flacco, A. Bicchi, and R. Schiavi, "Nonlinear decoupled motion-stiffness control and collision detection/reaction for the vsa-ii variable stiffness device," in *Intelligent Robots and Systems, 2009. IROS 2009. IEEE/RSJ International Conference on*, pp. 5487 –5494, 2009.
- [4] A. Pervez and J. Ryu, "Safe physical human robot interaction-past, present and future," *Journal of Mechanical Science and Technology*, vol. 22, pp. 469–483, 2008.
- [5] S. Katsura, Y. Matsumoto, and K. Ohnishi, "Analysis and experimental validation of force bandwidth for force control," *Industrial Electronics, IEEE Transactions on*, vol. 53, pp. 922 – 928, june 2006.
- [6] H. Sneider and P. Frank, "Observer-based supervision and fault detection in robots using nonlinear and fuzzy logic residual evaluation," *Control Systems Technology, IEEE Transactions on*, vol. 4, pp. 274 –282, May 1996.
- [7] W.-H. Chen, D. Ballance, P. Gawthrop, and J. O'Reilly, "A nonlinear disturbance observer for robotic manipulators," *Industrial Electronics, IEEE Transactions on*, vol. 47, pp. 932 –938, Aug. 2000.
- [8] A. Stotsky and I. Kolmanovsky, "Application of input estimation techniques to charge estimation and control in automotive engines," *Control Engineering Practice*, vol. 10, no. 12, pp. 1371 – 1383, 2002.
- [9] A. D. Luca, A. Albu-Schaffer, S. Haddadin, and G. Hirzinger, "Collision detection and safe reaction with the dlr-iii lightweight manipulator arm," in *Intelligent Robots and Systems, 2006 IEEE/RSJ International Conference on*, pp. 1623 –1630, oct. 2006.

- [10] S. Morinaga and K. Kosuge, “Collision detection system for manipulator based on adaptive impedance control law,” in *Robotics and Automation, 2003. Proceedings. ICRA '03. IEEE International Conference on*, vol. 1, pp. 1080 – 1085 vol.1, sept. 2003.
- [11] S. Takakura, T. Murakami, and K. Ohnishi, “An approach to collision detection and recovery motion in industrial robot,” in *Industrial Electronics Society, 1989. IECON '89., 15th Annual Conference of IEEE*, pp. 421 –426 vol.2, nov 1989.
- [12] C. Canudas de Wit, H. Olsson, K. Astrom, and P. Lischinsky, “A new model for control of systems with friction,” *Automatic Control, IEEE Transactions on*, vol. 40, pp. 419 –425, mar 1995.
- [13] V. Sotoudehnejad, A. Takhmar, M. Kermani, and I. Polushin, “Counteracting modeling errors for sensitive observer-based manipulator collision detection,” in *Intelligent Robots and Systems (IROS), 2012 IEEE/RSJ International Conference on*, pp. 4315 –4320, oct. 2012.



## **Chapter 5**

# **Improved Observer-Based Collision Detection Using Time-Variant Thresholds**

### **5.1 Introduction**

Human robot interaction has become an active research area in recent years, with the hope of building robots that can interact with humans in unstructured environments [1], [2], [3], [4], [5]. The idea of robots permeating into the human environment presents a set of challenging problems to which providing a plausible solution requires new approaches in mechanical design, sensors and actuators [6], [7], computer vision, control algorithms, and artificial intelligence.

One of the challenges facing researchers is evaluating the interaction of the robot with its environment. The evaluation can be achieved using vision, tactile, or sonar sensors [8], [9]. The evaluation becomes more important if the robot physically interacts with humans. These types of interaction concern the safety of the humans involved [10], [11], [12], [13]. In such cases, more reliable schemes for human-robot interactions are required. One way to better understand the interactions of the robot with the environment is to find the forces that are acting on the robot. These forces could be obtained either using force sensors or force observers. Force, torque, and tactile sensors are usually costly and require extra physical space. Thus, if external torques could be found without sensors, it would be of great advantage. Torque observers based on joint position and velocity are good techniques for

obtaining the value of the external torques. The downside of using observers is the need for the dynamics information of the robot which entails accurate modeling of the robot. Several observer-based schemes have been proposed in the literature for obtaining the value of the external torques [14], [15], [16], [17], [18]. In [14], an external torque observer for a robot based on the motor current and speed was proposed. However, the observer did not take the robot dynamics into consideration. In [15], a nonlinear torque observer based on a velocity residual was developed. The heuristic approach adopted in this method hampers the use of robot dynamics for the development of a more accurate adaptive threshold. In [16], a nonlinear torque observer for two link manipulators to estimate friction was proposed. Although the estimated values of the friction forces were close to their real values, this method became of minimum use when robots with more than two joints were concerned. The notion of high gain observers, originally proposed in [17], was modified for observing torque in robot manipulators [18]. In [19], an adaptive control scheme was used to detect collisions. However the scheme did not directly consider the effects of modeling inaccuracies in collision detection. The aforementioned methods commonly assumed that a reasonably accurate model of the robot was available. These methods considered inaccuracies in the model as additional disturbances on the observer output.

In this paper, in order to more effectively deal with the uncertainties in the robot dynamics and friction modeling and to detect collisions more accurately, we combine the high-gain observer scheme in [18] with time-variant thresholds. The evaluation of the collisions is performed using time-variant thresholds. This means if the robot is moving at high velocities, human safety during interactions with the robot is at higher risk compared to low velocity movements [12]. Hence time-variant thresholds are obtained with more emphasis on high velocity movements. To the best of our knowledge, time-variant thresholds have not been proposed previously.

The idea of time-variant thresholds is illustrated in Figure 5.1, where constant and time-variant thresholds are compared. In Figure 5.1 the blue line represents the difference between actual and estimated torque values, i.e. torque residual. In this figure it is assumed that changes in the value of the torque residual during time-span  $T1$  are due to modeling errors while similar changes in time-span  $T2$  are as a result of a collision. If the value of a constant threshold is set such that it detects a collision at  $T2$ , it will also trigger a false detection at  $T1$ . On the other hand, a time-variant threshold is able to correctly detect the collision at  $T2$  while avoiding false detection at  $T1$ . One should also note that time-variant thresholds are more effective in accurate detection of collisions on less accurately modeled

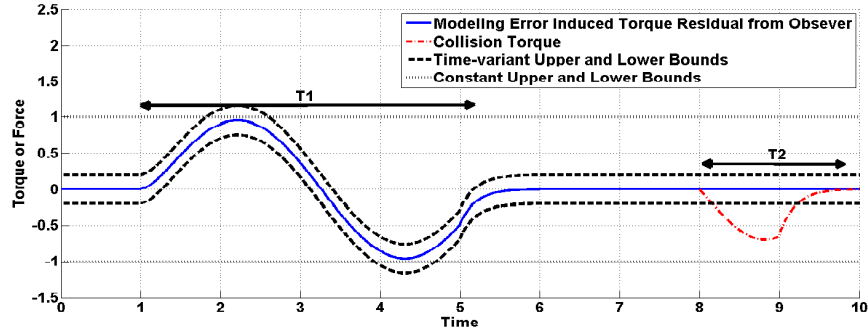


Figure 5.1: Time-variant threshold concept

manipulators.

– The organization of the paper is as follows. In section 5.2, dynamic modeling of manipulators, LuGre friction modeling, and torque observers are reviewed. Section 5.3 provides the mathematics behind the proposed time-variant collision detection threshold that includes uncertainties in sensor readings, dynamic modeling, and friction modeling. Of particular importance are the uncertainties in the physical parameters of the manipulators such as mass, inertia, center of gravity, etc., which contribute to a major time-varying component of the threshold value during high velocity periods. Section 5.4 provides the simulation results of applying the proposed method to a typical manipulator with six degrees of freedom. This includes a model of a human developed using LifeModeler software in order to demonstrate the capabilities of the proposed time-variant threshold in detecting collisions with humans. In Section 5.5, the proposed scheme is applied on a KUKA Light-Weight Robot shown in Figure 5.2. Modeling errors in KUKA Light-Weight Robot show the capabilities of time-variant thresholds. The results show that collision detection accuracy of the Light-Weight Robot is improved using time-variant thresholds compared to constant thresholds. Section 5.6 concludes the paper and discusses future work.

## 5.2 Manipulator Modeling, Friction Modeling and Collision Torque Observer

A manipulator's general dynamic equation is given by,

$$M(q)\ddot{q} + C(q, \dot{q})\dot{q} + g(q) = \tau_m + \tau_d + \tau_c - \tau_{fr} \quad (5.1)$$

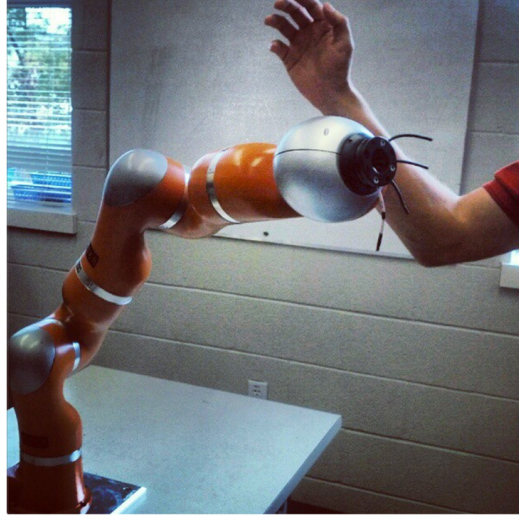


Figure 5.2: Collision with KUKA Light-Weight Robot IV+

where  $q$  denotes the joint space position of the manipulator,  $M(q)$  is the link inertia matrix,  $C(q, \dot{q})$  is the Centrifugal and Coriolis matrix, and  $g(q)$  is the gravitational vector. Also in this equation,  $\tau_m$  represents the torque vector exerted by the motors,  $\tau_{fr}$  is the friction torque vector acting on the manipulator,  $\tau_d$  represents disturbance torque vector, and  $\tau_c$  represents collision torque vector. Vectors  $\tau_d$  and  $\tau_c$  together represent external torques acting on the manipulator. To identify the external torques in the dynamic equation, various types of observers have been used in the literature, including high gain observers and sliding mode observers [17], observers based on adaptive control law [19], and nonlinear disturbance observers [16]. The common characteristic of these observers is their complex dynamics which requires unnecessary complicated error analysis. In this paper, the observer discussed in [18] is used, since this observer can be applied to any manipulator without further modifications. This observer is defined as an  $N$ -dimensional residual for collision torque  $\tau_c$ ,

$$r(t) = K_I \left[ p(t) - \int_0^t (\tau_m + \tau_d + C^T(q, \dot{q})\dot{q} - \tau_{fr} - g(q) + r(u))du - p(0) \right] \quad (5.2)$$

where  $N$  is the number of robot joints,  $K_I$  is the observer gain, and  $p(t) = M(q)\dot{q}$  is the generalized momentum of the robot. In (5.2),  $r(t)$  represents the first-order filtered value of  $\tau_c$  [18], i.e.  $r(t) = K_I/(s + K_I)\tau_c$ , where  $s$  represents Laplace transform variable. It is

not possible to accurately calculate  $r(t)$  due to the existence of errors in dynamic modeling, friction identification, sensor readings, and the actual value of  $\tau_d$ . Hence, one is limited to,

$$\hat{r}(t) = K_I \left[ \hat{p}(t) - \int_0^t (\hat{\tau}_m + \hat{C}^T(\hat{q}, \dot{\hat{q}}) \dot{\hat{q}} - \hat{\tau}_{fr} - \hat{g}(\hat{q}) + \hat{r}(u)) du - \hat{p}(0) \right] \quad (5.3)$$

where the hatted values are the approximations obtained through either modeling, calculations, or real-time sensor readings.

To model friction  $\tau_{fr}$  various methods have been proposed [20], [21], [22], [23], [24], [25]. In this paper, the LuGre model from [26] is used for estimating friction forces as follows,

$$\dot{z} = \dot{q}_j - \frac{\sigma_0 |\dot{q}_j|}{s(\dot{q}_j)} z; \quad (5.4a)$$

$$\tau_{fr,j} = \sigma_1 \dot{z} + \sigma_0 z + \sigma_2 \dot{q}_j; \quad (5.4b)$$

$$s(\dot{q}_j) = F_c + (F_s - F_c) e^{-\alpha |\dot{q}_j|} \quad (5.4c)$$

where  $z$  represents the deflection of bristle-like elements used for characterizing the friction force in the model,  $\tau_{fr,j}$  is joint  $j$  friction torque,  $\sigma_0$ ,  $\sigma_1$ , and  $\sigma_2$  are the stiffness, damping and viscous friction coefficients, respectively, and  $F_c$  and  $F_s$  are Coulomb and stiction friction torques, respectively. The value of  $\alpha$  represents the nature of the transitions between  $F_c$  and  $F_s$ . An approximation of the LuGre model is given by,

$$\dot{\hat{z}} = \dot{\hat{q}}_j - \frac{\hat{\sigma}_0 |\dot{\hat{q}}_j|}{\hat{s}(\dot{\hat{q}}_j)} \hat{z}; \quad (5.5a)$$

$$\hat{\tau}_{fr,j} = \hat{\sigma}_1 \dot{\hat{z}} + \hat{\sigma}_0 \hat{z} + \hat{\sigma}_2 \dot{\hat{q}}_j; \quad (5.5b)$$

$$\hat{s}(\dot{\hat{q}}_j) = \hat{F}_c + (\hat{F}_s - \hat{F}_c) e^{-\alpha |\dot{\hat{q}}_j|} \quad (5.5c)$$

Equations (5.2) and (5.3) show that as long as there is no collision,  $r(t) = 0$  and  $\hat{r}(t) \approx 0$ . In order to use  $\hat{r}(t)$ , at least a constant threshold  $b$  must be defined such that whenever  $|\hat{r}(t)| > b$ , a collision is detected. It is a common practice to define such a threshold and detect a collision when this threshold is surpassed [18]. Usually, the value for the threshold is determined experimentally [27], [19]. This technique does not provide an effective method for finding collision torques by itself, since  $\hat{r}(t)$  is an approximation of  $r(t)$ . Some considerations need to be made so as to reduce the impact of approximating  $r(t)$  in collision detection accuracy. To this end, the next section discusses the notion of a time-variant threshold for errors in  $\hat{r}(t)$ .

### 5.3 Residue Error Bounds

In this section the bounds for errors in  $\hat{r}(t)$  are found assuming that there is no collision. These bounds would also serve as the thresholds for  $\hat{r}(t)$ . To this purpose,  $r_e(t)$  is defined as,

$$r_e(t) = \hat{r}(t) - r(t) \quad (5.6)$$

#### 5.3.1 Constant Bounds

To calculate a bound for  $r_e(t)$ , a straight forward method is to directly subtract (5.2) from (5.3), i.e.,

$$\begin{aligned} r_e(t) = & K_I \left[ \hat{M}(\hat{q})\hat{q} - M(q)\dot{q} - \int_0^t (\tau_{me} - \tau_d - \hat{\tau}_{fr} \right. \\ & + \tau_{fr} + \hat{C}^T(\hat{q}, \hat{q})\hat{q} - C^T(q, \dot{q})\dot{q} - \hat{g}(\hat{q}) + g(q) \\ & \left. + r_e)du - \hat{M}(\hat{q}(0))\hat{q}(0) - M(q(0))\dot{q}(0) \right] \end{aligned} \quad (5.7)$$

By denoting  $p_e(t) = \hat{M}(\hat{q})\hat{q} - M(q)\dot{q}$ ,  $V_e(t) = \hat{C}^T(\hat{q}, \hat{q})\hat{q} - C^T(q, \dot{q})\dot{q}$ ,  $g_e(t) = \hat{g}(\hat{q}) - g(q)$ ,  $\tau_{fre} = \hat{\tau}_{fr} - \tau_{fr}$ , and by taking the Laplace transform of (5.7), the following expression for  $r_e$  is obtained,

$$\begin{aligned} R_e(s) = & \frac{s}{s + K_I} K_I \mathcal{L} \left\{ p_e(t) - \int_0^t (\tau_{me} - \tau_d + V_e(u) \right. \\ & \left. - g_e(u) - \tau_{fre})du - p_e(0) \right\} \end{aligned} \quad (5.8)$$

Because of the time constant  $K_I$ ,  $p_e(0)$  only has a transient effect on  $r_e(t)$  and hence could be ignored. Converting (5.8) to the time domain yields,

$$\begin{aligned} r_e(t) = & K_I \left[ p_e(t) - K_I \int_0^t e^{-K_I(t-u)} p_e(u) du \right] \\ & - K_I \int_0^t e^{-K_I(t-u)} (\tau_{me} - \tau_d + V_e(u) - g_e(u) - \tau_{fre}) dt \end{aligned} \quad (5.9)$$

In this paper, for the sake of simplicity in writing, the  $L_\infty$  norm of a vector is defined as  $\|\cdot\|_\infty = \left[ \|\cdot\|_{\infty,1}, \dots, \|\cdot\|_{\infty,j}, \dots, \|\cdot\|_{\infty,N} \right]^T$  where  $\|\cdot\|_{\infty,j} = \sup_{t,j} |\cdot|$ ,  $j = 1, \dots, N$  is the  $L_\infty$  norm of

the  $j$ th component of the vector.

The vectorized  $L_\infty$  norm applied to (5.9), yields the maximum of each component of the vectors across the time span  $t$ . A maximum bound for  $|r_e(t)|$ , in which  $|\cdot|$  is the component-to-component absolute value of the vector, is found as,

$$|r_e(t)| \leq b_1 \quad (5.10)$$

in that,

$$\begin{aligned} b_1 = & 2K_I \|p_e(t)\|_\infty + \|V_e(t) - g_e(t)\|_\infty \\ & + \|\tau_{me}(t) - \tau_d(t)\|_\infty + \|\tau_{fre}(t)\|_\infty \end{aligned} \quad (5.11)$$

Since it is difficult to determine the exact values of the right-hand side terms of (5.11), the maximum bound defined in (5.10) is not of much use in its current form. This equation is only to demonstrate the needs for a constant maximum bound for collision detection purposes. One can obtain such a value experimentally.

More importantly, from (5.9), it can be concluded that the maximum value of the term  $2\|p_e(t)\|_\infty$  in (5.11) is only reached if  $p_e(t)$  instantaneously changes from its minimum to its maximum possible value. This change,  $\frac{dp_e(t)}{dt}$ , is dependent on  $M(q(t))$  and  $\hat{M}(\hat{q}(t))$ , where  $t$  spans the time interval before the convolution attenuates  $p_e(t)$  in the integral. Thus, one can argue that there exists a time-variant bound that  $M(q(t))$  and  $\hat{M}(\hat{q}(t))$  contribute to. This idea is explained in the next section.

### 5.3.2 Proposed Time-variant Bounds

To obtain time-variant bounds for  $r_e(t)$ , which serve as the thresholds for  $\hat{r}(t)$ , let us use a different formulation of (5.7) using the linearity in parameters property [28]. The left-hand side of (5.1) can be expressed as,

$$M(q)\ddot{q} + C(q, \dot{q})\dot{q} + g(q) = Y(q, \dot{q}, \ddot{q})\Theta \quad (5.12)$$

where  $\Theta$  is a constant vector containing minimal inertial parameters of the manipulator which includes the mass, the center of mass, and inertia tensor of the robot links [29]. It can be easily deduced that each individual component in (5.12) is linear in terms of  $\Theta$ , i.e.

$M(q)\ddot{q} = Y_M(q, \ddot{q})\Theta$ ;  $C(q, \dot{q})\dot{q} = Y_C(q, \dot{q})\Theta$ ;  $g(q) = Y_g(q)\Theta$ . Thus (5.7) becomes,

$$\begin{aligned} r_e(t) = & K_I \left[ (Y_M(\hat{q}, \dot{\hat{q}}) - Y_M(q, \dot{q}))\Theta + Y_M(\hat{q}, \dot{\hat{q}})\Theta_e \right. \\ & - \int_0^t [\tau_{me} - \tau_d + (Y_{C^T}(\hat{q}, \dot{\hat{q}}) - Y_{C^T}(q, \dot{q}))]\Theta \\ & + Y_{C^T}(\hat{q}, \dot{\hat{q}})\Theta_e - (Y_g(\hat{q}) - Y_g(q))\Theta - Y_g(\hat{q})\Theta_e \\ & \left. - \tau_{fre} + r_e \right] du - p_e(0) \end{aligned} \quad (5.13)$$

Denoting  $Y_{Me}(t) = Y_M(\hat{q}, \dot{\hat{q}}) - Y_M(q, \dot{q})$ ,  $Y_{C^Te}(t) = Y_{C^T}(\hat{q}, \dot{\hat{q}}) - Y_{C^T}(q, \dot{q})$ ,  $Y_{ge}(t) = Y_g(\hat{q}) - Y_g(q)$ , and by taking the Laplace Transform of (5.13) the following is obtained,

$$\begin{aligned} r_e(s) = & \frac{s}{s + K_I} K_I \mathcal{L} \left\{ Y_{Me}(t)\hat{\Theta} + (Y_M(\hat{q}, \dot{\hat{q}}) - Y_{Me}(t))\Theta_e \right. \\ & \left. - p_e(0) \right\} - \frac{K_I}{s + K_I} \mathcal{L} \left\{ \tau_{me} - \tau_d + Y_{C^Te}(t)\hat{\Theta} + (Y_{C^T}(\hat{q}, \dot{\hat{q}}) \right. \\ & \left. - Y_{C^Te}(t))\Theta_e - Y_{ge}(t)\hat{\Theta} - (Y_g(\hat{q}) - Y_{ge}(t))\Theta_e - \tau_{fre} \right\} \end{aligned} \quad (5.14)$$

As in (5.9),  $p_e(0)$  has been ignored due to its transient effect. Rewriting and rearranging (5.14) in the time domain gives,

$$\begin{aligned} r_e(t) = & K_I \left[ Y_{Me}(t) - \int_0^t e^{-K_I(t-u)} (K_I Y_{Me}(u) + Y_{C^Te}(u) \right. \\ & \left. - Y_{ge}(u)) du \right] \hat{\Theta} + K_I \left[ Y_M(\hat{q}, \dot{\hat{q}}) - Y_{Me}(t) \right. \\ & \left. - \int_0^t e^{-K_I(t-u)} \left[ K_I (Y_M(\hat{q}, \dot{\hat{q}}) - Y_{Me}(u)) \right. \right. \\ & \left. \left. + Y_{C^T}(\hat{q}, \dot{\hat{q}}) - Y_{C^Te}(u) - (Y_g(\hat{q}) - Y_{ge}(u)) \right] du \right] \Theta_e \\ & - K_I \int_0^t e^{-K_I(t-u)} (\tau_{me} - \tau_d - \tau_{fre}) du \end{aligned} \quad (5.15)$$

Excluding the inaccuracies in motor modeling and unmodeled dynamics of the robot, the inaccuracy in the manipulator modeling is represented by  $\Theta_e$ . The following formulation for  $\Theta_e$  proves to be very effective in obtaining the simulation and experimental results in sections 5.4, and 5.5, respectively.

$$\Theta_e = \epsilon \hat{\Theta} + \delta_{\hat{\Theta}} \quad (5.16)$$



where

$$\epsilon = \text{diag}(\epsilon_1, \epsilon_2, \dots, \epsilon_p); \delta_{\hat{\Theta}} = [\delta_{\hat{\Theta},1}, \delta_{\hat{\Theta},2}, \dots, \delta_{\hat{\Theta},p}]^T \quad (5.17)$$

In other words,  $\epsilon$  is a diagonal constant matrix which needs to be tuned and  $\delta_{\hat{\Theta}}$  compensates for the difference between  $\Theta_e$  and  $\epsilon\hat{\Theta}$ . Also,  $p$  is the number of minimal inertial parameters. To include the effect of friction in time-variant thresholds,  $\tau_{fre}$  is rewritten as

$$\tau_{fre}(t) = \epsilon_{fr}\hat{\tau}_{fr}(t) + \delta_{fr}(t) \quad (5.18)$$

where

$$\begin{aligned} \epsilon_{fr} &= \text{diag}(\epsilon_{fr,1}, \epsilon_{fr,2}, \dots, \epsilon_{fr,n}); \\ \delta_{fr}(t) &= [\delta_{fr,1}(t), \delta_{fr,2}(t), \dots, \delta_{fr,n}(t)]^T \end{aligned} \quad (5.19)$$

Again,  $\epsilon_{fr}$  is a diagonal constant matrix which needs to be tuned and  $\delta_{fr}(t)$  compensates for the difference between  $\tau_{fre}(t)$  and  $\epsilon_{fr}\hat{\tau}_{fr}(t)$ . To justify the particular formulation given in equation (5.18), it is assumed, for obvious reasons, that human safety is more jeopardized during faster robot motions. During faster motions, the dominant part of the friction is viscous friction which is linear in terms of joint velocity. Hence friction modeling error would be, to some extent, linear in terms of  $\hat{\tau}_{fr}(t)$ . This linear formulation proves to be useful in obtaining the simulation results of section 5.4 that incorporate the LuGre friction model. By defining,

$$\begin{aligned} H(t) &= K_I \left[ Y_M(\hat{q}, \hat{\dot{q}}) - \int_0^t e^{-K_I(t-u)} (K_I Y_M(\hat{q}, \hat{\dot{q}}) \right. \\ &\quad \left. + Y_{C^T}(\hat{q}, \hat{\dot{q}}) - Y_g(\hat{q})) du \right] \end{aligned} \quad (5.20)$$

and using (5.18) and (5.16), equation (5.15) can be rewritten as,

$$\begin{aligned} r_e(t) &- \epsilon_{fr} K_I \int_0^t e^{-K_I(t-u)} \hat{\tau}_{fr}(t) du - H(t) \epsilon \hat{\Theta} \\ &= K_I \left[ Y_{Me}(t) - \int_0^t e^{-K_I(t-u)} (K_I Y_{Me}(u) \right. \\ &\quad \left. + Y_{(C^T-g)e}(u)) du \right] (\hat{\Theta} - \Theta_e) + H(t) \delta_{\hat{\Theta}} \\ &- K_I \int_0^t e^{-K_I(t-u)} (\tau_{me} - \tau_d - \delta_{fr}) du \end{aligned} \quad (5.21)$$

where  $Y_{(C^T-g)e}(t) = Y_{C^T e}(t) - Y_{ge}(t)$ . Hence, the time-variant bounds for  $r_e(t)$  are found as,

$$b_{2L}(t) \leq r_e(t) \leq b_{2H}(t) \quad (5.22)$$

where

$$b_{2H}(t) = b_{2C} + b_{2V}(t); \quad b_{2L}(t) = -b_{2C} + b_{2V}(t) \quad (5.23)$$

$$\begin{aligned} b_{2C} = & (2K_I \|Y_{Me}(t)\|_\infty + \|Y_{(C^T-g)e}(t)\|_\infty)(|\hat{\Theta}| + |\Theta_e|) \\ & + \|\tau_{me}(t) - \tau_d(t)\|_\infty + \|\delta_{fr}(t)\|_\infty \end{aligned} \quad (5.24)$$

$$\begin{aligned} b_{2V}(t) = & |H(t)| |\delta_{\hat{\Theta}}| + H(t) \epsilon \hat{\Theta} \\ & + \epsilon_{fr} K_I \int_0^t e^{-K_I(t-u)} \hat{\tau}_{fr}(u) du \end{aligned} \quad (5.25)$$

As before,  $|\cdot|$  denotes a component by component absolute value operator.

Contrary to  $b_1(t)$ ,  $b_{2H}(t)$  and  $b_{2L}(t)$ , are bounds that depend on the trajectory of the robot. These bounds can decrease or increase the maximum and minimum values that  $r_e(t)$  can take without triggering a collision. When inaccuracies in the robot and friction modeling appear as positive collision torques in robot dynamics, the bounds  $b_{2H}(t)$  and  $b_{2L}(t)$  are increased and whenever these inaccuracies appear as negative collision torques,  $b_{2H}(t)$  and  $b_{2L}(t)$  are decreased. To use these time-variant bounds easier, some minor changes need to be made which are discussed in subsection 5.3.3.

### 5.3.3 Implementation Notes

Implementation of  $b_{2H}(t)$  and  $b_{2L}(t)$  involves finding  $H(t)$  in (5.20) which in turn requires all the  $Y$  matrices. Unfortunately, calculating the  $Y$  matrices is not easy for manipulators with multiple joints. Moreover, in (5.25), tuning the value of  $\epsilon$  and determining an upper bound for  $|\delta_{\hat{\Theta}}|$  are non-trivial tasks. To overcome these downsides, a joint-by-joint view of (5.16) is considered here,

$$\Theta_e = \gamma_j \hat{\Theta} + \delta_{\hat{\Theta},j} \quad (5.26)$$

where  $\gamma_j$  is a scalar value to be tuned for each joint. Using (5.18) and (5.26), the residual error given in (5.15) for joint  $j$  can be rewritten as,

$$\begin{aligned}
& r_{e,j}(t) - \epsilon_{fr,j} K_I \int_0^t e^{-K_{I,j}(t-u)} \hat{\tau}_{fr,j}(t) du - \gamma_j H_j(t) \hat{\Theta} \\
&= K_{I,j} \left[ Y_{Me,j}(t) - \int_0^t e^{-K_{I,j}(t-u)} (K_{I,j} Y_{Me,j}(u) \right. \\
&\quad \left. + Y_{(C^T-g)e,j}(u)) du \right] (\hat{\Theta} - \Theta_e) + H_j(t) \delta_{\hat{\Theta},j} \\
&\quad - K_I \int_0^t e^{-K_{I,j}(t-u)} (\tau_{me,j} - \tau_{d,j} - \delta_{fr,j}) du
\end{aligned} \tag{5.27}$$

where the subscript  $j$  denotes the  $j$ th row of the corresponding vector or matrix. This formulation of residual error lends itself to new definitions for  $b_{2C,j}$  and  $b_{2V,j}(t)$  originally defined in (5.24) and (5.25), respectively. These new definitions are,

$$\begin{aligned}
b_{2C,j} &= \|H_j(t) \delta_{\hat{\Theta},j}\|_{\infty} + (2K_{I,j} \|Y_{Me,j}(t)\|_{\infty} \\
&\quad + \|Y_{(C^T-g)e,j}(t)\|_{\infty}) (|\hat{\Theta}| + |\Theta_e|) \\
&\quad + \|\tau_{me,j}(t) - \tau_{d,j}(t)\|_{\infty} + \|\delta_{fr,j}(t)\|_{\infty}
\end{aligned} \tag{5.28}$$

$$b_{2V,j}(t) = \gamma_j h(t) + \epsilon_{fr,j} K_I \int_0^t e^{-K_{I,j}(t-u)} \hat{\tau}_{fr,j}(u) du \tag{5.29}$$

where,

$$\begin{aligned}
h(t) &= K_I \left[ \hat{p}(t) - \int_0^t e^{-K_I(t-u)} (K_I \hat{p}(u) \right. \\
&\quad \left. + \hat{C}^T(\hat{q}, \hat{q}) \hat{q} - \hat{g}(\hat{q})) du \right]
\end{aligned} \tag{5.30}$$

The reason for assuming  $H_j(t) \delta_{\hat{\Theta},j}$  as a constant term of  $b_{2C,j}$  is that otherwise it requires obtaining all  $Y$  matrices in (5.20) for obtaining  $b_{2V,j}$ . As mentioned earlier, calculating  $Y$  matrices is not an easy task for manipulators with multiple joints. Moreover, an estimate of  $\delta_{\hat{\Theta},j}$  is not readily available.

As long as there is no external collision torques on the manipulator,  $r(t) = 0$ , which in turn using (5.6) results in  $\hat{r}(t) = r_e(t)$ . Consequently having,

$$|\hat{r}(t)| > b_{2C} + b_{2V}(t) \quad \text{or} \quad |\hat{r}(t)| < -b_{2C} + b_{2V}(t) \tag{5.31}$$

is an indication of a collision.

To implement (5.28) and (5.29) in practice, involving robot manipulators, usually one does not necessarily have access to individual values such as  $\|p_e^{\hat{\Theta}}(t)\|_{\infty}$  or  $\|\delta_{fr}(t)\|_{\infty}$ , unless with extensive experiments on the robot. A remedy for this problem is to present  $b_1(t)$ ,  $b_{2H(t)}$  and  $b_{2L(t)}$  after combining the constant terms in (5.11), (5.28), and (5.29), and obtaining these constant values through experiments. Using this method, if  $K_I$  is kept at a constant value throughout all experiments, (5.11) would turn into,

$$b_1 = K_I \beta_1 + \beta_2 = \beta \quad (5.32)$$

and if  $\gamma$  and  $\epsilon_{fr}$  are known,  $b_{2H}(t)$  and  $b_{2L}(t)$  become,

$$\begin{aligned} b_{2H}(t) &= \alpha_1 + (K_I \alpha_2 + \alpha_3)(\hat{\Theta} + \alpha_4) + \alpha_5 \\ &\quad + \gamma h(t) + \epsilon_{fr} K_I \int_0^t e^{-K_I(t-u)} \hat{\tau}_{fr}(u) du \end{aligned} \quad (5.33a)$$

$$\begin{aligned} &= \alpha + \gamma h(t) + \epsilon_{fr} K_I \int_0^t e^{-K_I(t-u)} \hat{\tau}_{fr}(u) du; \\ b_{2L}(t) &= -\alpha + \gamma h(t) + \epsilon_{fr} K_I \int_0^t e^{-K_I(t-u)} \hat{\tau}_{fr}(u) du \end{aligned} \quad (5.33b)$$

The values of  $\beta$ ,  $\alpha$ ,  $\gamma$  and  $\epsilon_{fr}$  can be tuned experimentally by having the robot follow few different trajectories. Tuning  $\gamma$  and  $\epsilon_{fr}$  properly gives (5.33) the ability to detect collisions more accurately as compared with the constant threshold approach given in (5.32).

## 5.4 Simulations

In this section we evaluate the effectiveness of time-variant thresholds on collision detection and compare it to constant thresholds using a complete simulated model of PUMA 560 shown in Figure 5.3. PUMA 650 is selected due to the availability of its complete model in the literature. The model of PUMA 560 have been reported in several articles [30], [31], [32], [33]. The model parameters used here are taken from [31]. As there is no information about the friction modeling of the wrist, which includes the last three joints of PUMA robot, these joints are excluded from collision detection analyses. The effect of these joints have been considered in calculating the inertia of the robot simulated.

An estimation of the inertia parameters within 15% error is assumed. The LuGre model is considered for friction modeling and the parameters of the estimated model are assumed to

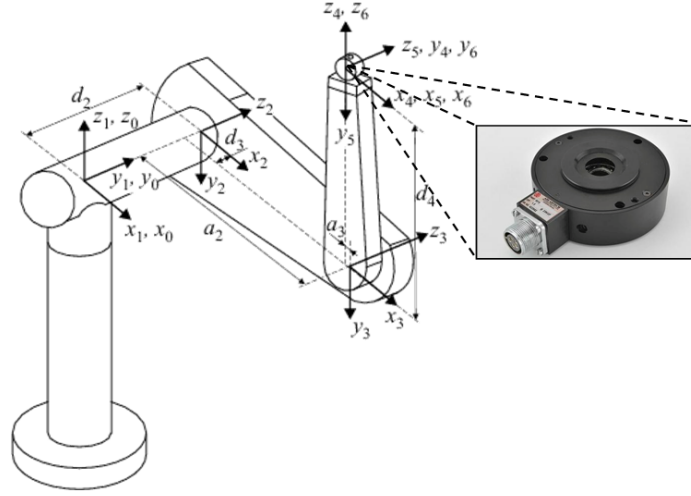


Figure 5.3: PUMA 560

Table 5.1: Simulated Trajectory Points

time(s)	$q_1$	$q_2$	$q_3$	$q_4$	$q_5$	$q_6$
0	0	-90	90	0	0	0
1.25	0	-90	90	0	0	0
2.5	45	-90	135	0	90	135
3.75	0	-45	90	180	0	0
5	0	-90	90	0	0	0

have 15% error. Parameter estimations are obtained by using random functions. Due to the large number of parameters, their values are not included in this paper. The robot controller used in these simulations is a PID controller with gravity and friction compensation.

#### 5.4.1 Collision Detection

PUMA 560 is set to follow a trajectory comprised of multiple time-stamped via points for each joint angle as listed in Table 5.1. The trajectory for each joint is constructed using a five-order polynomial passing through the given points. The gains of the PID controller for the first three joints are given in Table 5.2.

To calculate the time-variant term of the thresholds,  $b_{2V}(t)$  given in (5.29), the values of  $\gamma$  and  $\epsilon_{fr}$  must be known. These values and the value of  $\alpha$  in (5.33b) are found by comparing  $\hat{r}_e(t)$ ,  $h(t)$  and  $K_I \int_0^t e^{-K_I(t-u)} \hat{\tau}_{fr}(u) du$  for various trajectories. For the first three joints, the

Table 5.2: PID Controller Gains for a Simulated PUMA 560.

Joint	P	I	D
1	4500	0.7	80
2	12000	0.5	80
3	2500	0.1	30

Table 5.3: Values of  $\alpha$ ,  $\gamma$  and  $\epsilon_{fr}$  for a Simulated PUMA 560.

Joint	1	2	3
$\alpha$	0.2212	0.3653	0.2311
$\gamma$	-0.0456	-0.036	-0.078
$\epsilon_{fr}$	-1.74	1.98	0.29

values of  $\gamma$ ,  $\epsilon_{fr}$  and  $\alpha$  are given in Table 5.3. It is assumed that  $K_I = 20$  for all joints. The simulation results for the trajectory described by Table 5.1 are shown in Figure 5.4. As observed, despite significant variations in the value of the residue signal no collision has been detected. One is able to observe that the appropriate changes in  $b_{2V}(t)$  counteracts the changes in  $\hat{r}(t)$  and hence no collision is detected.

In order to further evaluate this technique using realistic force/torque data (with noise), an ATI force/torque sensor shown in Figure 5.3 was used to imitate a possible human collision with a robot. Collision forces  $f_c(t)$  and torques  $m_c(t)$  applied by the hand to the sensor are shown in Figure 5.5. The obtained data was applied to the last joint of PUMA to simulate the propagation of the collision forces/torques in all joints of the robot,

$$\tau_c(t) = J_c^T(q) \begin{bmatrix} f_c(t) \\ m_c(t) \end{bmatrix} \quad (5.34)$$

where  $J_c^T(q)$  is the Jacobian of the manipulator at the point of collision  $c$ ; in this case the end effector.

The results in Figure 5.6 show the upper bound  $b_{2H}(t)$  and the lower bound  $b_{2L}(t)$ , collision torques  $\tau_c$ , and the residue  $\hat{r}(t)$ . Also in this figure, the constant thresholds considered to be the absolute maximum values of  $\hat{r}(t)$  in Figure 5.4 are shown. The constant thresholds for the first three joints are 0.95, 2.6, 0.45 N.m, respectively. Table 5.4 compares the results for collision detection using the proposed time-variant thresholds and constant thresholds for the actual data acquired using ATI sensor. It is assumed that whenever a joint's residue

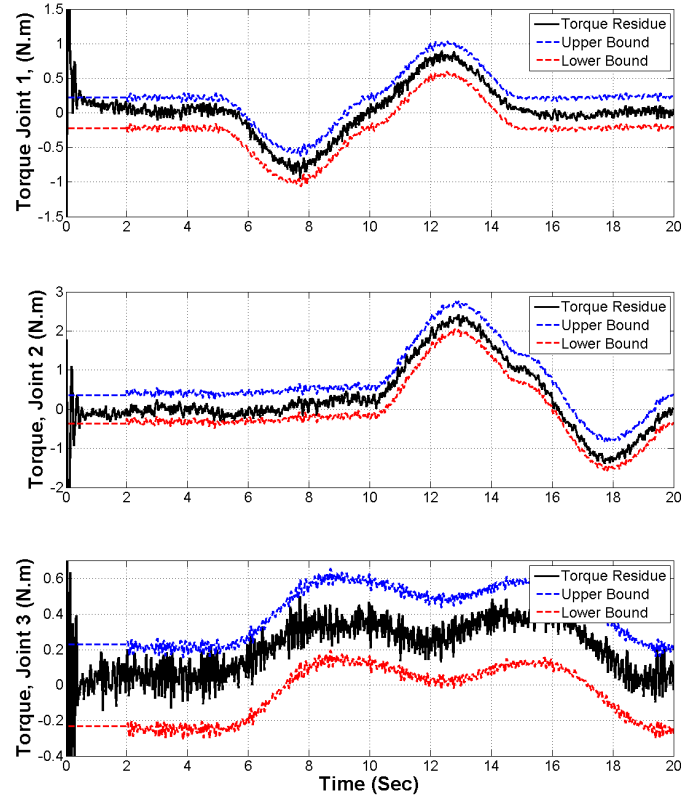


Figure 5.4: Collision residue  $\hat{r}(t)$  and thresholds  $b_{2H}(t)$  and  $b_{2L}(t)$  for a simulated PUMA 560.

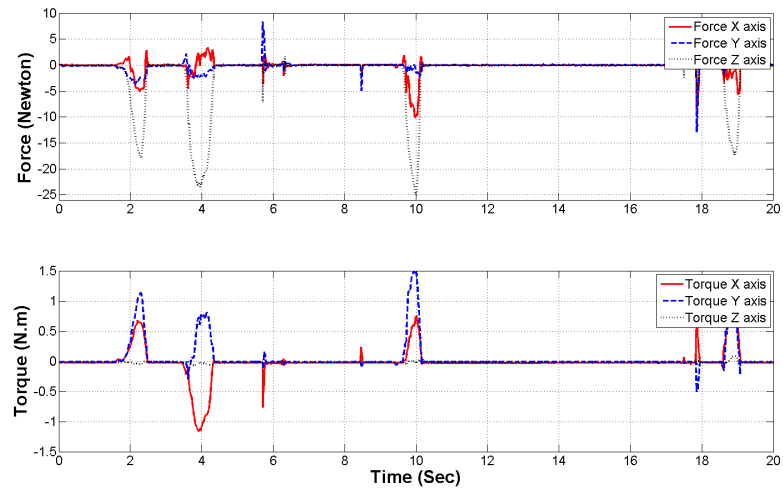


Figure 5.5: Collision forces/torques applied to the last joint of PUMA 560

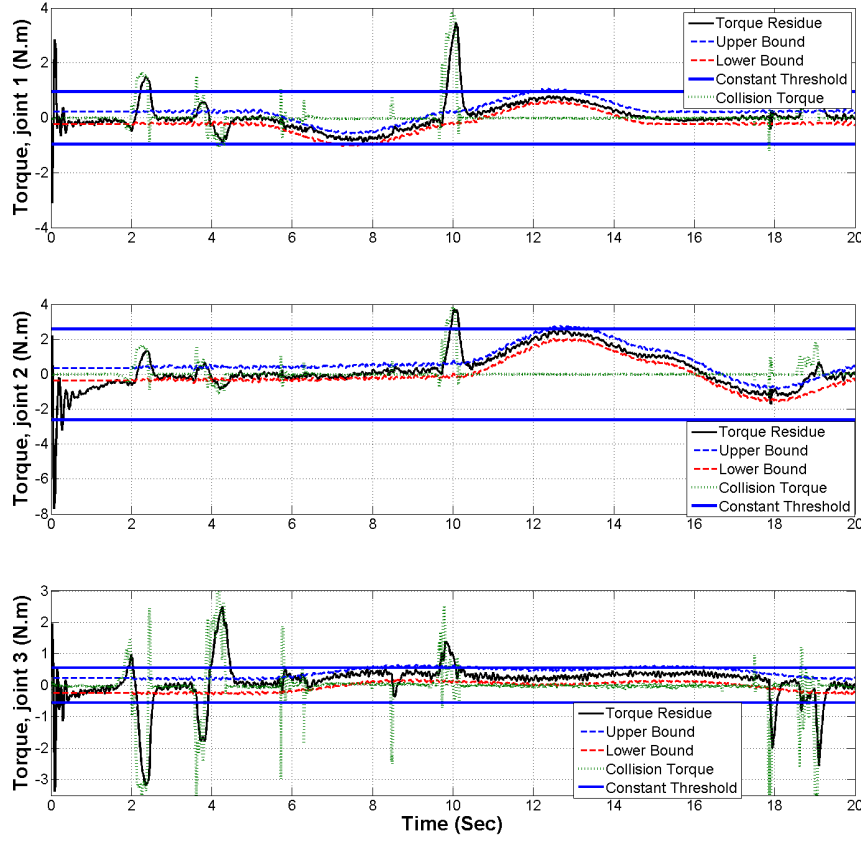


Figure 5.6: Collision residue  $\hat{r}(t)$  compared to the collision torques  $\tau_c$  for PUMA 560.

crosses the corresponding threshold value, it triggers a collision signal and when the residue returns within its respective thresholds, it deactivates collision detection. The results in Table 5.4 clearly show that the proposed time-variant method is able to detect all but one of the collisions without setting off any false collision. There is a delay in the detection that depends on the value of  $K_I$ . As it is clear from Figure 5.6 and Table 5.4, constant thresholds can miss too many actual collisions due to the shortcoming described previously. In fact, there is no constant threshold that can be obtained from (5.32) to detect all collisions correctly and avoid erroneous trigger of unreal collisions. This fact is clearly illustrated in Figure 5.6 if one notices the large values of  $\hat{r}(t)$  due to modeling errors and not actual collision forces. A constant threshold will trigger false detections to these large values of  $\hat{r}(t)$ , if it is set small enough to detect the collisions occurring at  $t = 6.26\text{sec}$  and  $t = 8.49\text{sec}$ .



Table 5.4: Collision detection times in the first three joints of PUMA 560

Collision Number	Time-variant Threshold Detection Delay (Sec)		Constant Threshold Detection Delay(Sec)	
	Collision Starts	Collision ends	Collision Starts	Collision Ends
1	0.27	0.10	0.31	0.05
2	0.14	0.20	0.16	0.11
3	0.05	0.03	Does not Detect	Does not Detect
4	0.03	0.09	Does not Detect	Does not Detect
5	0.04	0.11	Does not Detect	Does not Detect
6	0.05	0.13	0.04	0.03
7	Does not Detect	Does not Detect	Does not Detect	Does not Detect
8	0.04	0.18	0.05	0.11
9	0.06	0.18	0.07	0.14

### 5.4.2 Collision with Human Arm

The model of PUMA 560 with the same parameters and PID control described in section 5.4.1 was imported from MATLAB into Multi-Body Dynamics Adams software. The same values of  $\gamma$ ,  $\epsilon_{fr}$  and  $\alpha$  as given in Table 5.3 were used. It was assumed that the end-effector of the robot was holding an aluminum shaft with a mass of 2.86 kg. The shaft is shown in Figure 5.7 using a black cylinder. Using LifeModeler software, a human model with passive joints was created in MD Adams to simulate the human body. The aluminum shaft was moved by the robot such that it collided with the human arm twice at speeds of 0.307 meter/sec and 0.423 meter/sec. Four snapshots of this scenario at various times are shown in Figure 5.7. The collisions with the human arm were constructed by rotating the first joint of PUMA 560, while keeping the other joints at constant relative positions. The collision forces are shown in Figure 5.8. The residues obtained using (5.3), and the upper and lower bounds  $b_{2H}(t)$  and  $b_{2L}(t)$  given in (5.33) for the first three joints of PUMA 560 are depicted in Figure 5.9. It is easy to see that no constant threshold is able to detect the collisions correctly on the first joint, whereas the time-variant thresholds detect both collisions successfully. Table 5.5, shows how fast the proposed time-variant thresholds works for collision detection in the first three joints of the robot. With the first collision happening at 1.58sec, the third joint is able to detect the collision only 20 milliseconds later

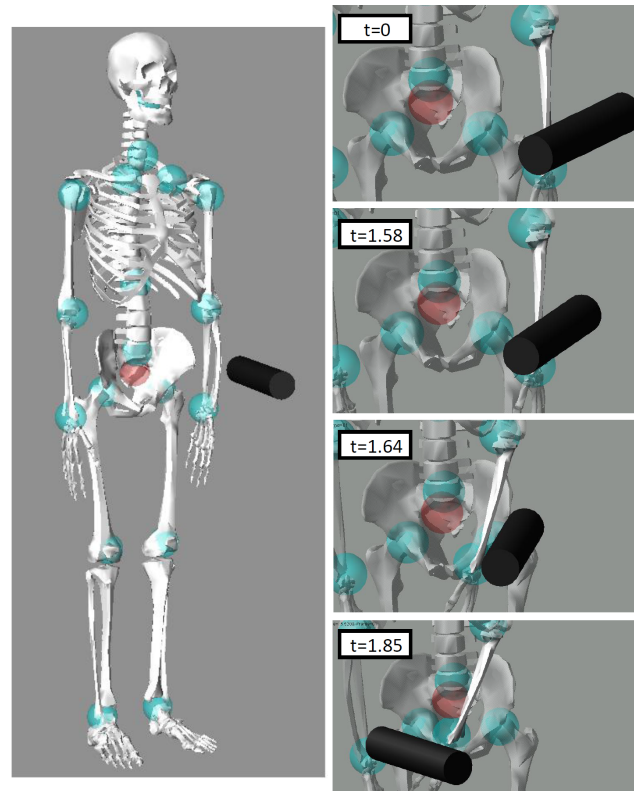


Figure 5.7: Snapshots of a modeled human in LifeModeler software during two collisions with a robot (PUMA 560).

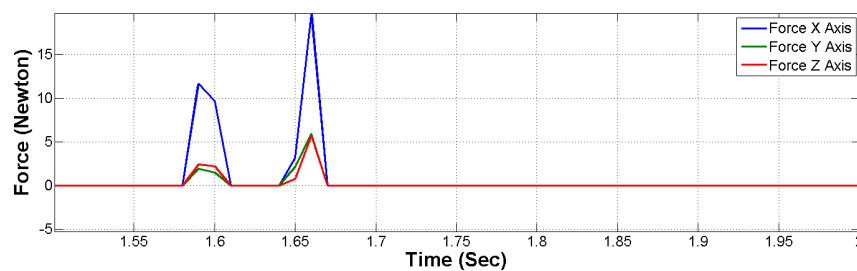


Figure 5.8: Collision forces between the human arm and an aluminum shaft held by PUMA 560.

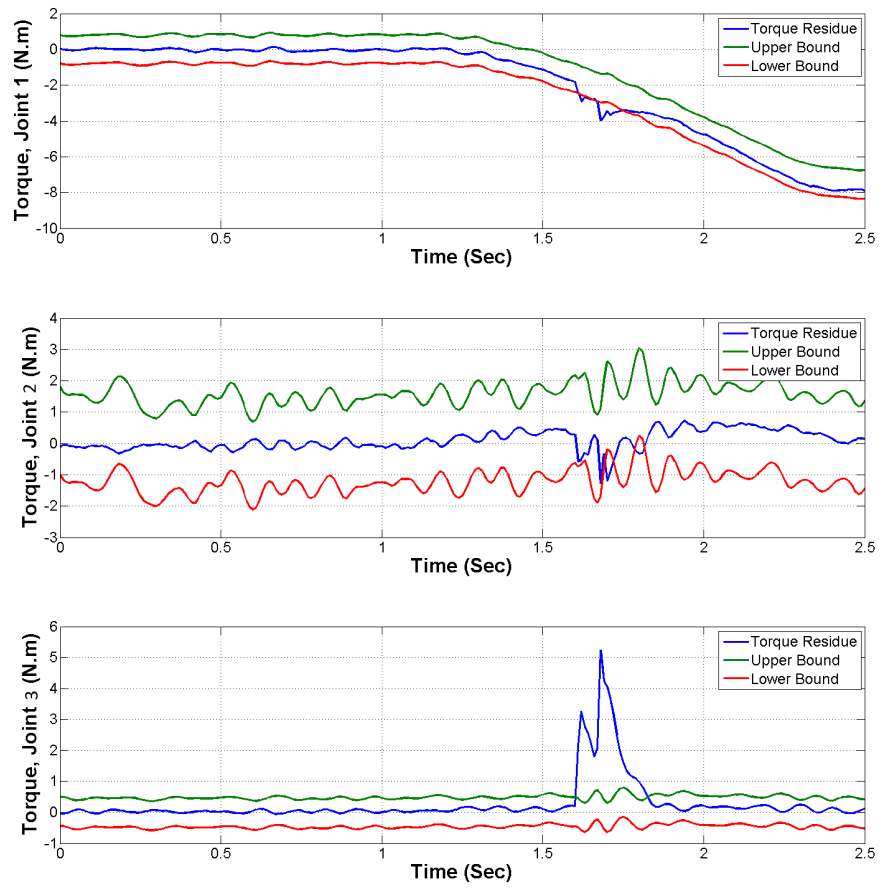


Figure 5.9: Collision residue  $\hat{r}(t)$  and upper and lower collision detection bounds for PUMA 560.

Table 5.5: Collision detection with the human arm using time-variant thresholds in the first three joints of PUMA 560.

Collision Starts (Sec)	Joint 1	Joint 2	Joint 3
1.58	1.61	-	1.60
1.64	1.66	1.69	1.66

at 1.60sec. Similarly, the second collision at 1.64sec is detected with 20 milliseconds delay at 1.66sec by joints 1 and 3. Only the second joint is not able to detect the first collision, and the reason is that the collision forces are almost perpendicular to the second joint axis, creating little amount of external torque on that joint.

## 5.5 Experimental Results

In this section, the results of section 5.3 are applied to the KUKA Light-Weight Robot IV+ (KUKA-LWR) shown in Figure 5.10. The Fast Research Interface (FRI) module in the KUKA-LWR controller gives direct access to the mass matrix  $M(q)$  and the gravity vector  $g(q)$  without the need to find minimal inertial parameters. The values for  $C(q, \dot{q})$  matrix are not accessible through the FRI module. However, the  $C(q, \dot{q})\dot{q}$  amounts to almost 2% of the total torque value in KUKA-LWR and it can be safely ignored in (5.3). i.e.,

$$\hat{C}^T(\hat{q}, \hat{\dot{q}})\hat{\dot{q}} \approx 0 \quad (5.35)$$

While KUKA-LWR can measure the torque at each joint of the robot, the focus of this paper is to study sensorless collision detection. As a result, the experimental results obtained in this section are only based on torque residuals, without using the torque sensor readings for collision detection.

In order to provide a command torque in KUKA-LWR, the FRI module must run in Impedance Control mode. The Impedance Control mode includes automatic gravity and friction compensation. Hence, the commanded torque exerted on each joint is equal to,

$$\tau_m = \tau_{m,FRI} + g(q)_{comp} + \tau_{fr,comp} \quad (5.36)$$

where  $\tau_{m,FRI}$  is the motor torque, and  $g(q)_{comp}$  and  $\tau_{fr,comp}$  are the gravity and friction compensation terms added to the motor torque by FRI module in Impedance Control mode.

In these experiments, only the first three joints of KUKA-LWR were considered. Joints 4-7



Figure 5.10: KUKA Light-Weight Robot IV+

were kept at their zero position throughout the experiments. The results presented in this section can be extended to joints 4-7 but are chosen not to in favour of the simplicity of the text. To control KUKA-LWR, a sampling rate of 3ms was used. A PD controller with friction compensation and automatic gravity compensation was used in Impedance Control mode. The gains of the PD controller are given in Table 5.6.

A number of preliminary experiments that are not reported in this paper were conducted to measure the error in friction compensation, i.e.,

$$\tau_{fre} = \hat{\tau}_{fr} - \tau_{fr} \quad (5.37)$$

The results from these experiments indicated that for every joint,  $\tau_{fre}$  defined in (5.37) is found to have a hysteretic nature. Figure 5.11 demonstrates the results for Joint 1 for different velocities from -2.0 to 2.0 rad/sec in which the hysteretic nature of  $\tau_{fre}$  is apparent. It is therefore, suitable to model  $\tau_{fre,j}$  as,

$$\tau_{fre,j} = -C_j \frac{|\dot{q}_j|}{\dot{q}_j} \quad (5.38)$$

This new model for  $\tau_{fre}$  should be used instead of (5.18) to obtain friction error in KUKA-LWR. In other words, in KUKA-LWR the friction error is not linearly proportional to the

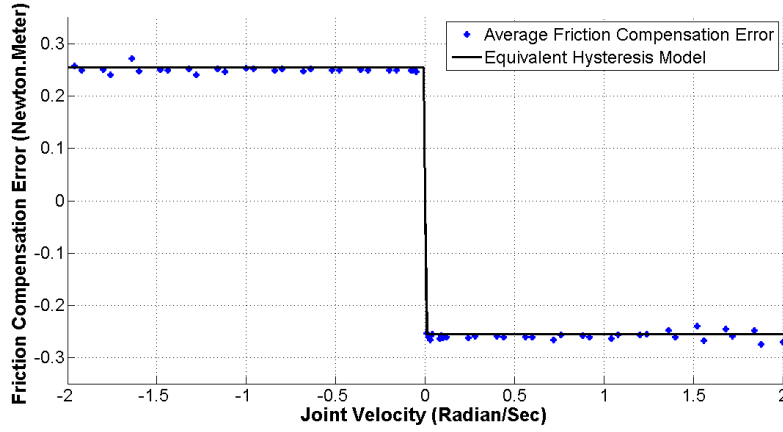
Figure 5.11: Hysteretic nature of  $\tau_{fre}$  in joint 1 of KUKA-LWR

Table 5.6: PD controller values for KUKA-LWR

Joint	P	D
1	132	13.2
2	1120	112
3	124	12.4

estimated value of the friction (i.e.,  $\hat{\tau}_{fr}$ ) as in (5.18), instead it has hysteretic behaviour. This hysteretic behaviour perhaps is due to the hysteresis that exists in torque sensor measurements. The new model of  $\tau_{fre}$  provides new time-variant thresholds. These time-variant thresholds are defined as,

$$b_{2H}(t) = \alpha + \gamma h(t) - CK_I \int_0^t e^{-K_I(t-u)} \frac{|\dot{q}_j(u)|}{\dot{q}_j(u)} du \quad (5.39a)$$

$$b_{2L}(t) = -\alpha + \gamma h(t) - CK_I \int_0^t e^{-K_I(t-u)} \frac{|\dot{q}_j(u)|}{\dot{q}_j(u)} du \quad (5.39b)$$

where  $\alpha$ ,  $\gamma$ , and  $C$  are vectors determined experimentally for  $b_{2H}(t)$  and  $b_{2L}(t)$  by comparing the values of  $\hat{r}_e(t)$ ,  $h(t)$ , and  $-K_I \int_0^t e^{-K_I(t-u)} \frac{|\dot{q}_j(u)|}{\dot{q}_j(u)} du$  for various trajectories. For the first three joints, the values of  $\gamma$ ,  $\alpha$  and  $C$  are given in Table 5.7. To compare the time-variant thresholds given in (5.39) with the constant threshold defined in (5.32), the values of  $\beta$  and  $eff = \frac{\alpha}{\beta}$  are also included in Table 5.7. Note that the smaller values of  $eff$  represent more effectiveness of the time-variant threshold. For KUKA-LWR, the inaccuracies in the estimation of the minimal inertial parameters have a larger effect on the lower joints. These

Table 5.7: Experimental values of  $\alpha_H$ ,  $\alpha_L$ ,  $\gamma$  for KUKA-LWR

Joint	1	2	3
$\alpha$	2.0137	1.8727	2.3715
$\gamma$	0.0020	5.0523e-004	0.0521
$C$	0.2678	0.5654	0.4367
$\beta$	2.5662	2.4758	2.8413
$eff = \alpha/\beta$	0.7847	0.7564	0.8347

inaccuracies have resulted in smaller values of  $eff$  for joints 1 and 2. This demonstrates the effect of modeling inaccuracies on external torque residues and validates our approach in obtaining time-variant thresholds.

The results of an experiment with no collision using KUKA-LWR on a trajectory described in Table 5.8 are shown in Figure 5.12. In this experiment the value of  $K_I$  was set to 20 for all joints. The results for collision detection using time-variant and constant thresholds are compared in Figure 5.13, where the upper threshold  $b_{2H}(t)$ , the lower threshold  $b_{2L}(t)$ , the residue  $\hat{r}(t)$ , along with the constant thresholds are shown. The collision forces in this experiment were exerted on the second joint of KUKA-LWR. Table 5.9 summarizes the results of this comparison and clearly shows the advantage of using time-variant thresholds in collision detection. A collision has occurred whenever a joint residue crosses its corresponding threshold. As observed, the collisions detected by the time-variant thresholds are either missed or detected with delays using constant thresholds. The results also indicate that small collision forces are detected neither with time-variant nor constant thresholds.

## 5.6 CONCLUSION

In this paper, time-variant thresholds for collision detection in robot manipulators were proposed. It was shown both theoretically and experimentally that the proposed thresholds were more effective in detecting collisions than any constant threshold. Time-variant thresholds are easy to use for collision detection in robot manipulators as they require tuning of three unknown parameters per joint. The proposed time-variant thresholds require the knowledge of torques resulted from model uncertainties which in turn, make collision detection based on time-variant thresholds more effective for the lower joints of a manip-

Table 5.8: Trajectory Points of KUKA-LWR

time(s)	$q_1$	$q_2$	$q_3$
0	0	0	0
3	25	25	25
15	-168	-6	88
27	27	-70	-70
36	0	100	44
47	168	-37	-88
56	0	115	-168
69	168	6	-88
83	-55	4	1
96	34	-4	-1
107	-165	-115	169
122	165	115	-169
133	-165	-85	-169
146	165	-85	169
160	27	-70	-70

Table 5.9: Collision detection times in the first three joints of KUKA-LWR

Collision Number	Time-variant Threshold Detection time (Sec)	Constant Threshold Detection Delay(Sec)
1	3.36	Does not Detect
2	7.39	Does not Detect
3	21.83	Does not Detect
4	28.43	0.01
5	38.92	0.03
6	50.18	0.42
7	62.59	Does not Detect
8	76.13	0.05
9	97.84	0.06
10	98.22	Does not Detect



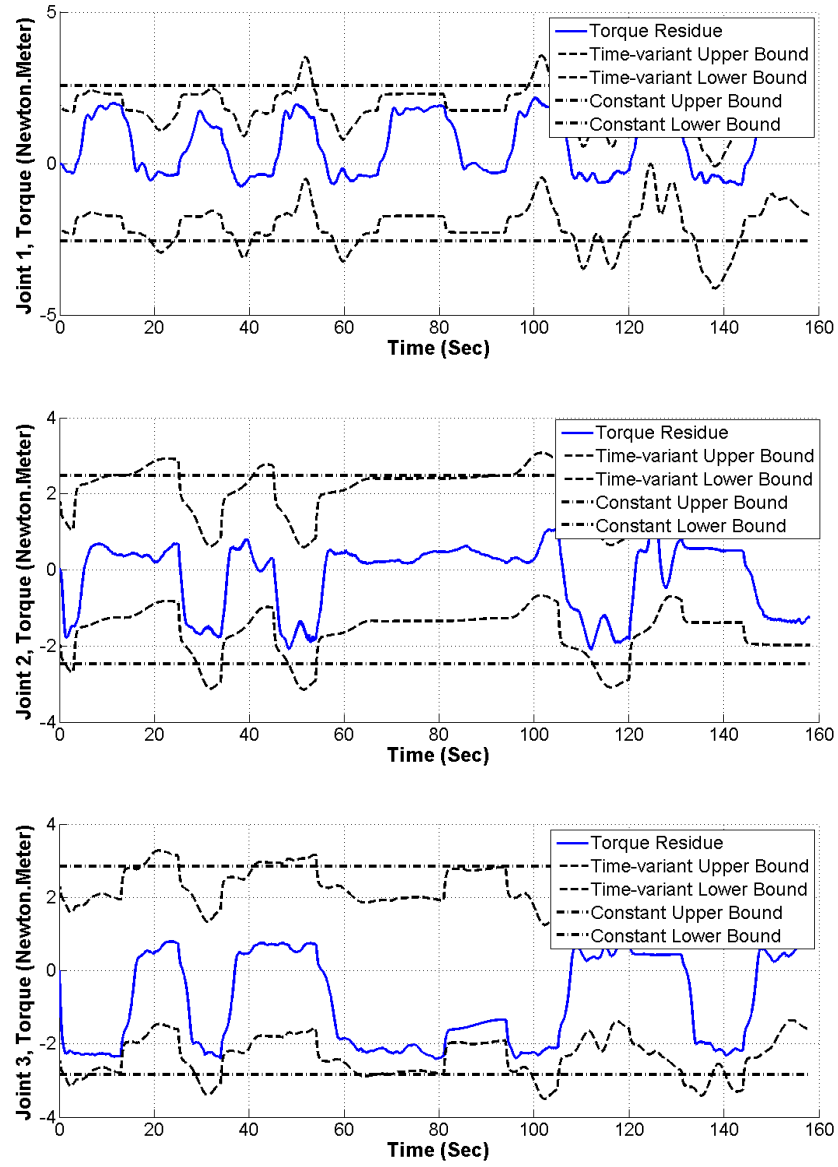


Figure 5.12: Collision residues  $\hat{r}(t)$  and bounds  $b_{2H}(t)$  and  $b_{2L}(t)$  for KUKA-LWR in the absence of collision forces

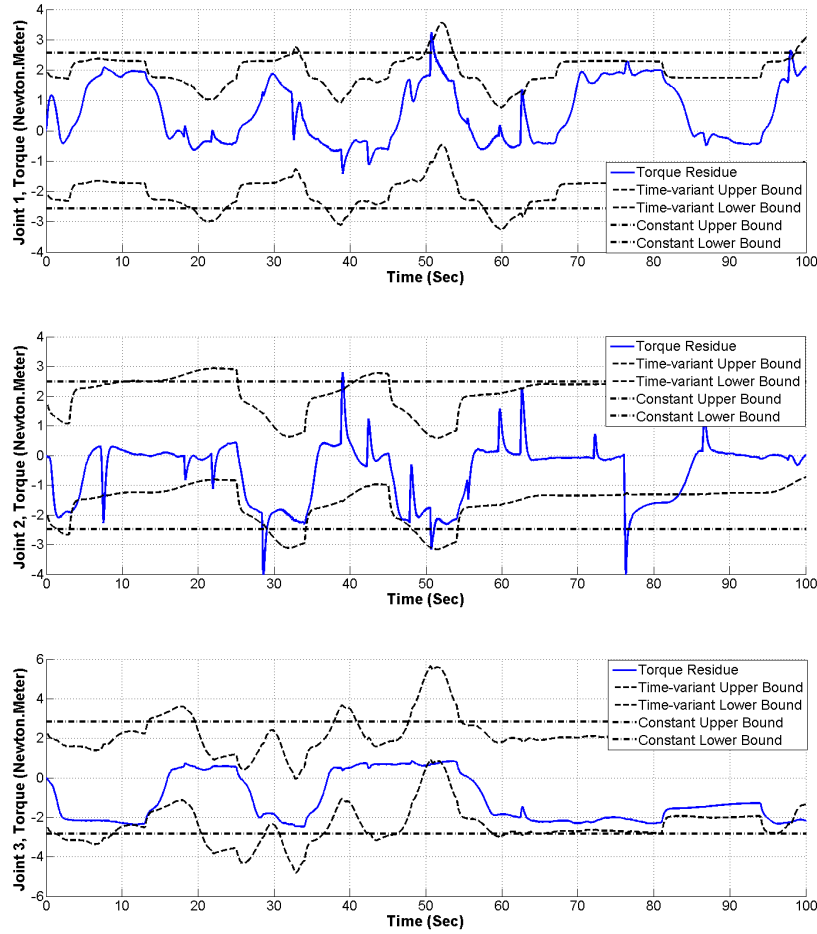


Figure 5.13: Collision residues  $\hat{r}(t)$ , time-variant thresholds, and constant thresholds for KUKA-LWR in the presence of collision forces

ulator. It was also shown that the proposed thresholds were effective during fast robot motions, when the friction forces were mainly due to viscous frictions. Simulation results using LifeModeler software and experimental results on KUKA Light-Weight Robot were presented to validate this approach. Future work will include obtaining similar time-variant thresholds for the observer model given in (5.2) within the task space of a manipulator. It is conjectured that comparing the results with those obtained within the joint space of the manipulator will lead to possible improvements in collision detection capabilities of the observer. Moreover, comprehensive studies of various types of robot collisions with different part of the human in LifeModeler environment will be an important step in order to establish new standards for characterizing human-safe robots.

## Bibliography

- [1] K. Ikuta, H. Ishii, and M. Nokata, “Safety evaluation method of design and control for human-care robots,” *International Journal of Robotics Research*, vol. 22, pp. 281–297, May 2003.
- [2] A. D. Santis, B. Siciliano, A. D. Luca, and A. Bicchi, “An atlas of physical human-robot interaction,” *Mechanism and Machine Theory*, vol. 43, no. 3, pp. 253 – 270, 2008.
- [3] A. De Luca, F. Flacco, A. Bicchi, and R. Schiavi, “Nonlinear decoupled motion-stiffness control and collision detection/reaction for the vsa-ii variable stiffness device,” in *Intelligent Robots and Systems, 2009. IROS 2009. IEEE/RSJ International Conference on*, pp. 5487 –5494, Oct. 2009.
- [4] A. Pervez and J. Ryu, “Safe physical human robot interaction-past, present and future,” *Journal of Mechanical Science and Technology*, vol. 22, pp. 469–483, 2008.
- [5] T. Fong, I. Nourbakhsh, and K. Dautenhahn, “A survey of socially interactive robots,” *Robotics and Autonomous Systems*, vol. 42, no. 3-4, pp. 143–166, 2003.
- [6] V. Lumelsky, M. Shur, and S. Wagner, “Sensitive skin,” *Sensors Journal, IEEE*, vol. 1, pp. 41 –51, June 2001.
- [7] A. Shafer and M. Kermani, “On the feasibility and suitability of mr and er based actuators in human friendly manipulators,” in *Intelligent Robots and Systems, 2009. IROS 2009. IEEE/RSJ International Conference on*, pp. 2904 –2909, oct. 2009.
- [8] E. Cheung and V. Lumelsky, “A sensitive skin system for motion control of robot arm manipulators,” *Robotics and Autonomous Systems*, vol. 10, no. 1, pp. 9–32, 1992.
- [9] P. Schmidt, E. Mael, and R. Wurtz, “A sensor for dynamic tactile information with applications in human-robot interaction and object exploration,” *Robotics and Autonomous Systems*, vol. 54, no. 12, pp. 1005–1014, 2006.
- [10] A. Bicchi, M. A. Peshkin, and J. E. Colgate, “Safety for physical human-robot interaction,” in *Springer Handbook of Robotics* (B. Siciliano and O. Khatib, eds.), pp. 1335–1348, Springer Berlin Heidelberg, 2008.

- [11] D. KuliA and E. Croft, "Real-time safety for human-robot interaction," *Robotics and Autonomous Systems*, vol. 54, no. 1, pp. 1–12, 2006.
- [12] S. Haddadin, A. Albu-Schaffer, M. Frommberger, J. Rossmann, and G. Hirzinger, "The dlr crash report: Towards a standard crash-testing protocol for robot safety - part ii: Discussions," in *Robotics and Automation, 2009. ICRA '09. IEEE International Conference on*, pp. 280 –287, May 2009.
- [13] S. Haddadin, A. Albu-schaffer, and G. Hirzinger, "Safety evaluation of physical human-robot interaction via crash-testing," in *In Robotics: Science and Systems Conf. RSS2007*, pp. 217–224, 2007.
- [14] S. Katsura, Y. Matsumoto, and K. Ohnishi, "Analysis and experimental validation of force bandwidth for force control," *Industrial Electronics, IEEE Transactions on*, vol. 53, pp. 922 – 928, june 2006.
- [15] H. Sneider and P. Frank, "Observer-based supervision and fault detection in robots using nonlinear and fuzzy logic residual evaluation," *Control Systems Technology, IEEE Transactions on*, vol. 4, pp. 274 –282, May 1996.
- [16] W.-H. Chen, D. Ballance, P. Gawthrop, and J. O'Reilly, "A nonlinear disturbance observer for robotic manipulators," *Industrial Electronics, IEEE Transactions on*, vol. 47, pp. 932 –938, Aug. 2000.
- [17] A. Stotsky and I. Kolmanovsky, "Application of input estimation techniques to charge estimation and control in automotive engines," *Control Engineering Practice*, vol. 10, no. 12, pp. 1371 – 1383, 2002.
- [18] A. D. Luca, A. Albu-Schaffer, S. Haddadin, and G. Hirzinger, "Collision detection and safe reaction with the dlr-iii lightweight manipulator arm," in *Intelligent Robots and Systems, 2006 IEEE/RSJ International Conference on*, pp. 1623 –1630, oct. 2006.
- [19] S. Morinaga and K. Kosuge, "Collision detection system for manipulator based on adaptive impedance control law," in *Robotics and Automation, 2003. Proceedings. ICRA '03. IEEE International Conference on*, vol. 1, pp. 1080 – 1085 vol.1, sept. 2003.
- [20] P. R. Dahl, "A solid friction model," *Industrial Electronics, IEEE Transactions on*, may 1968.

- [21] H. Olsson, K. J. Astrom, C. C. de Wit, M. Gafvert, and P. Lischinsky, “Friction models and friction compensation,” *Eur. J. Control*, vol. 4, no. 3, pp. 176–195, 1998.
- [22] C. Canudas de Wit, H. Olsson, K. Astrom, and P. Lischinsky, “A new model for control of systems with friction,” *Automatic Control, IEEE Transactions on*, vol. 40, pp. 419–425, mar 1995.
- [23] C. Canudas de Wit, P. Tsiotras, E. Velenis, M. Basset, and G. Gissinger, “Dynamic friction models for road/tire longitudinal interaction,” *Vehicle System Dynamics*, vol. 39, no. 3, pp. 189–226, 2003.
- [24] D. Rigos and S. Fassois, “Friction identification based upon the lugre and maxwell slip models,” *Control Systems Technology, IEEE Transactions on*, vol. 17, pp. 153–160, jan. 2009.
- [25] J. Swevers, F. Al-Bender, C. Ganseman, and T. Projogo, “An integrated friction model structure with improved presliding behavior for accurate friction compensation,” *Automatic Control, IEEE Transactions on*, vol. 45, pp. 675–686, apr 2000.
- [26] M. Kermani, R. Patel, and M. Moallem, “Friction identification and compensation in robotic manipulators,” *Instrumentation and Measurement, IEEE Transactions on*, vol. 56, pp. 2346–2353, dec. 2007.
- [27] S. Takakura, T. Murakami, and K. Ohnishi, “An approach to collision detection and recovery motion in industrial robot,” in *Industrial Electronics Society, 1989. IECON '89., 15th Annual Conference of IEEE*, pp. 421–426 vol.2, nov 1989.
- [28] J. J. Craig, *Introduction to Robotics: Mechanics and Control*. Boston, MA, USA: Addison-Wesley Longman Publishing Co., 2nd ed., 1989.
- [29] M. Gautier and W. Khalil, “A direct determination of minimum inertial parameters of robots,” in *Robotics and Automation, 1988. Proceedings., 1988 IEEE International Conference on*, pp. 1682–1687 vol.3, apr 1988.
- [30] B. Armstrong, O. Khatib, and J. Burdick, “The explicit dynamic model and inertial parameters of the puma 560 arm,” in *Robotics and Automation. Proceedings. 1986 IEEE International Conference on*, vol. 3, pp. 510–518, Apr. 1986.

- [31] P. Corke and B. Armstrong-Helouvry, "A search for consensus among model parameters reported for the puma 560 robot," in *Robotics and Automation, 1994. Proceedings., 1994 IEEE International Conference on*, pp. 1608–1613 vol.2, May 1994.
- [32] H. Y. Kim and D. A. Streit, "Configuration dependent stiffness of the puma 560 manipulator: Analytical and experimental results," *Mechanism and Machine Theory*, vol. 30, no. 8, pp. 1269–1277, 1995.
- [33] K. P. Valavanis, T. B. Larsson, and S. P. Gardner, "Pd and pid model-based control stability analysis of the puma-560 robot manipulator under model mismatch," *Journal of Intelligent Robotic Systems*, vol. 7, pp. 233–254, 1993.

# Chapter 6

## Concluding Remarks and Future Work

This chapter discusses the main contributions of this work and makes suggestions for future research in the area of safe human-robot interaction and collision detection.

### 6.1 Conclusions

The key contributions of this thesis are as follows:

1. Chapter 2 discussed modeling of KUKA Light-Weight Robot IV+ (KUKA-LWR). This robot, developed at DLR laboratories [1], is frequently used for research purposes. To model the robot, the regressor matrix and minimal inertial parameters formulations were obtained. Extensive experiments were conducted to obtain the friction model of KUKA-LWR. Even though the LuGre model was employed to obtain the friction model [2], it is shown that both link side and motor side friction of KUKA-LWR could be best explained using a Coulomb model. A contribution of this chapter is the identification of the minimal inertial parameters of the robot, and a study on the effects of torque sensor calibrations in the KUKA-LWR controller. The novelty of the work presented in this chapter in terms of modeling technique includes the application of relative weights (see [3]) in the regression analysis of the minimal inertial parameters. Relative weight analysis was used to consider the covariance in the identification procedure to determine the importance of each minimal inertial parameter in the model. Small relative weights were used as a criteria to remove the corresponding parameters that can not be accurately identified. This in turn improved the identification of the remaining parameters.



Moreover, the KUKA-LWR controller allows access to the mass matrix and the gravity vector values. Procedures were devised to obtain the minimal inertial parameters using the mass matrix and the gravity vector provided by the controller. The minimal inertial parameters obtained by these procedures were compared to the results obtained by regression analysis.

2. Inaccuracies in robot models diminish the quality of external force/torque observer results. Chapter 3 provided a comprehensive study considering modeling inaccuracies and robot state approximation errors in external force/torque estimation and collision detection. One of the contributions of this chapter was providing the formulation for external force/torque estimation errors by concurrently considering modeling inaccuracies, and velocity and acceleration approximation errors. Another contribution was the development of model-based time-varying thresholds based on the proposed formulation. Based on these thresholds, a novel collision detection capability metric for comparing robots, trajectories, and robot state approximation filters was developed. Also, the problem of obtaining optimal trajectories with regards to external force/torque estimations was defined. The solution to this problem can help in ensuring safety of the user by timely detection of collisions. The optimal trajectory problem was developed such that it can be solved by Euler-Lagrange equations. Also discussions were presented about the capability of the proposed method to automatically compensate effects of manipulation of unknown objects in the model-based thresholds. This property makes the proposed thresholds suitable for unstructured environments. Further discussions were provided with regards to controller design, effects of friction and unmodeled dynamics.

Collision detection experiments were conducted on KUKA-LWR to show the efficacy of the proposed model-based collision detection thresholds. The collision detection metric of different trajectories achieving the same task on KUKA-LWR were compared. The results show the capability of the proposed metric in anticipating collision detection efficiency.

3. Inaccurate friction modeling results in poor external force/torque observer performance. Friction modeling is a well-studied subject in the literature [4]. The model of the friction of a robotic system might change as a result of age, and temperature. Usually the experiments regarding friction modeling are time-consuming and might not be appropriate for every application. Given that friction models are velocity de-

pendent [5], the goal of Chapter 4 was defined as considering effects of velocity in modeling inaccuracies in observers and in collision detection without resorting to remodeling the robot. The main contribution of Chapter 4 was the proposal of velocity-based collision detection thresholds to achieve this goal. Robots with and without joint force/torque sensors were studied. The effects of modeling inaccuracies in the residual signal from the generalized momentum-based observer, proposed in [6], was investigated. This in turn led to theoretical formulation of the deterministic velocity-based thresholds.

In order to identify the time the collision occurs, Endevco® Piezoresistive 2000 g accelerometers were installed in a Humanetics® Hybrid III 50th Male Dummy. Experimental results from conducting collisions between KUKA-LWR and the dummy validated the proposed thresholds. The velocity-based methodology can be used to augment the model-based thresholds developed in Chapter 3 to achieve more accurate thresholds.

4. Effects of modeling inaccuracies on force/torque observers, specially errors in minimal inertial parameter estimations, can be further studied on a joint-by-joint basis. By avoiding the complexity of model-based and velocity-based thresholds, a heuristic method was given in Chapter 5 for improving collision detection. Considering a linear relationship between the approximation error and the estimated value of the minimal inertial parameters, a signal was defined for collision detection threshold adjustment. Simulation results on PUMA 560 robot were given to validate the concept. Calibration of the proposed collision detection signal was also discussed. It was shown that this signal can be calibrated together with the friction modeling adjustment signal. To this end, experiments on KUKA-LWR showed that using the proposed heuristic method, given an appropriate friction model, effects of friction modeling errors and minimal inertial parameter inaccuracies can be mitigated simultaneously.

## 6.2 Suggestions for Future Work

The work in this thesis can be continued in several directions. Some suggestions for future research are given here:

1. Availability of an accurate model of the actuator helps in determining the external

forces/torques and collision detection. Considering that soft actuation systems, such as [7], [8], [9] and [10] usually have complex mechanisms, it is essential to obtain a very accurate model of the joints dynamics. Although without an accurate model, the heuristic method in Chapter 5 can still be employed, and the model-based and velocity-based thresholds can still be determined. However in such cases, due to presence of not so small disturbances caused by unavailability of the actuator model, the efficacy of the proposed thresholds are reduced. Therefore the actuator dynamics of a human-safe robot must be available and accurately identified.

2. Utilization of dirty derivatives or other computational methods to obtain accelerations is not satisfactory in case of non-smooth actual trajectories, specially in real-time applications. Acceleration and velocity can be better estimated using non-causal filters such as the Savitsky-Golay filter [11]. Such filters are useful in measurement of external forces/torques in applications where time-delay is acceptable. However, considering human-safety, collision detection requires fast online computation of acceleration and velocity, which is usually erroneous. Availability of accelerometers and to a lesser extent tachometers in human-safe robots can significantly lower collision detection thresholds. Future work can consist of installation of such sensors in manipulators for comparison of external force/torque estimation capability with manipulators without such sensors.
3. Motor inertia is a major contributor to the maximum collision force in physical human-robot interaction [12]. Therefore reducing the effective motor inertia in robot dynamics is desirable. MR-Fluid robots are capable of disconnecting the motor inertia from the link inertia [13]. This capability of MR-Fluid actuators makes them a viable option for development of human safe-robots. A comparison between MR-Fluid robots and other manipulators in terms of maximum collision forces can establish MR-Fluids as a major human-safe actuation mechanism. The proposed collision detection thresholds along with trajectory planning considerations will be applied to MR-Fluid robots in upcoming research. Theoretical formulation of the proposed collision detection thresholds predicts that application of such thresholds to MR-Fluid robots would further reduce maximum possible human-robot collision forces. Furthermore, extensive studies done in our lab on hysteresis modeling of MR-Fluid actuators, such as [14], will help in development of fast and accurate collision detection strategies.

4. The time-varying thresholds proposed in this thesis have multiple parameters that need to be determined before the thresholds are implemented. Tuning these parameters requires information about the implemented robot state estimation method and experimental data. Although parameter tuning in each chapter of this work is separately explained, there is a need for a standardized technique to tune the time-varying thresholds. This can be subject of future work.
5. In chapter 3, effects of trajectory planning on external force/torque estimation and collision detection was studied. A calculus of variations problem to maximize external force/torque estimation precision was proposed. However, the solution to this optimization problem was not investigated. Future work should contain solving this problem. Moreover, upon availability of the actuator model, accelerometers or tachometers, the optimal collision detection trajectory for performing a given task must be reformulated.
6. The external force/torque observers can, to a good extent, only detect at which joint the collision has occurred. Employing the Jacobian matrix of a manipulator along with the observer help in obtaining more information about collision forces/torques at each joint. Given the collision data, Jacobian matrix can be used to determine the maximum possible external force/torque that could've occurred at each joint. To this end, the exterior design of each link must also be considered.
7. One aspect of research in safe physical human-robot interaction is the studies on distinguishing between user commands and accidental collisions. Any interaction with the environment can increase or decrease the internal energy of the manipulator. The interactions can be categorized into passive and active interactions. Preparing a Programming by Demonstration scheme that makes use of such a passive-active categorization to make the robot able to identify the intention of its user can be an objective of future work. The importance of such research is in its direct effect on the safety of the users. Artificial damping can be added through the controller to the robot when interacting with the user to make the distinction of intentional interaction from accidental collision easier.

## Bibliography

- [1] A. Albu-Schaffer, S. Haddadin, C. Ott, A. Stemmer, T. Wimbock, and G. Hirzinger, “The dlr lightweight robot: Design and control concepts for robots in human environments,” *Industrial Robot*, vol. 34, no. 5, pp. 376–385, 2007.
- [2] M. Kermani, R. Patel, and M. Moallem, “Friction identification and compensation in robotic manipulators,” *Instrumentation and Measurement, IEEE Trans. on*, vol. 56, pp. 2346–2353, dec. 2007.
- [3] S. Tonidandel and J. LeBreton, “Relative importance analysis: A useful supplement to regression analysis,” *Journal of Business and Psychology*, vol. 26, no. 1, pp. 1–9, 2011.
- [4] H. Olsson, K. Astrom, C. C. de Wit, M. Gafvert, and P. Lischinsky, “Friction models and friction compensation,” *European Journal of Control*, vol. 4, no. 3, pp. 176 – 195, 1998.
- [5] C. Canudas de Wit, H. Olsson, K. Astrom, and P. Lischinsky, “A new model for control of systems with friction,” *Automatic Control, IEEE Trans. on*, vol. 40, pp. 419–425, mar 1995.
- [6] A. D. Luca, A. Albu-Schaffer, S. Haddadin, and G. Hirzinger, “Collision detection and safe reaction with the dlr-iii lightweight manipulator arm,” in *Intelligent Robots and Systems, 2006 IEEE/RSJ International Conference on*, pp. 1623–1630, oct. 2006.
- [7] A. Bicchi and G. Tonietti, “Fast and ”soft-arm” tactics [robot arm design],” *Robotics Automation Magazine, IEEE*, vol. 11, pp. 22 – 33, june 2004.
- [8] A. Bicchi, S. Rizzini, and G. Tonietti, “Compliant design for intrinsic safety: general issues and preliminary design,” in *Intelligent Robots and Systems, Proceedings. 2001 IEEE/RSJ International Conference on*, vol. 4, pp. 1864–1869 vol.4, 2001.
- [9] M. Zinn, O. Khatib, B. Roth, and J. K. Salisbury, “A new actuation approach for human friendly robot design,” in *International Symposium on Experimental Robotics, S. Angelo d’Ischia, I*, pp. 379–398, 2002.

- [10] P. Yadmellat, A. S. Shafer, and M. R. Kermani, “Design and development of a safe robot manipulator using a new actuation concept,” in *Robotics and Automation (ICRA), 2013 IEEE International Conference on*, pp. 337–342, 2013.
- [11] A. Savitzky and M. J. E. Golay, “Smoothing and differentiation of data by simplified least squares procedures.,” *Analytical Chemistry*, vol. 36, no. 8, pp. 1627–1639, 1964.
- [12] A. D. Santis, B. Siciliano, A. D. Luca, and A. Bicchi, “An atlas of physical human-robot interaction,” *Mechanism and Machine Theory*, vol. 43, no. 3, pp. 253 – 270, 2008.
- [13] A. Shafer and M. Kermani, “Design and validation of a magneto-rheological clutch for practical control applications in human-friendly manipulation,” in *Robotics and Automation (ICRA), 2011 IEEE International Conference on*, pp. 4266–4271, 2011.
- [14] P. Yadmellat and M. Kermani, “Output torque modeling of a magneto-rheological based actuator,” in *IFAC World Congress*, vol. 18, pp. 1052–1057, 2011.

# **Appendix A**

## **Downloadable Files**

All files are available at <http://publish.uwo.ca/~vsotoude/>.

## Appendix B

### Time-Domain Solution to the External Force/Torque Observer

Equation (4.5) is obtained by taking the Laplace transform of (4.4),

$$\hat{r}(s) = K_I \left[ \hat{p}(s) - \frac{(\hat{\tau}_m + \hat{C}^T(\hat{q}, \hat{q})\hat{q} - \hat{g}(\hat{q}) - \hat{\tau}_{fr} + \hat{r})}{s} - \frac{\hat{p}(0)}{s} \right] \quad (\text{B.1})$$

therefore,

$$\hat{r}(s) = \frac{K_I s}{s + K_I} \hat{p}(s) - \frac{K_I}{s + K_I} \left[ (\hat{\tau}_m + \hat{C}^T(\hat{q}, \hat{q})\hat{q} - \hat{g}(\hat{q}) - \hat{\tau}_{fr}) - \hat{p}(0) \right] \quad (\text{B.2})$$

and by taking the inverse Laplace transform of (B.2),

$$\hat{r}(t) = K_I \left[ \delta(t) - K_I e^{-K_I t} \right] * \hat{p}(t) - K_I e^{-K_I t} * \left[ (\hat{\tau}_m + \hat{C}^T(\hat{q}, \hat{q})\hat{q} - \hat{g}(\hat{q}) - \hat{\tau}_{fr}) - \hat{p}(0) \right] \quad (\text{B.3})$$

The term  $-K_I e^{-K_I t} * \hat{p}(0)$  is the transient response and is assumed to be negligible after a certain time period. Hence (B.3) can be written as,

$$\hat{r}(t) = K_I \left[ \hat{p}(t) - K_I (e^{-K_I t} * \hat{p}(t)) \right] - K_I (e^{-K_I t} * (\hat{\tau}_m + \hat{C}^T(\hat{q}, \hat{q})\hat{q} - \hat{g}(\hat{q}) - \hat{\tau}_{fr})) \quad (\text{B.4})$$



# Curriculum Vitae

**Name:**                   Vahid Sotoudehnejad

**Post-Secondary**   The University of Western Ontario

**Education and**     London, Ontario, Canada

**Degrees:**           2009 - 2013 Ph.D.

Electrical and Computer Engineering Dept., Robotics and Control

Isfahan University of Technology

Isfahan, Iran

2006 - 2008 M.Sc.

Electrical and Computer Engineering Dept., Control Systems

**Related Work**     Teaching Assistant

**Experience:**       The University of Western Ontario

2010 - 2013

## Related Publications:

Sotoudehnejad V.; Kermani M.R., “On Determining Collision Detection Thresholds and Trajectory Planning for Manipulators with Regards to External Torque Estimation Precision,” Submitted to Robotics, IEEE Transactions on.

Sotoudehnejad, V.; Takhmar, A.; Kermani, M.R.; Polushin, I.G., “Counteracting modeling errors for sensitive observer-based manipulator collision detection,” Intelligent Robots and Systems (IROS), 2012 IEEE/RSJ International Conference on , vol., no., pp.4315,4320, 7-12 Oct. 2012.

Sotoudehnejad V.; Kermani M.R., “On Dynamic Model Identification of KUKA Light-Weight Robot IV+,” Submitted to Advanced Robotics.

Sotoudehnejad, V.; Kermani, M.R., “Improved Observer-Based Collision Detection Using Time-Variant Thresholds,” Submitted to Robotics and Autonomous Systems.

Sotoudehnejad, V.; Kermani, M.R., “Velocity-Based Thresholds for Improving Collision Detection in Manipulators,” Submitted to Robotics and Automation (ICRA), 2014 IEEE International Conference on.